Unraveling the Complexity of Mid-Gestation Placental Immunity

by

Jessica Mae Toothaker

Bachelor of Science, Syracuse University, 2017

Submitted to the Graduate Faculty of the

School of Medicine in partial fulfillment

of the requirements for the degree of

Doctor of Philosophy

University of Pittsburgh

2021

UNIVERSITY OF PITTSBURGH

SCHOOL OF MEDICINE

This dissertation was presented

by

Jessica Mae Toothaker

It was defended on

April 22, 2021

and approved by

Carolyn Coyne, Professor, Department of Pediatrics

Daniel Kaplan, Professor, Departments of Dermatology and Immunology

Warren Shlomchik, Professor, Departments of Medicine and Immunology

Matthew Nicotra, Assistant Professor, Department of Surgery

Dissertation Director: Liza Konnikova, Assistant Professor, Department of Pediatrics and Immunology

Unraveling the Complexity of Mid-Gestation Placental Immunity

Jessica Toothaker, PhD

University of Pittsburgh, 2021

Maintenance of healthy pregnancy is reliant on successful balance between the fetal and maternal immune systems. Although maternal mechanisms responsible have been well studied, those used by the fetal immune system remain poorly understood. Using suspension mass cytometry and various imaging modalities, this dissertation reports a complex immune system within the mid-gestation (18-23 weeks) human placental villi (PV). Further, we identified immunosuppressive signatures in innate immune cells and antigen presenting cells that potentially maintain immune homeostasis in utero. Consistent with recent reports in other fetal organs, T cells with memory phenotypes were detected within the PV tissue and vasculature. Moreover, we determined PV T cells could be activated to upregulate CD69 and proliferate after TCR stimulation and when exposed to maternal uterine antigens. In addition, this dissertation explored the role of PV immune cells in a non-human primate model of intra-amniotic inflammation. This study showed that pregnancy-matched choriodecidua and PV have distinct immunological profiles in rhesus pregnancies. In the choriodecidua, the abundance of neutrophils, multiple populations of antigen-presenting cells, and two populations of natural killer (NK) cells changed with prenatal IA LPS exposure. In contrast, in immune cells within the PV we observed alterations in the abundance of B cells, monocytes, and CD8 T cells. Prior work has illustrated that IA inflammation leads to an increase in tumor necrosis factor alpha (TNFα) at the fetal–maternal interface. In this study, pretreatment with a TNF blockade partially reversed inflammation in the PV. Furthermore, immune cells in the PV sensed LPS during our experimental window, and subsequently activated

T cells to produce proinflammatory cytokines. Moreover, this study was the first report of memory T cells in third-trimester non-human primate PV and provided evidence that manipulation of immune cells in the PV at the fetal–maternal interface should be considered as a potential therapeutic target for IA inflammation.

Table of Contents

List of Tables

List of Figures

Preface

When I began my PhD journey in Pittsburgh, Pennsylvania three and a half years ago, I never imagined I would be finishing my dissertation while in quarantine from an apartment in Connecticut. Through all the "normal" hardships of getting a PhD and novel hardships of finishing a dissertation in the height of a global pandemic and in the midst of a relocation I remain passionate for the work presented in this dissertation and optimistic for the future of scientific research in the post-SARS-CoV-2 era. I would not have made it through these tumultuous times and my time in graduate school overall without the support from the individuals referenced in this preface.

To begin I thank my mentor Dr. Liza Konnikova for her guidance, scientific knowledge and time invested in my training. Though I still believe Dr. Konnikova has figured out a way to get more than 24 hours out of every day, I will always be inspired by her ability to be a successful scientist, physician, parent and mentor all at the same time. I am particularly thankful for her ability to know when I needed help thinking through an experiment but also giving me the space to problem solve on my own. It has been one of the pleasures of my life to be a part of growing Dr. Konnikova's lab from the ground (or myself and one other person) up to the accomplished research team it is today.

I would also like to thank all of the current and past members of the Konnikova lab and our partner lab the Yimlamai lab for your help in my pursuit of a PhD. Specifically, Dr. Bunmi Olaloye, Stephanie Stras, Rebecca Case, Collin McCourt and Blake McCourt from the Konnikova lab and Dr. Dean Yimlamai, Meghan Mooring, Ye Liu and Connor Yao from the Yimlamai lab. I have been blessed to enjoy coming to work every day and have greatly benefited from all of your scientific expertise and emotional/social support throughout this journey. Additionally, I would

like to thank the members of my dissertation committee: Dr. Carolyn Coyne, Dr. Matt Nicotra, Dr. Warren Shlomchik, and Dr. Dan Kaplan for your scientific insight, support and flexibility during my move, and presentation feedback which greatly enhanced my scientific communication skills and overall self-confidence as a researcher.

Additionally, I wish to thank my parents, Mary and Scott Toothaker, older brother Adam Toothaker and soon-to-be sister-in-law Alana Assanmacher. I truly appreciate the examples of hard work and success you all have set for me. Your unwavering support of my quest to finish this degree through all of the missed phone calls and family gatherings means the world to me. Lastly, I thank my partner Blake McCourt. I cannot express how much it means to me that his first response to hearing the lab was relocating was “great when do we leave?” I cannot thank him enough for his support for myself and my career, and willingness to move his life and start a new job (in the same lab as myself no less). I am so thankful to have found both love for my research and love from Blake during my time in graduate school.

1.0 Introduction

1.1 Human Placental Anatomy

1.1.1 Timeline of Placental Development

The human placenta is the physical barrier at the fetal-maternal interface tasked with protecting the fetal cavity, transferring maternal nutrients, removing fetal waste, regulating gas exchange and producing hormones to sustain pregnancy throughout gestation (~40 weeks) (**Fig 1A)**[1]. Upon fertilization and a series of myotic divisions the morula segregates into the trophectoderm that is the precursor cell structure to the placental villi (PV) and fetal membranes (amnion and chorion) **(Fig 1B)**. The primitive PV structures begin to form on the seventh day post conception as they initiate contact with the uterus and begin the implantation process. Secure attachment of the blastocyst (precursor cells of the fetus) to the decidua (mucosal uterine lining) is mediated by trophoblast cells of the PV that produce many signaling molecules including hormones, cytokines and integrins[1]. As invasion of the decidua and uterus progresses, PV trophoblast differentiation from individual cytotrophoblast to multinucleated syncytiotrophoblasts begins, ultimately forming the syncytium, which will be elaborated on in Section 1.1.4. Maternal blood flow is directed to surround the PV at the end of the first trimester initiating transfer of oxygen and nutrients between mother and fetus **(Fig 1A)**[1]. Placental growth continues throughout the second and third trimesters **(Fig 1A)** and is delivered in the third stage of labor following delivery of the fetus at a size proportional to that of the fetus[1].

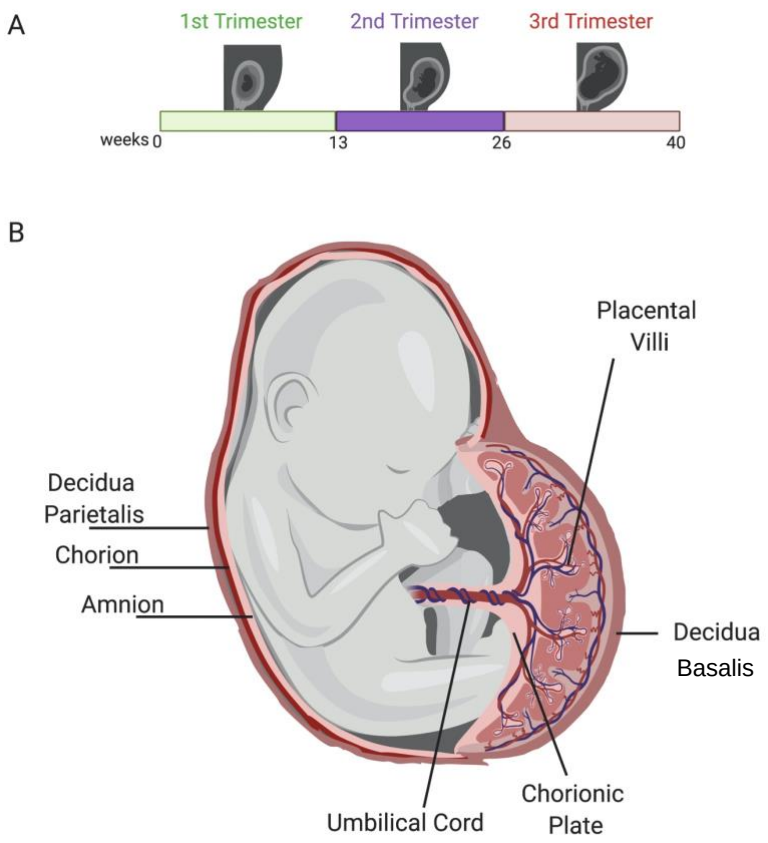

Figure 1 Summation of human pregnancy

(A) Timeline of human gestation. (B) Diagram of the human fetal maternal interface.

1.1.2 Decidual formation and cellular composition

Decidualization of the human endometrium occurs throughout the menstrual cycle of healthy nonpregnant women. It forms during the secretory phase approximately 6 days post-ovulation and is routinely shed during menses after a failure of implantation[2]. During decidualization, mesenchymal cells transition from elongated to cuboidal epithelial-like states. This differentiation is largely driven by female sex hormones, specifically estradiol and progesterone produced by the ovaries[2]. In the pregnant uterus, the decidua is segregated into the decidua parietalis, which lines the fetal membranes and the decidua basalis surrounding the PV.

This site of attachment of the PV to the decidua basalis is collectively referred to as the basal plate **(Fig 1B)**. Within this location, the decidua plays many critical roles in maintaining a healthy pregnancy. The decidua must regulate trophoblast invasion, both to ensure trophoblasts have invaded deep enough to secure placental attachment for a bipedal pregnancy (fighting against gravity) and to prevent trophoblasts from invading too deeply into the uterus[3]. At each site of anchored PV **(Fig 2)**, extravillous trophoblasts (EVTs) form long cell columns protruding into the decidua. Additionally, the decidua basalis is tasked with remodeling maternal spiral arteries and promoting angiogenesis to redirect blood flow to accommodate the developing fetus[2]. Furthermore, the decidua must protect the fetus from environmental exposure such as oxidative stress. Interestingly, the decidualized cuboidal cells described above have been reported to be resistant to radical oxygen species as one potential mechanism of fetal protection[4]. Lastly, the decidua has a key role in maintaining immune homeostasis by balancing the promotion of tolerance towards the foreign paternal antigens displayed on fetal derived cells while also conferring protection against pathogens. The specific cell types and unique functionality of decidual immune cells will be further explored in Section 1.2.1.

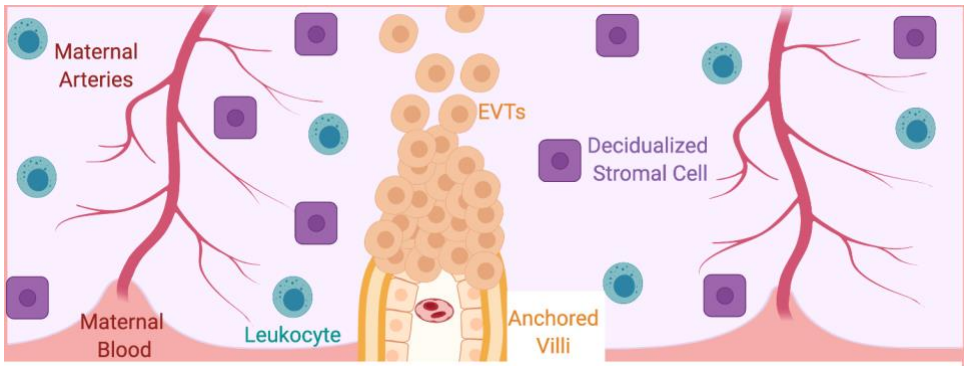

Figure 2 Cell types of the decidua basalis

1.1.3 Composition and function of the fetal membranes

The fetal membranes comprised of the amnion and the chorion encase the fetus floating in amniotic fluid and form the amniotic sac. The membranes are in contact with the decidua parietalis lining the uterus and also the PV at the chorionic plate **(Fig 1B)**. The fetal-facing membrane is the amnion. Though the amnion is only ~0.5cm thick, it is a complex organ made up of five distinct layers: epithelium, basement membrane, compact layer, fibroblast layer and spongy layer[5] **(Fig 3)**. Underneath the spongy layer of the amnion, there are 4 additional tissue layers comprising the chorion: cellular layer, reticular layer, pseudo-basement layer and trophoblast layer[5] which is connected to the PV (**Fig 3)**. At the chorionic plate, the umbilical cord is centralized containing the fetal blood supply. In contrast, the amnion is non-vascular and the chorion only houses blood vessels within the reticular layer[5]. As blood flow is highly limited in the fetal membranes, it is unlikely they play a large role in mediating nutrient, gas and waste exchange. As such, the primary function of the fetal membranes is to secure and protect the fetus and amniotic fluid components throughout pregnancy. However, there is evidence suggesting the membranes have important fetal-maternal signaling functions for maintaining pregnancies. For example, multiple studies have investigated the role of prostaglandin synthesis and metabolism in the fetal membranes[6,7].

Additionally, signaling by cells in the fetal membranes is critical for successful parturition. Rupture of the membranes and subsequent release of the amnionic fluid is dictated by site-specific accumulation of metallomatrix proteins (MMPs) leading to membrane weakening and ultimate rupture[8]. While the mechanisms responsible for the initiation of this labor cascade are still unclear, multiple studies have highlighted key immunological events within the fetal membranes related to parturition such as: selective chemotaxis of leukocytes in the fetal membranes during labor[9], upregulation of MMPs by membrane explants after exposure to inflammatory stimulants[10], and a

three-fold increase in immune cells in fetal membranes that experienced labor compared to membranes from deliveries without labor[11].

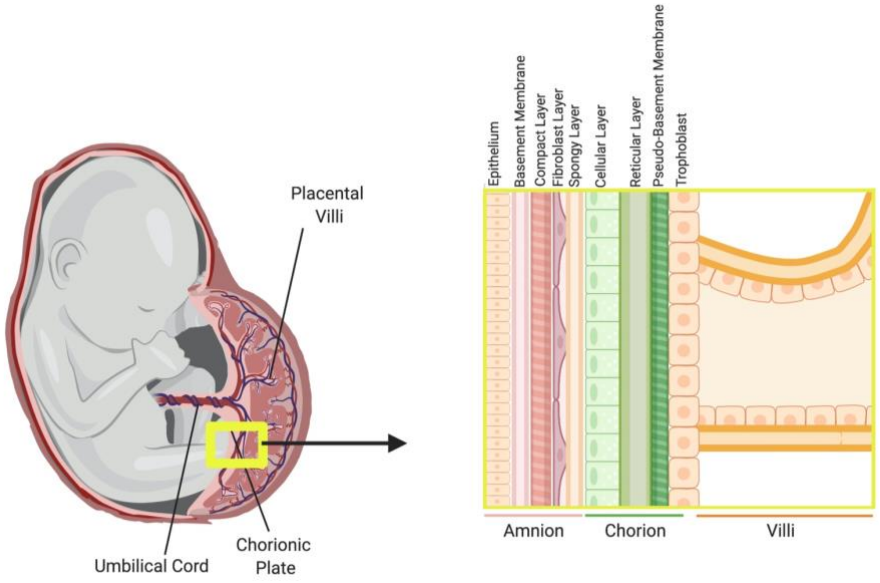

Figure 3 Layers of the fetal membranes

1.1.4 Cell types of the placental villi

The placental villi (PV) comprise the bulk by mass of the placenta. The PV tree network is rooted in the chorionic plate on the fetal side and branches out in multiple directions until it reaches the maternal decidua. The specific PV that are embedded in the decidua are termed anchoring villi. In contrast, the villi sprouting off the stem villous are termed floating villi in the intervillous space **(Fig 4A)**. These tree-like projections have an outer layer of multinucleated syncytiotrophoblasts that are bathed in maternal blood from the intervillous space and an inner layer of mononuclear cytotrophoblasts[1] **(Fig 4B)**. As the placenta grows the syncytiotrophoblast layer sheds off cell clumps referred to as syncytial knots and these cells are then replaced with fusion of individual cytotrophoblasts. Syncytiotrophoblasts and cytotrophoblasts perform a variety of functions to help

maintain healthy pregnancy including secretion of pregnancy supporting hormones[12], clearance of fetal waste[13], and deterrence of pathogens[14] among others. The third type of trophoblast cell are extravillous trophoblasts (EVTs) which are located at the tip of anchoring PV in the decidua. EVTs are highly migratory cells involved in multiple physiologic processes through their communication with maternal NK cells, endothelial and stromal cells to coordinate vascular remodeling among other functions[15].

Comprised within the bounds of these trophoblast layers (intravillous space) is the villi stroma made up of undifferentiated and differentiated stromal cell types, endothelial cells of the fetal vasculature network, and resident macrophages (Mϕ) (Hofbauer cells)[1] **(Fig 4B-C)**. All of the placental villi cell types are of fetal origin. As gestation progresses, the intravillous space becomes more and more compact with cells, likely limiting cellular migration. The influx of cells in the stroma is coupled with the reduction of collagen and other extracellular structures and an increase in vascularization. All of these stromal changes happening with pregnancy progression likely allow for easier diffusion of nutrients and gases between mother and fetus[1].

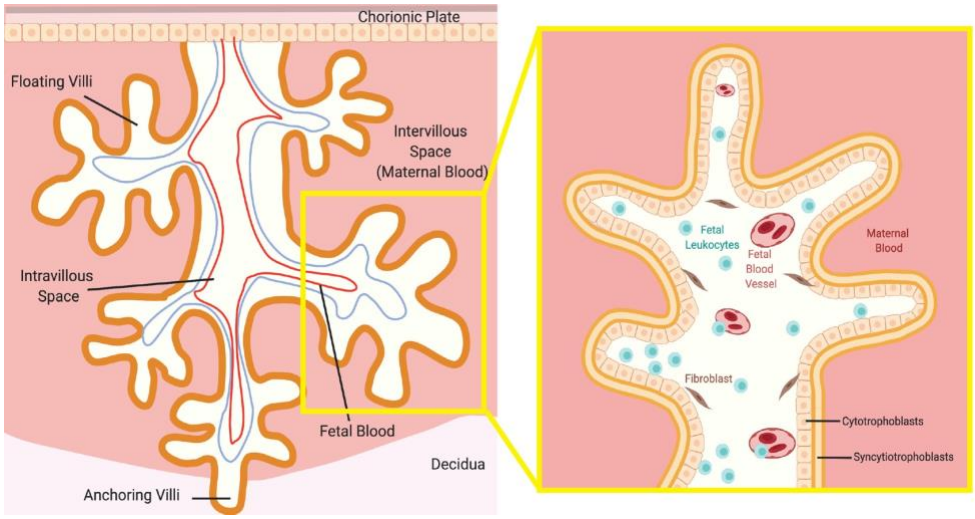

Figure 4 Placental villi anatomy

1.1.5 Experimental models of placental biology

Placentas are classified based on a number of factors: (1) the developmental origin of the embryonic membranes (chorioallantoic), (2) shape (discoid, cotyledonary, diffuse or zonary) (3) contact with maternal tissue (deciduate vs nondeciduate), (4) depth of trophoblast invasion, (hemochorial, epitheliochorial, endotheliochorial) and (5) PV shape (villous vs. labyrinth)[16]. Based on these classifications the human placenta is chorioallantoic, single discoid, deciduate, hemochorial, and villous respectively[16]. While all mammalian placentas are classified as chorioallantoic, they are variable between species in all other classifications. Some species including mice and primates are deciduate, meaning that trophoblasts are invasive and that maternal and fetal placental tissue is shed after delivery. In contrast a nondeciduate placenta, present in many farm animals, has superficial trophoblast invasion without fusion of fetal and maternal tissues. As such, fetal tissues can be cleanly shed from the uterus at delivery[16]. Furthermore, the hemichorial classification (the most invasive type of trophoblast invasion) of human placentas means that fetal placental cells have eroded uterine tissue and are in direct contact with maternal blood.

Murine models are often used to study placentation as the mouse placenta is also reflective of the deciduate and singular discoid classification of the human placenta[17]. Although the mouse, like humans, has a hemichorial placenta, the anatomy of the placenta differs[18,19]. In brief, the mouse PV are organized into a labyrinth structure contrasting the free-floating villous PV of the human placenta. In the mouse, maternal blood flows through sinuses into this labyrinth coming into contact with the mononuclear cytotrophoblasts while the fetal blood supply is in contact with the multinucleated syncytiotrophoblast cells[19]. As such, the blood-trophoblast relationship is

inverse of that seen in humans in which the syncytiotrophoblasts are bathed in maternal blood **(Fig 4)**.

Moreover, it has been postulated that human pregnancy is more symbiotic between maternal and fetal mechanisms than murine pregnancies[20]. This notion is supported by phenomena like progesterone production, which is made exclusively in maternal ovaries in mice, but switches in humans to the fetal placenta early in gestation[18]. These stark differences support the theory that some of the tissue-specific immune mechanisms within the placental layers may have different functions between species. While mouse models do lead to important discoveries about placental development and pregnancy regulation, the physiologic differences between species leads to gaps in knowledge that can be filled by studying additional model systems. However, clear ethical and logistical concerns bar the manipulation of human subjects to investigate the causes of pathological pregnancies. Therefore, alternative model organisms, particularly non-human primate macaques, are used for such purposes. Though financially burdensome, the macaque placenta has clear advantages over the murine placenta. Specifically, the gestation duration of 166 days[21] is far more comparable to that of humans (~280 days) than murine pregnancies at only 19.5 days. Additionally, the average offspring number for macaques is 1 per gestation with the frequency of twin pregnancies reported by one study at only 0.027%[22], compared to mice with litter sizes that can range from 6-14 pups on average[23]. Lastly, the macaque placenta is classified almost identical to human placentas except for having a bidiscoid shape.

1.2 Immunology of Pregnancy

1.2.1 Maternal Immunity

The female immune system is altered during pregnancy both in the periphery and within the uterine environment. Specifically, the maternal immune system must maintain a delicate immune homeostasis balancing tolerance towards foreign paternal antigens displayed on the fetus while also preventing infection from pathogens[24]. Further challenging to maternal immunity is the changing of physiological demands that differ throughout gestation, i.e. immune mechanisms needed for successful implantation are likely distinct from those necessary at mid-gestation and further distinct from those involved in parturition.

Peripheral immunity- Seminal work from Agaheepour and colleagues first illustrated the heterogeneity of immunological changes in maternal peripheral blood throughout pregnancy. Using mass cytometry (CyTOF) this work demonstrated not only that the landscape of immune cells changes across gestation, but also found gestation-specific signaling, and stimulation potential in many immune populations[25]. In addition to multicellular surveys of the peripheral maternal immune system[25,26], cell type specific modulations to peripheral immunity have been reported as well[27,28]. A trend across multiple studies has shown increased innate immune function, likely as a mechanism to protect and support the developing fetus at various stages of gestation. For example, enhanced anti-viral activity has been observed in monocytes and plasmacytoid dendritic cells[27]. Additionally, there is increased interferon (IFN) induced STAT1 signaling in monocytes, myeloid DCs and NK cells[25] and an increase in complement activity[28]. Conversely, it is reported that components of the peripheral adaptive immune system are repressed during pregnancy. Notably, peripheral B cells are reduced and promote a tolerogenic phenotype during

pregnancy[29] and there is an accumulation of T regulatory cells (Tregs) in early pregnancy[30]. Studies of autoimmunity during pregnancy further support an immunosuppressive phenotype among some peripheral immune cells during pregnancy as there is a reduction in autoimmune flares during pregnancy for women with multiple autoimmune diseases such as rheumatoid arthritis[31]. Interestingly, it has been shown that Tregs isolated from pregnant mice are sufficient to protect against collagen-induced rheumatoid arthritis in mice[32].

Decidual immunity- Reviews by Erlebacher [33] and Liu [34] summarize the studies that have been instrumental to our understanding of maternal tolerance; the most substantial discoveries include the identification of specialized tolerant uterine natural killer (uNK) cells, Mϕs, dendritic cells (DCs) and T cells in the decidua. This work has revealed that the decidua is comprised of about 40% leukocytes [35,36], primarily comprised of NK cells [37], Mϕs [38], and T cells [39]; with DCs [40,41], B cells [42], NKT [43] and γδ T cells [44] being much more rare. Along with the differential abundance of decidual immune subsets, much is also known about their function. NK cells are not only the most abundant immune cells in the decidua, but also have specialized phenotypes and function. Over 90% of decidual NK cells (dNKs) are $CD56^{hi}$ $CD16^{lo}$ in direct contrast with peripheral NK cells which are predominantly $CD56^{lo}CD16^{hi}$ [45,46]. This reversal of surface marker expression is indicative of reduced cytotoxicity in dNKs to prevent destruction of placental cells[46], and it has been reported that dNKs instead secrete pro-angiogenic factors[47]. Moreover, dNKs may directly recognize fetal trophoblasts through KIR2D/HLA-C recognition[48] suggesting dNKs may regulate trophoblast invasion. Additionally, it has been shown the dNKs can transfer granulysin to kill bacteria in infected trophoblasts[49]. T cell immunity in the decidua is also functionally distinct. It is well-reported that decidual Tregs are vital to implantation, exemplified by impaired breeding in Treg deficient mice[50], and associations with Treg malfunction and clinical fertility

complications[51]. Salvany-Celades and colleagues showed that human decidual Tregs can be classified into three subtypes based on expression of FOXP3, PD-1 and TIGIT each with a unique transcriptional profile and immunosuppressive capabilities[52]. Further controlling T cell activity in the decidua, dendritic cells have been shown to preferentially skew CD4 T cells to a T helper type 2 (TH2) phenotype in the decidua[53]. Moreover, unique properties of decidual B cells have been reported such as the IL-33 regulated production of progesterone-induced blocking factor in maintaining healthy pregnancy[54].

1.2.2 Placental Villi Immunity

Trophoblast-mediated immunity- One of the strongest forms of immune protection within the PV is the structure of the tissue itself. The outermost syncytiotrophoblast layer **(Fig 4)** is one long continuous cytoplasm with many nuclei. Therefore, no cellular junctions can be used by pathogens to infect the placenta, nor can cell-to-cell connections be susceptible to immunomodulation[55]. This lack of cell junctions coupled with a dense cytoskeleton on the apical (maternal) facing side of the syncytiotrophoblast layer[56] results in few pathogens with infectious capabilities to vertically transmit infection across the placenta. Notable exceptions to this are TORCHZ pathogens such as Toxoplasmosis, Other (syphilis, varicella-zoster, parovirus B16), Rubella, Cytomegalovirus, and Herpes and Zika. In addition to being a structural deterrent, trophoblasts also constitutively secrete anti-pathogenic products including antiviral interferons[57] and microRNAs[14,57]. If pathogens bypass the secreted factors, syncytiotrophoblasts are also capable of sensing pathogen associated molecular patterns (PAMPs) through pattern recognition receptors including toll-like receptors (TLRs) and retinoic-acid gene I (RIG-I)-like receptors[58,59]. Moreover, there are reports that trophoblasts can attract peripheral maternal T cells and NK cells

into the decidua to protect the fetus from potential pathogens[60]. However, trophoblasts must also prevent recognition and subsequent rejection of the maternal immune system against paternal antigens displayed by the fetus. There have been reports that potentially pathogenic maternal T cells can recognize fetal antigens[61]. While prevention of this fetal-antigen induced inflammation is controlled in part by maternal immunosuppressive mechanisms such as fetal-specific Tregs[62,63], trophoblasts also may help control the maternal T cell response by modifying maternal T cell development to favor Th2 phenotypes[64]. Furthermore, trophoblasts prevent direct detection by maternal T cells by not expressing any histocompatibility (MHC) class II[65] or canonical MHC class I proteins[55].

Leukocytes- The most well studied immune cell type in the PV are the tissue-resident placental Hofbauer cells. Hofbauer cells are yolk-sac derived and appear as early as 18 days post conception and persist until delivery[66,67]. Though some functions of Hofbauer cells remain elusive, it is believed that Hofbauer cells are phenotypically and functionally consistent with an M2 Mϕ polarization[67]. This is supported by the surface expression of CD163 a marker associated with M2 Mϕ, an epigenetic profile consistent with M2 over M1 transcription[68], and a proangiogenic phenotype[69]. However, recent work by Thomas and colleagues demonstrated that Hofbauer cells can have some M1-like activity by showing that first trimester PV do have phagocytic capabilities and can be stimulated through TLR4[66] showing that Hofbauer cells may also directly protect the fetus from pathogens as well. Though it is believed that Hofbauer cells are the predominant fetal-derived immune cells in the PV, there are multiple reports showing additional PV immune populations.

One well reported finding is that the placenta is a site of hematopoiesis during development[70]. Additionally, placental hematopoiesis is unique from initial hematopoiesis in the

yolk sac in that the placenta generates hematopoietic stem cells (HSCs) with the potential to differentiate into many immune cell subsets including lymphocytes, while yolk sac hematopoiesis is restricted to myeloid and erythroid lineages[71]. Moreover, the placenta maintains a large pool of HSCs, multiplying 20x over between 11.5 and 12.5 days post conception in mice[71]. The robust abundance of HSCs with the multi-lineage differentiation potential strongly suggests that the PV contain other immune cell populations in addition to Hofbauer cells. Specifically, as early as 1979, B cell precursors were identified in single cell suspensions from mouse placentas[72]. Moreover, T cells have been detected both in single cell suspensions[73] and with immunohistochemistry[74] in human PV. Furthermore, a recent single cell survey of term and preterm placental tissues revealed the detection of NK cells, B cells and T cells in the PV in healthy term placentas that did not undergo labor suggesting that multiple immune cell types are present in the PV independent of the labor cascade in utero [75]. Collectively, these studies demonstrate that there is a more complex immune landscape within the PV than has been previously appreciated, and further research is needed to identify the phenotypic and functional capacity of PV immune cells.

1.2.3 Pathologic Placental Inflammation

Intra-amniotic inflammation is believed to be driven by both pathogen and sterile inflammatory processes[76]. Downstream morbidities of intra-amniotic inflammation include placental dysfunction, intrauterine growth restriction, preeclampsia, and spontaneous preterm labor. Each of these pathologies is also associated with preterm birth, currently the number one cause of mortality in children under five years of age[77]. Differential inflammatory signatures are detected in PTB compared to term births in the placenta[75,78], amniotic fluid[79–81], fetal membranes[75,78], uterus[54,75,78,82] and peripheral sites[83]. Although intra-amniotic inflammation by

definition is restricted to the fetal-maternal interface and the amniotic fluid, pathogen-associated intra-amniotic inflammation leads to inflammatory responses in multiple other fetal organs including the brain, lungs, skin, and gut in humans and animals[84,85]. Much of the work investigating infection-driven inflammation at the fetal-maternal interface has focused on the maternally-derived decidua and/or the fetus-derived fetal membranes[86–90]. Yet, the fetus-derived PV have not been thoroughly investigated, even though this tissue is in contact with the fetal membranes at one end, invades into the maternal decidua at the other, and forms the bulk of the fetal-maternal interface by mass **(Fig 1,4)**. Specifically, within the PV, pathological lesions of inflammatory origin are detected in 27% of preterm deliveries[91]. Additionally, villitis of unknown origin (VUE), an inflammatory disorder of the placental villi (PV) involving both innate and adaptive immune cells occurs without documented infection in 5-15% of all deliveries[92]. Collectively, this shows that the role played by PV-derived immune cells during intra-amniotic inflammation and other obstetric complications should be investigated further.

1.3 Fetal & Neonatal Immune System

Historically, the fetal and neonatal immune systems have been described as immature, underdeveloped, and primitive. This hypothesis was supported by poor vaccine responses in neonates[93], high susceptibility to infection[94], and the predominance of naïve lymphocytes in human cord blood[95]. However, novel insights suggest that the fetal and neonatal immune systems are mature and developed, though potentially with altered function. Work supporting this concept includes: the *in utero* maturation following education of fetal Tregs[96], detection of novel immunosuppressive cell types[97–99], and the presence of *in utero* memory lymphocytes[100–104].

However, our knowledge about the immunological capabilities of the fetal cells at the fetal maternal interface is incomplete.

A collection of recent single cell RNA-sequencing studies of the first trimester fetal-maternal interface revealed multiple previously undocumented PV cell types and cell-cell interactions [105,106]. Similarly, detection of novel cell populations and interactions was observed in third trimester surveys[75,107]. Of interest, the work by Pique-Regi identifying PV-specific immune cell signatures is notable for the presence of both resting and activated T cells of fetal origin in term PV[75]. However, it remains unclear if memory lymphocyte populations are present in the placenta at mid-gestation. Furthermore, it is unknown if the activated T cells identified by Pique-Regi were activated prior or subsequent to labor/delivery [75]. And, if functional, activated immune cells are present within the PV at mid-gestation, what mechanisms prevent these cells from initiating intra-amniotic inflammation?

2.0 Human placental villi immune cells help maintain homeostasis in utero

2.1 Study Goals

Based on the collection of prior work documented in Chapter 1, and specifically in reference to the work by Pique-Regi and colleagues[75], we hypothesized that the active PV immune system detected in the third trimester must be present and poised to participate in immune functions at mid-gestation. To investigate this hypothesis, we used single-cell technology as this approach generates large amounts of data using small amounts of tissue and has previously led to discoveries of new cell types in placental tissues[75,105–107] and other fetal organs[100–102,108–110]. We elected to use mass cytometry by time of flight (CyTOF) over single-cell RNA-sequencing for our investigation. While both technologies are beneficial for characterizing cellular phenotypes, single cell RNA-sequencing is biased towards the detection of the most abundant transcripts in a cell and is dependent on depth of sequencing[111]. Moreover, mRNA is typically expressed at a much lower magnitude than protein levels (2 vs 6-7 orders of magnitude respectively)[112]. As we were primarily interested in immune markers, which in general are not the highest expressed transcripts per cell, we elected to use the proteomic approach of CyTOF, and complimentary techniques for our target investigation to phenotype PV immune cells. In this study we aimed to (1) to characterize the complexity and diversity of PV immune cells in the mid-gestation human placenta; (2) determine if intravillous PV immune cells were circulatory or tissue resident populations; (3) elucidate if mid-gestation PV immune cells were mature and functional; (4) uncover if PV immune contributed to immune homeostasis in utero; and (5) determine if PV immune cells could be activated ex vivo.

2.2 Materials and methods

Table 1 Patient Demographics

Demographic Information				Experimental Use							
Sample Number	Gestational Age	Sex	Maternal Age Range	RNA seq	qPCR	FISH	CyTOF	IMC	RISH	TCR Stim	Decidua Stim
1130	23 weeks	F	25-30	✓			✓		✓		✓
1143	23 weeks	M	20-25	✓		✓					✓
1146	23 weeks	F	25-30	✓			✓				✓
1081	22 weeks	M	25-30		✓						
1131	18 weeks	M	20-25		✓		✓				
1132	22 weeks	M	30-35		✓		✓				✓
1186	18-19 weeks	M	30-35		✓			✓		✓	
1100A	21 weeks	N/A	34-40		✓						
1102	21 weeks	F	40-45		✓		✓				
1055	23 weeks	F	35-40		✓						
1108	22 weeks	F	25-30			✓	✓		✓		
1038	21 weeks	M	N/A				✓				
1042	22 weeks	M	N/A				✓				
1094	17 weeks	F	25-30				✓			✓	
1106	21 weeks	F	30-35				✓		✓		✓
1165	18 weeks	M	20-25				✓	✓	✓	✓	✓
PO38	23 weeks	F	N/A				✓				
1217	21 weeks	N/A	N/A								✓
1199*	17 weeks	M	35-40								✓

* denotes unknown genetic abnormality

Placental tissue collection: Human products of conception were obtained through the University of Pittsburgh Biospecimen core after IRB approval (IRB# PRO18010491) (**Table 1**). PV were separated using forceps under a light dissection microscope (Fisherbrand #420430PHF10) from the chorionic and amniotic membranes lining the chorionic plate (CP) and from the decidua basalis (referred to as decidua throughout manuscript) on the basal plate side of the placenta. Tissue was thoroughly washed with sterile PBS prior to cryopreservation and subsequent single cell isolation as previously described[113].

RNA sequencing: Snap frozen placental tissues were shipped on dry ice to MedGenome for mRNA extraction and library preparation. RNA extractions were completed with the Qiagen All Prep Kit (#80204). cDNA synthesis was prepped with the Takara SMART-seq kit (#634894) and NexteraXT (FC-131-1024, Illumina) was used to fragment and add sequencing adaptors. Quality control was completed by MedGenome via Qubit Fluorometric Quantitation and TapeStation BioAnalyzer. Libraries were sequenced on the NovaSeq6000 for Paired End 150 base pairs for 90 million reads per sample.

RNA sequencing analysis: FASTQ files were imported and subsequently analyzed with CLC Genomics Workbench 20.0 (https://digitalinsights.qiagen.com). Briefly, paired reads were first trimmed with a quality limit of 0.05, ambiguous limit of 2 with automated read through adapter trimming from the 3'-end with a maximum length of 150. Trimmed reads were then mapped to the homo_sapiens_sequence_hg38 reference sequence. Differential gene expression was computed in CLC Genomics with an Across groups ANOVA-like comparison. Significantly differentially expressed genes were delineated as those with a p-value <0.05, False-Discovery Rate <20% and fold-change > absolute value of 2. Heatmaps for gene expression were created with Morpheus (https://software.broadinstitute.org/morpheus).

RISH: Formalin fixed samples were sectioned and embedded in paraffin by the Pitt Biospecimen Core. Staining was completed per manufacturer's instructions for RNAScope® multiplex V2 detection kit (ACD Bio) coupled with immunofluorescent protein staining for Cytokeratin19 (ab52625 Abcam) at 1:250 dilution. Echo® Revolve microscope at 20x was used to image sections. All images were batch processed using FIJI[114], and all edits were made to every pixel in an image identically across all patients per experiment. Quantification of cell populations was done using a custom pipeline in CellProfiler[115].

FISH*:* In situ hybridization for the Y chromosome was adapted from the protocol outlined in[116]. Briefly, slides were deparaffinized with a series of xylene and ethanol washes. Target retrieval was done at 95^{oC} for 10 minutes, slides were placed in 70% ethanol, 85% ethanol and 100% ethanol for 2 minutes each. DYZ3 probe (D5J10-034, Abbott Laboratories) was diluted 1:10 in LSI/WCP hybridization buffer (D6J67-011, Abbott Laboratories) and incubated for 5 minutes at 83^{oC} prior to overnight hybridization at 37^{oC}. Slides were soaked in SSC/0.1% NP-40 (ab142227, Abcam) to remove cover slips and placed in 2X SSC/0.1% NP-40 for 2 minutes at 74^{oC} before mounting with antifade plus Propidium Iodide (p36935, Invitrogen). Slides were imaged on the LSM 710 (Leica Biosystems) confocal at the Yale Center for Cellular and Molecular Imaging.

RNA extraction and qPCR: RNA was extracted from snap-frozen villi samples using the RNAEasy Minikit (#217004, Qiagen) RNA was converted to cDNA using iScript (#1708891, BioRad) reagents according to manufacturer protocol. Samples were run on the Taqman StepOnePlus Real-Time PCR System (Applied Biosciences) machine with probes for *ACTB* (Hs01060665_g1) as housekeeping gene and with either *XIST* (Hs01079824_m1) or EIF3AY (Hs01040047) all from Qiagen. Values undeterminable were given cycle values of 40 for quantification purposes.

Immunofluorescent staining: Slides with 10um sections of FFPE tissue were deparaffinized with a series of xylene and ethanol washes. Antigen retrieval was performed in the Biocare Medical LLC decloaking chamber (NC0436641) for 1 hour with citrate-based antigen retrieval buffer (H-3300, Vector Laboratories) and washed with PBS. Slides were then blocked for 30 minutes with 10% horse serum prior to overnight incubation at 4^{o}C with primary antibodies: CD163 (ab87099, Abcam); CD45 (20103-1-AP, Proteintech); PD-1 (AF1086, R&D Systems); CD3 (ab135372, Abcam); Cytokeratin19 (AF3506, R&D Systems) . Slides were washed with PBS

and incubated with secondary antibodies for 45 minutes at RT. Slides were mounted with Antifade mounting media + DAPI (H-1300, Vectashield).

Table 2 Imaging Mass Cytometry Panel

Metal	Target	Clone	Vendor
115In	CD44	IM7	BioLegend
142Nd	CD19	6OMP31	Fluidigm
143Nd	Vimentin	D21H3	Fluidigm
144Nd	CD14	EPR3653	Fluidigm
147Sm	CD163	EDHu-1	Fluidigm
148Nd	PanKeratin	C11	Fluidigm
151Eu	CD31	EPR3094	Fluidigm
152Sm	CD45	D8M81	Fluidigm
156Gd	CD4	EPR6855	Fluidigm
160Gd	IgG	MHK49	Fluidigm
161Dy	Ki67	8D5	BioLegend
162Dy	CD8a	C8/144B	Fluidigm
164Dy	pZAP70	Y319	Cell Signaling
165Ho	pCREB	87G3	Cell Signaling
166Er	CD45RA	HI100	Fluidigm
167Er	p44/42	D13.14.4E	Cell Signaling
169Tm	pSTAT3	A1600213	Cell Signaling
170Er	CD3	polyclonal	Fluidigm
171Yb	CD66a	CD66a-B1.1	Fluidigm
173Yb	CD45RO	UCHL1	Fluidigm
174Yb	HLA-DR	LN3	Fluidigm
175Lu	pS6	D57.2.2E	Cell Signaling
176Yb	pHistoneH3	HTA28	Fluidigm

Imaging mass cytometry: Slides with 4um sections of FFPE tissue were deparaffinized with a series of xylene and ethanol washes. Antigen retrieval was performed at 95^{oC} for 20 minutes using 1X Antigen Retrieval Buffer (#CTS013 R&D) and washed with water and dPBS. Slides were then blocked for 30 minutes with 3% BSA in dPBS prior to overnight incubation at 4^{o}C with a primary antibody cocktail **(Table 2)**. Slides were rinsed and co-stained with 191/193 DNA-intercalator (Fluidigm), rinsed and air dried for >20 minutes prior to analysis. Slides were analyzed

on the Hyperion Mass Cytometer with an ablation energy of 4 and frequency of 100Hz for ~30 minutes per section.

Imaging mass cytometry data analysis*:* Representative images were generated using Histocat++ software[117]. Further analysis of image data was performed using the IMC segmentation pipeline as published [118]. Briefly, files were loaded to Histocat 1.7.6.1 [119], visualized and analyzed as follows. Phenograph clustering of cells was performed using major lineage markers to identify cell populations of interest. Clusters were visualized using the tsne function and plots generated. Heatmap for cluster identification was generated with Morpheus (https://software.broadinstitute.org/morpheus). Nearest neighborhood analysis was performed to identify neighboring cells within 3 pixels to identify interactions present in >10% of images with a of p-value of 0.01.

CyTOF staining*:* Samples were stained with antibody cocktail (**Table 3**) per previously published protocol[100] and incubated with 191Ir/193Ir DNA intercalator (Fluidigm) and shipped overnight to the Longwood Medical Area CyTOF Core. Data was normalized and exported as FCS files, downloaded and uploaded to Premium Cytobank® platform. Any files with insufficient cell number were excluded from analysis **(Table 4)**. Gating and analysis was completed with cytofkit[120] as published[100]. Cluster abundance was extracted, and statistically analyzed using R.

Table 3 CyTOF Panel

Metal	Target	Clone	Vendor
89Y	CD45	HI30	Fluidigm
113In	CD88	P12/1	BioRad
115In	CD44	IM7	BioLegend
141Pr	CD66b	G10F5	BioLegend
142Nd	CD19	HIB19	BioLegend
143Nd	HLA-DR	L243	Fluidigm
144Nd	CD69	FN50	Fluidigm
145Nd	cRTH2	BM16	BioLegend
146Nd	CD8a	RPA.T8	BioLegend
147Sm	CD10	HI10a	BioLegend
148Nd	CD28	CD28.2	BioLegend
149Sm	CD25	2A3	Fluidigm
150Nd	CD38	HIT2	BioLegend
151Eu	CD123	TUGH4	BioLegend
152Sm	CD14	M5E2	BioLegend
153Eu	CD45RA	HI100	BioLegend
154Sm	CD163	GHI/61	Fludigim
155Gd	CD27	L128	Fluidigm
156Gd	CCR4	SIDI8BEE	eBiosciences
158Gd	CD3	UCHT1	BioLegend
159Tb	CD11c	Bu15	BioLegend
160Gd	IgG	MHK49	Fluidigm
161Dy	CD16	3G8	BioLegend
162Dy	CD56	NCAM16.2	BioLegend
163Dy	CXCR3	G025H7	Fluidigm
164Dy	CD161	HP-3G10	BioLegend
165Ho	LAG3	11C3C65	Fluidigm
166Er	HLA-G	87G	BioLegend
167Er	Lox1	331212	R&D Systems
168Er	CD127	A019D5	Fludiigm
169Tm	CD11b	M1/70	BioLegend
170Er	CCR7	G043H7	BiolLegend
171Yb	CD68	Y1/82A	Fluidigm
172Yb	CD274(PD-L1)	29E.2A3	BioLegend
173Yb	CD335	9E2	BioLegend
174Yb	CD4	SK3	Fluidigm
175Lu	PD-1	EH12.2H7	Fluidigm
176Yb	IL-10	JES3-19F1	BioLegend
209Bi	CXCR5	MU5UBEE	eBiosciences

Table 4 Files Omitted From CyTOF Analysis

Sample Name	Figures Excluded
1102 Decidua	7-10,13-14,17-18
1165 CP	7-10,13-14,17-18
PO38 PV	7-10,13-14
1094 CP	9-10, 13-14
1130 CP	9-10, 13-14
1131 CP	9-10, 13-14

Stimulation of PV T cells: *αCD3/αCD28:* Cells were isolated from cryopreserved PV samples as described throughout manuscript. Dead cells were removed prior to stimulation using Millitenyl dead cell removal kit (130-090-101 Millitenyl Biotec). Cells were incubated with CFSE (65-0850-85) alone or with αCD3 (clone HIT3a, #300302, Biolegend) and αCD28 (clone CD28.2, 302902, Biolegend) soluble antibodies for 72 hours rotating at 37^{oC} + 5% CO_2. GolgiPlug (51-2301K2, BD Biosciences) and GolgiStop (51-2092K2, BD Biosciences) were added for the last 4 hours of stimulation.

Flow cytometry αCD3/αCD28*:* Post stimulation cells were washed with PBS and incubated with Propidium Iodide (PI) live/dead stain (421301, Biolegend). PI was washed out and cells were resuspended and spun down in FACS buffer then incubated with Human TruStain FcX (Biolegend) for 10 minutes prior to the addition of a surface antibody cocktail containing the following antibodies: CD3 *PE-Cy7* (clone SK7, Biolegend), CD69 *PE,* (clone FN50, Biolegend), for 30 minutes. Cells were washed with FACs buffer and permeabilized with FOXP3 fix/perm (Invitrogen) overnight. Cells were washed with 1X FOXP3 Wash Buffer (Invitrogen) and incubated with intracellular antibodies: TNFα PacBlue (clone Mab11, Biolegend) and IFNγ *AF647* (clone B27, BD Biosciences) for 30 minutes.-Cells were washed, fixed for 10 minutes with

4% PFA and resuspended in FACs buffer. All samples were run on BD LSRII (BDBiosciences) at the Yale University Flow Cytometry core and output FCS files were analyzed with FlowJo®.

Stimulation of PV T cells lysed decidual cells: Single cells from PV and decidua were isolated from cryopreserved tissue as previously described[113]. PBMCs were thawed and DMSO was washed out. PV tissue was thawed and made into single-cell suspensions (as described above). Cells were incubated in 5mLs of media with GolgiPlug (51-2301K2, BD Biosciences) and GolgiStop (51-2092K2, BD Biosciences) and designated stimuli. For PMA condition, PMA (1:2000) (Sigma-Aldrich) and Ionomycin (1:1000) (Sigma-Aldrich) were added. Decidua and PBMC cells were lysed via ultracentrifugation at max speed for 7 minutes and 1mL of lysed components was added to appropriate conditions. PV cells were exposed to stimuli for 4 hours at 37^{oC} with 5% CO_2.

Flow Cytometry lysed decidual cells: Post stimulation cells were washed with PBS and incubated with Zombie Aqua live/dead stain (Biolegend). Zombie was washed out and cells were resuspended and spun down in FACS buffer then incubated with Human TruStain FcX (Biolegend) for 10 minutes prior to the addition of a surface antibody cocktail containing the following antibodies: CD3 *PE-Cy7* (clone SK7, Biolegend), CD45 *AF700* (clone MHCD4328, Thermofisher), CD4 *BV711* (clone SK3, BDBioscience), CD8 *PerCP-Cy5* (clone RPA-T8, eBioscience), CD69 *PE,* (clone FN50, Biolegend), and CD19 *PE-Cy5* (clone HIB19, Biolegend) for 30 minutes. Cells were washed with FACs buffer and permeabilized with FOXP3 fix/perm (Invitrogen) overnight. Cells were washed with 1X FOXP3 Wash Buffer (Invitrogen) and incubated with intracellular antibodies: TNFα *BV650* (clone Mab11, Biolegend) and IFNγ *AF647* (clone B27, BD Biosciences) for 30 minutes.-Cells were washed, fixed for 10 minutes with 4% PFA and resuspended in FACs buffer. All samples were run on BD LSRFortessa (BDBiosciences)

at the University of Pittsburgh Department of Pediatrics Flow Cytometry core and output FCS files were analyzed with FlowJo®.

Statistics*:* R version 3.6.1 with Kruskal-Wallis analysis and Dunn's multiple comparison test for post-hoc analysis among groups. One-tailed t-test was used to compare groups of two. Comparisons of mean expression values corrected using the Bonferroni method. P-values of 0.05 or less were significant.

Plot generation: Plots comparing multiple groups were generated using Prism GraphPad 8. In each plot, each data point represents one subject as per figure description.

Data and code availability: Data analyzed in this study has been stored according to IRB guidelines and is subject to institutional regulations. CyTOF data is available for public download on premium cytobank and RNA-sequencing data requests can be made to liza.konnikova@yale.edu.

2.3 Results

2.3.1 The human second trimester PV has tissue specific immune signatures

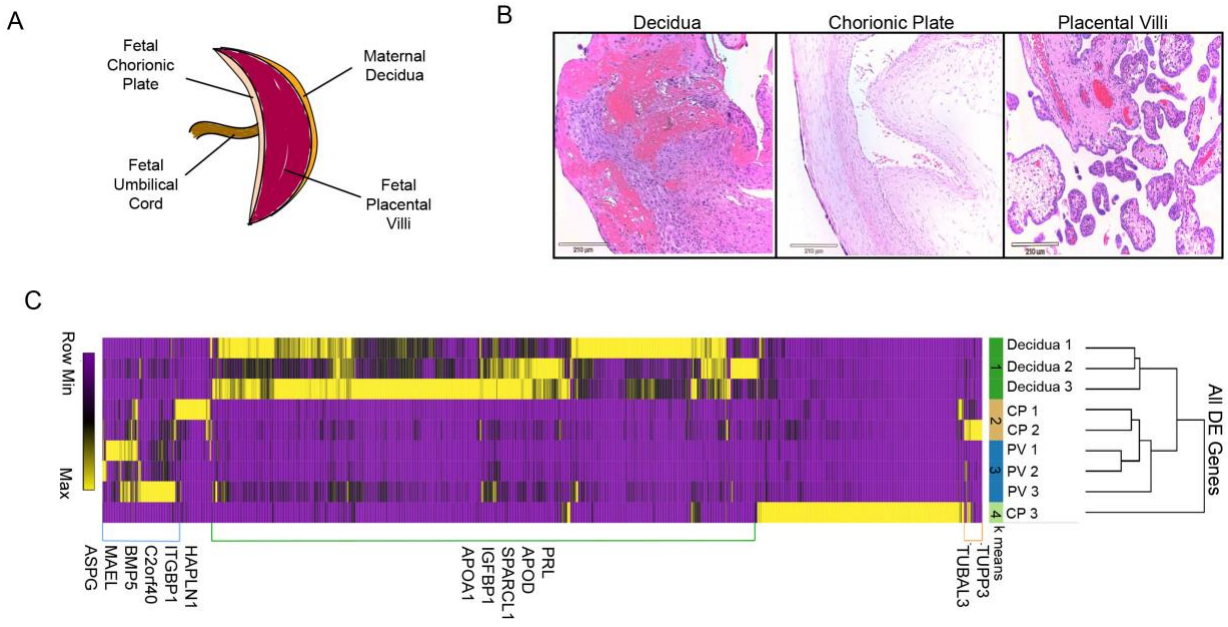

Figure 5 Confirmation of placental layer separation
(A) Diagram of placental tissues. (B) Representative H&E staining of layers of placental tissues. (C) All differentially expressed genes between three placental tissues with p value <0.05, false-discovery rate <20%, and fold change > absolute value 2.

We collected placental specimens from 19 second trimester products of conception, gestational age (GA) 17-23 weeks **(Table 1)**. Maternal decidua and fetal chorionic/amniotic membranes covering the chorionic plate (referred to hereafter as CP) were separated from the PV **(Fig 5A)** with forceps under a dissecting microscope. Separation of layers was initially confirmed by histology **(Fig 5B)**. To verify separation of placental layers, we used bulk RNAseq from 3 matched cases (**Table 1**). Differential expression analysis and hierarchical clustering confirmed segregation of layers based on transcription profiles with the exception of one outlier (CP3) sample which was enriched for inflammatory signatures, likely upregulated during the termination

procedure or secondary to undocumented *in utero* inflammation **(Fig 5C)**. This segregation of samples was confirmed with k-means clustering which grouped samples correctly by tissue with the exception of CP3 outlier **(Fig 5C)**. Moreover, we confirmed the enrichment of decidua and PV specific stromal genes previously reported in multiple studies [75,105,106] and detected two tubulin genes, TUPP3 and TUBAL3 enriched in all three CP samples.

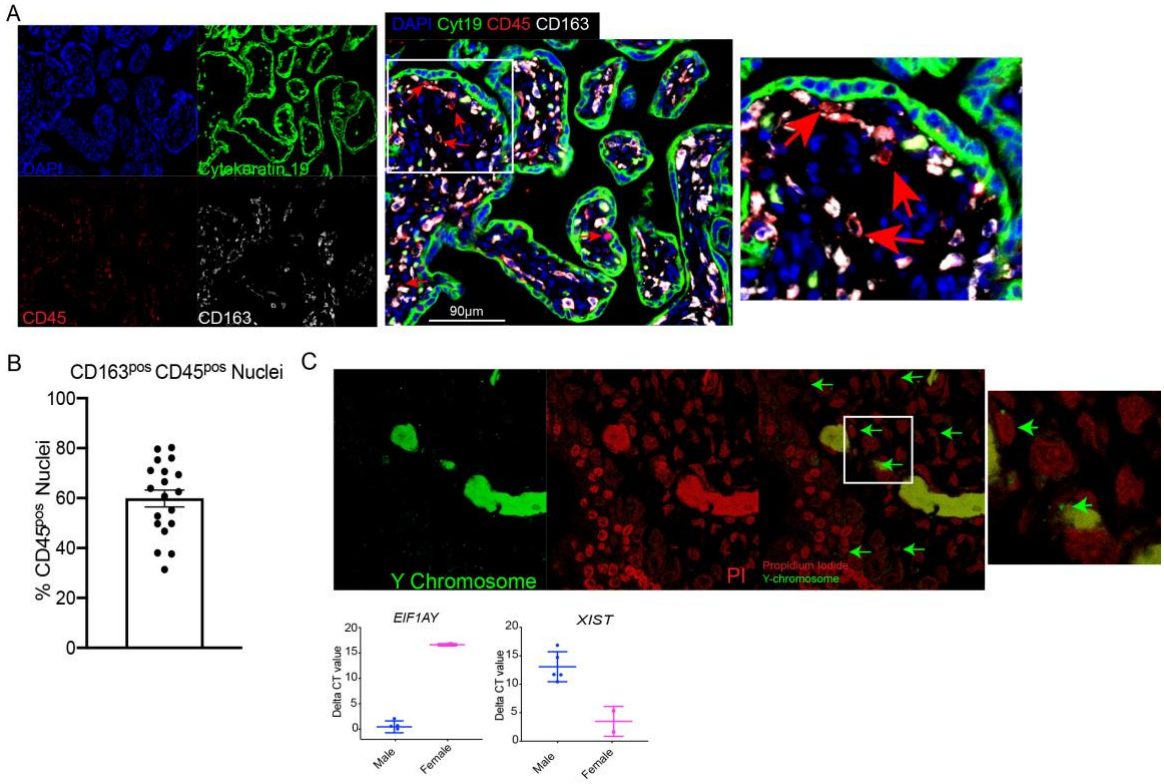

Figure 6 Detection of non-Hofbauer fetal immune cells in PV
(A) Representative image of CD45^{pos} CD163^{lo} cells within the intravillous space identified with immunofluorescence. (B) Quantification of %CD163^{pos} nuclei of CD45^{pos} nuclei per high power field. (C) Representative image for fluorescent *in situ* hybridization of Y chromosome in PV (top). Delta CT values of Y and X chromosome genes in male and female PV (bottom).

To determine if immune cells in the mid-gestation PV were solely reflective of the Hofbauer cell population we used immunofluorescence to co-stain for CD45, a marker of all hematopoietic cells and CD163, a classical PV resident Hofbauer cell marker [67]. Consistent with previous reports identifying non-Hofbauer immune subsets in the first and third trimester PV [74,75],

we detected $CD45^{pos}CD163^{lo}$ cells within the mid-gestation PV **(Fig 6A)** ranging in abundance from 20-70% of $CD45^{pos}$ nuclei per high power field **(Fig 6B)**. We also confirmed that immune cells present in PV samples were reflective of cells contained within the trophoblast layers (intravillous) and not simply contamination from maternal blood cells in the intervillous space **(Fig 6A, 4)**. Additionally, we detected the Y chromosome with *in situ* hybridization in many intravillous cells and had enriched expression of Y chromosome derived *EIF1AY* mRNA coupled with low expression of the X chromosome inactivation transcript *XIST* in male PV samples indicating that the majority of PV immune cells in our study were fetal in origin **(Fig 6C)**.

To gain insight into what the $CD45^{pos}CD163^{lo}$ immune cell subsets could be, we next assessed the expression of immune genes in our RNAseq dataset and confirmed the presence of a diverse immune landscape in second trimester placental tissues. Though most transcripts in the PV were expressed at lower levels than decidual counterparts (darker in color), transcripts for most major immune subtypes analyzed were detected in PV samples (circle size) including T cells, B cells, DCs and Mϕs **(Fig 7, Table 5)**.

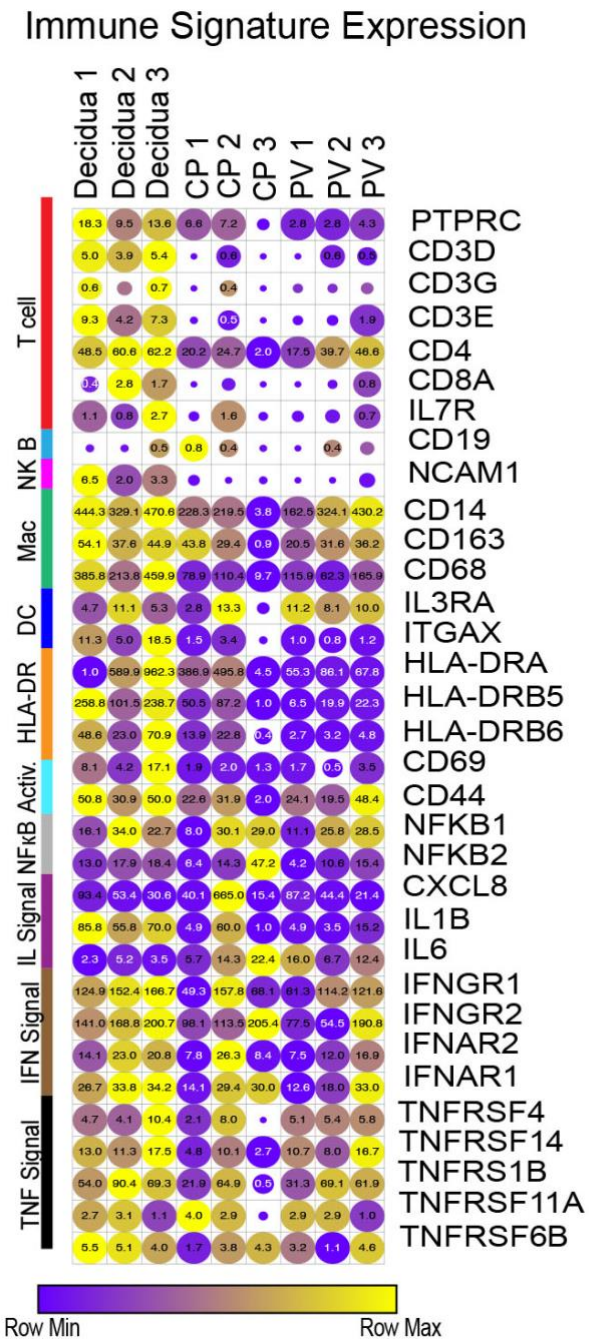

Figure 7 Immune transcripts in the mid-gestation placenta
Expression values of selected immune genes. Circle size indicative of expression value. Circle color indicative of relative expression across row.

Table 5 Selected Immune Genes

Gene Name	Expression Values								
	Decidua 1	Decidua 2	Decidua 3	CP1	CP2	CP3	PV1	PV2	PV3
PTPRC (CD45)	18.25	9.53	13.57	6.64	7.22	0.21	2.84	2.84	4.34
CD3D	5.02	3.87	5.38	0	0.64	0	0	0.65	0.47
CD3G	0.63	0.3	0.67	0	0.39	0	0.12	0.12	0.21
CD3E	9.3	4.15	7.35	0.04	0.53	0	0.13	0.17	1.85
CD4	48.51	60.61	62.16	20.23	24.72	2.04	17.55	39.68	46.63
CD8A	0.38	2.85	1.73	0	0.25	0	0	0.11	0.76
IL7R	1.08	0.75	2.66	0.14	1.56	0.1	0.19	0.29	0.71
CD19	0.06	0.05	0.49	0.79	0.44	0.03	0	0.42	0.27
NCAM1	6.53	2.02	3.29	0.18	0.02	0.06	0	0.01	0.33
CD14	444.26	329.06	470.57	228.26	219.48	3.83	162.49	324.13	430.24
CD163	54.09	37.6	44.92	43.76	29.41	0.9	20.53	31.63	36.2
CD68	385.84	213.79	459.9	78.93	110.38	9.69	115.92	62.35	165.92
IL3RA	4.65	11.15	5.31	2.78	13.33	0.21	11.2	8.06	9.96
ITGAX	11.27	4.97	18.49	1.46	3.36	0.06	0.98	0.75	1.18
HLA-DRA	1,690.96	589.86	962.34	386.91	495.82	4.53	55.26	86.08	67.75
HLA-DRB5	258.75	101.54	238.74	50.52	87.15	0.99	6.51	19.9	22.32
HLA-DRB6	48.63	23.05	70.91	13.91	22.82	0.4	2.66	3.21	4.85
CD69	8.06	4.16	17.1	1.93	2.04	1.32	1.72	0.48	3.53
CD44	50.77	30.92	50.01	22.61	31.86	2	24.06	19.52	48.42
NFKB1	16.11	34.05	22.71	7.99	30.13	28.96	11.12	25.79	28.47
NFKB2	13.03	17.85	18.36	6.42	14.28	47.22	4.15	10.58	15.45
CXCL8	93.43	53.42	30.57	40.08	665	15.41	87.19	44.44	21.43
IL1B	85.82	55.8	70	4.92	60.03	0.98	4.86	3.45	15.24
IL6	2.34	5.18	3.48	5.69	14.34	22.4	16.03	6.67	12.39
IFNGR1	124.86	152.35	166.72	49.29	157.79	68.13	61.25	114.17	121.57
IFNGR2	141.04	168.79	200.74	98.05	113.48	205.37	77.54	54.45	190.82
IFNAR2	14.09	22.98	20.82	7.76	26.34	8.35	7.52	11.98	16.93
IFNAR1	26.69	33.77	34.23	14.09	29.39	29.99	12.63	17.96	32.96
TNFRSF4	4.72	4.05	10.42	2.14	7.98	0	5.1	5.42	5.79
TNFRSF14	13.04	11.26	17.46	4.76	10.05	2.69	10.73	7.98	16.69
TNFRSF1B	54.03	90.41	69.25	21.9	64.87	0.52	31.26	69.05	61.91
TNFRSF11A	2.65	3.09	1.15	3.98	2.9	0.1	2.89	2.88	1.01
TNFRSF6B	5.54	5.05	4.01	1.69	3.81	4.28	3.22	1.14	4.59

Upon collection and separation, placental tissue was cryopreserved for CyTOF analysis, as previously described[100,113] and validated in **Fig 8A**, fixed with formalin prior to embedding in paraffin for imaging mass cytometry (IMC) and IF analysis or snap frozen for bulk RNA-sequencing (RNAseq) analysis. To survey the $CD45^{pos}$ populations in the PV, we used a panel of 38 metal conjugated antibodies **(Table 3)** and performed CyTOF analysis on 12 matched placental (decidua, CP and PV) samples **(Table 1)**. Briefly, cryopreserved tissues were batch thawed and digested to make single cell suspensions, stained with metal conjugated antibodies (**Table 3)** and analyzed using CyTOF[113]. FCS files from CyTOF analysis were pre-gated for DNA^{pos}, single, live, non-bead, $CD45^{pos}$ cells **(Fig 8B)**. After omitting samples with insufficient cell numbers (>750 $CD45^{pos}$ cells) we were left with 11 total samples for each tissue layer **(Table 4)**. $CD45^{pos}$ cells were clustered using Phenograph **(Fig 8C)** and clusters were identified based on mean metal intensities of surface markers with heatmaps generated with Clustergrammer **(Table 6, Fig 8D)**.

There were 31 unique clusters of immune cells within the mid-gestation placenta, belonging to Mϕ, DC, NK, CD4 T cell, CD8 T cell, double positive (DP) T cell, B cell and other immune cell type subsets **(Fig 8C, E)**. Each layer of the placenta housed a unique and complex immune profile **(Fig 8F)**. When all clusters belonging to the same immune subset were combined, the decidua had a greater abundance of NK cells compared to PV **(Fig 8E),** consistent with previous studies[37,121]. Additionally, there was a higher proportion of CD4 T cells in the decidua than either of the fetal layers, likely attributed to the documented high abundance of Tregs in the decidua **(Fig 8E)**. In contrast, the PV had a larger proportion of Mϕ than either the decidua or CP, potentially representing the Hofbauer population **(Fig 8E)**.

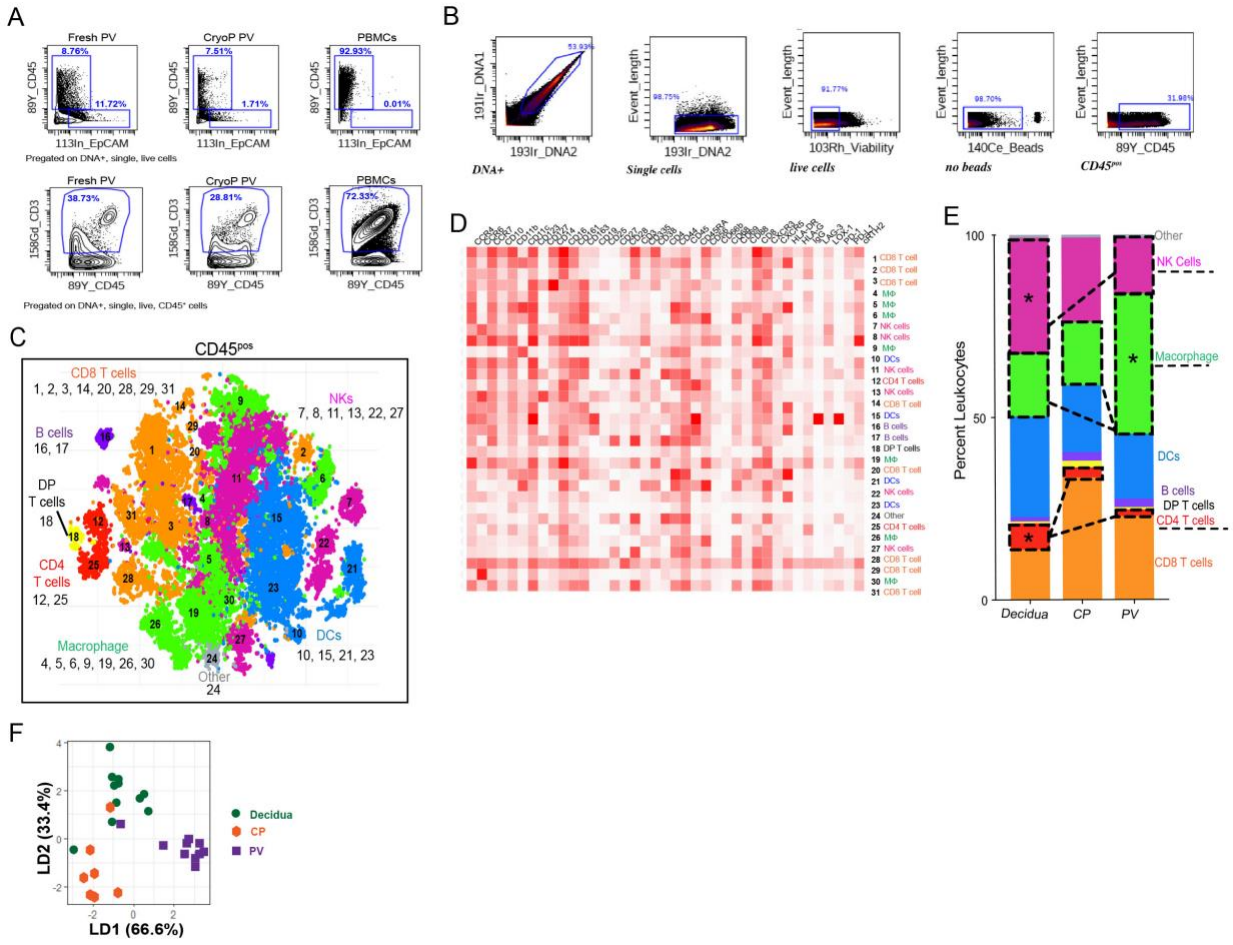

Figure 8 Global immune landscape of the mid-gestation placenta.

(A) Comparison of CyTOF analysis of CD45pos and T cell abundances between fresh PV, cryopreserved PV and frozen PBMCs. (B) Pre-gating strategy for CD45^{pos} population used in automated clustering. (C) tsne of CD45^{pos} cells on (n=33 total, n=11 per tissue) placental tissues used in CyTOF analysis. Clusters belonging to immune subtypes are color coded. (D) Clustergrammer heatmap for cell type identification of clusters. (E) Stacked bar graph of abundance of major immune subtypes. (E) Linkage Disequilibrium (LD) plot confirming segregation of placental layer immune profile). * = p value <0.05 upon post hoc analysis after Kruskal-Wallis (K-W) test.

Table 6 Cell Type Identification

Cell Type	Markers
Leukocytes/Immune Cells	CD45+
T Cells	CD45+CD3+
B Cells	CD45+CD3-CD19+
Innate Cells	CD45+CD3-CD19-
CD4 T cells	CD45+CD3+ CD4+
CD8 T cells	CD45+CD3+ CD8+
Double Positive T Cells	CD45+CD3+ CD4+ CD8+
Double Negative T Cells	CD45+CD3+ CD4- CD8-
Regulatory T cells	CD45+CD3+ CD4+ CD127lo CD25+
Mϕs	CD45+CD3-CD14+
NK Cells	CD45+CD3-CD19-CD14-CD56+
Dendritic Cells	CD45+CD3-CD19-CD14-CD56- HLA-DR+
Plasmacytoid Dendritic Cells	CD45+CD3-CD19-CD14-CD56- HLA-DR+ CD11b+
Myeloid Dendritic Cells	CD45+CD3-CD19-CD14-CD56- HLA-DR+ CD123+
Innate Lymphoid Cells	CD45+CD3-CD19- CD127+
Innate Lymphoid Cells Type 2	CD45+CD3-CD19- CD127+ cRTH2+
Dual Expressing Lymphocytes	CD45+CD3+ CD19+

When each cluster abundance was directly compared, 11/31 $CD45^{pos}$ clusters were differently distributed between the three layers of the placenta **(Fig 9A-C)**. The PV was uniquely enriched for cluster 19, $CCR7^{neg}$ Mϕ **(Fig 9A-B).** This robust PV enriched cluster likely represents Hofbauer cells (as prior reports show most Hofbauer cells are $CCR7^{neg}$ [122]). Moreover, this finding shows tissue-specificity of Hofbauer cells in our dataset as cluster 19 was largely undetectable in decidua and CP samples **(Fig 9B)**. Interestingly, we also found cluster 10, $CCR7^{neg}$ DCs, and cluster 3, $CD69^{neg}$ CD8 T cells, to be enriched in the PV over decidua **(Fig 9A-B)**. CCR7 is highly expressed on DCs homing to secondary lymphoid structures from peripheral tissue sites after antigen encounter [123], and CD69 is found to be upregulated on transiently on activated T cells[124] and constitutively on tissue resident memory T cells[125]. As PV enriched clusters 9 and 3 lacked these respective markers, we hypothesized that PV are poised (i.e., immune cell types are present) to participate in mature immune functions but may not be actively doing so during a time of

homeostasis seen at mid-gestation in healthy pregnancies. To further explore the idea that the PV house a mature immune system poised for activation, we next explored each immune cell subset more deeply.

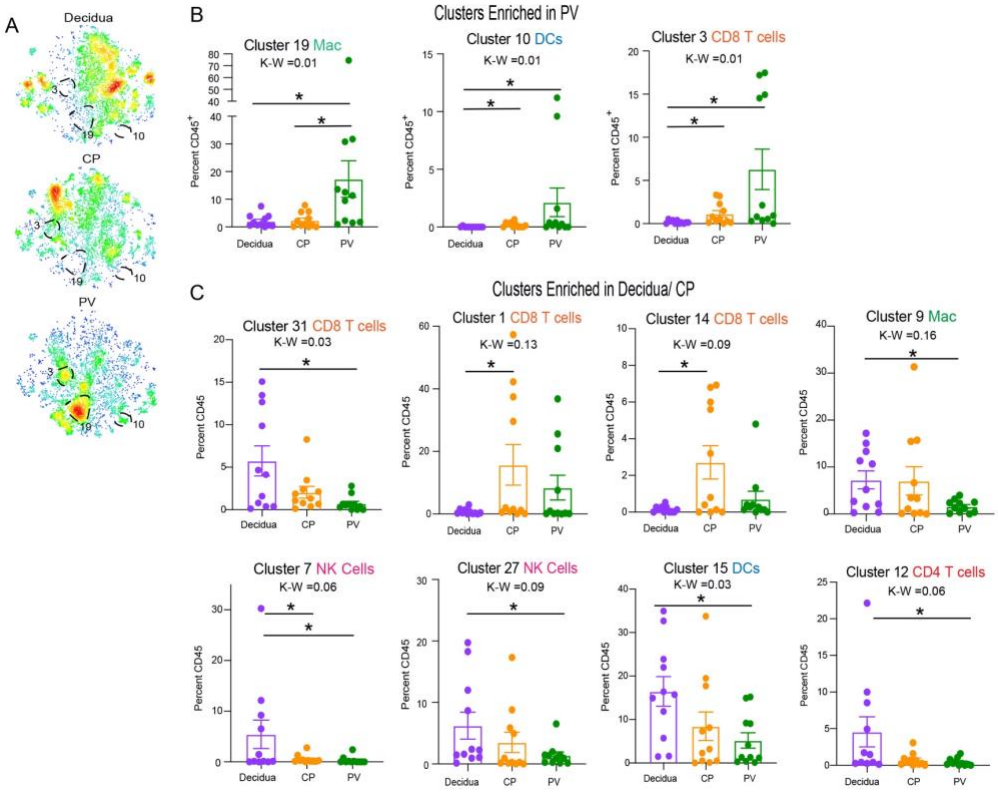

Figure 9 Tissue specific clusters of immune cells in mid-gestation placenta

(A) Density plot separated by tissue (n=11 per tissue) of cell populations with PV enriched clusters outlined. (B) Abundance of significant PV enriched clusters outlined in (A). (C) Abundance of decidua and CP enriched clusters. * = p value < 0.05 after posthoc analysis from Kruskal-Wallis (K-W) test.

2.3.2 PV innate cells have quiescent phenotypes

To evaluate PV innate cell subsets, which represents the first cells to sense foreign compounds we clustered on innate non-antigen presenting cells ($CD3^{neg}CD19^{neg}HLA\text{-}DR^{neg}$) (**Fig 10A)** and identified Mϕ, innate lymphoid cells (ILCs), NK cells and multiple other immune cell populations that we were unable to fully phenotype with our panel **(Table 3), (Fig 10B, 10C)**.

When comparing subtypes of immune cells, i.e., individual clusters of the same cell type added together, we confirmed our findings from the CD45 level (**Fig 10D)**, with the decidua having a larger proportion of NK cells and the PV having a larger proportion of Mϕ **(Fig 10D)**. The increased granularity of focusing on HLA-DR^{neg} innate cells specifically, revealed that the Mϕ populations contained both CD163^{pos} cells, likely representing the Hofbauer cell population, and also contained a significant proportion of CD163^{lo} Mϕ, presumably other non-Hofbauer cell Mϕ **(Fig 10D)**. HLA-DR^{neg} Mϕ in the decidua, in contrast were largely CD163^{pos}, consistent with the enriched CD163 gene signatures seen in the decidua from RNAseq data **(Fig 7)** and the previously document predominance of M2 Mϕs in the decidua[33]**.** The Mϕ profile in the CP was more equally split between the two phenotypes **(Fig 10D)**. At the individual cluster level, within the PV, there was enrichment of cluster 25 CD163^{lo} Mϕ and cluster 27 NK cells **(Fig 10E)**. While cluster 27 NK cells were abundant in all three layers and only slightly elevated in the PV, cluster 25 Mϕ were almost exclusively present in the PV with minimally presence in decidua and CP **(Fig 10E)**. Multiple clusters were enriched in either the decidua and/or CP **(Fig 10F)**.

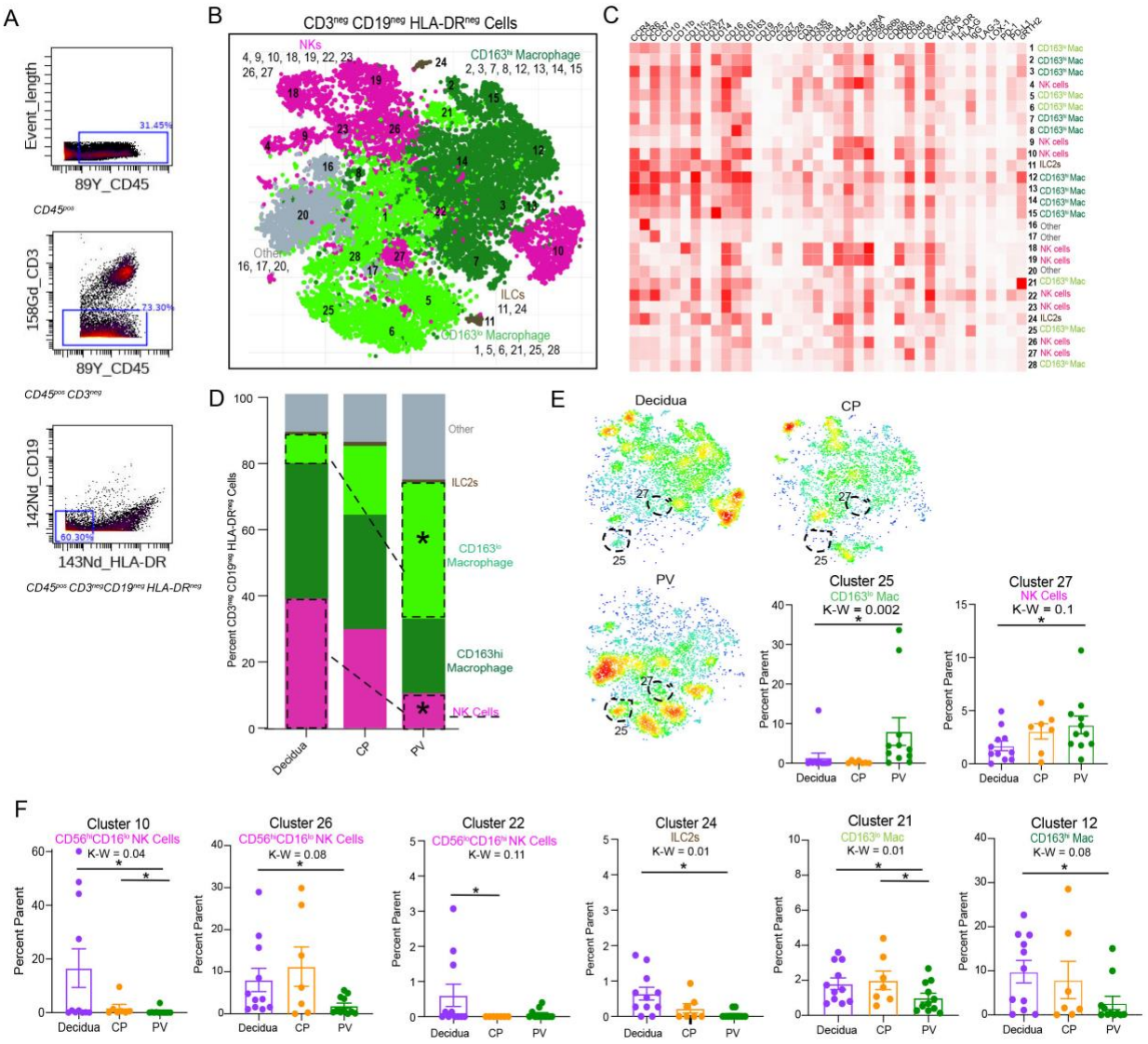

Figure 10 Tissue specificity of PV innate non-APC immune populations

(A) Pre-gating for innate non-APC population. (B) Combined CyTOF tsne for CD45^{pos} CD3^{neg} CD19^{neg} HLA-DR^{neg} cells. (C) Clustergrammer heatmap used for cluster identification. (D) Stacked bar graph of abundance of major immune subtypes. (E) Density plots separated by tissue of cell populations from (B). Statistically significantly abundant clusters in PV outlined (left). Quantitative data of PV abundant clusters outlined in density plots (right). (F) Quantitative data on abundance of decidua and CP enriched clusters. * = p value < 0.05 after posthoc analysis from Kruskal-Wallis (K-W) test.

To determine if PV NK and ILCs were expressing markers consistent with activation, we compared the mean metal intensities (MMIs) of CD69 and PD-1 two markers associated with activation of these cells[126–129]. We found that PV NK cells and ILCs expressed significantly lower amounts of both CD69 and PD-1 compared to decidual and CP counterparts **(Fig 11A)**. Next, to

examine if PV innate cells have migratory or tissue-retentive phenotypes we compared chemokine receptor (CCR) expression among innate subsets. Illustrated both visually **(Fig 11B)** and graphically **(Fig 11C)** we show that multiple populations of PV innate cells have reduced expression of four CCRs. Interestingly, we did not detect any significant reductions of CCRs on $CD163^{lo}$ Mϕs in the PV, suggesting that reduced chemotaxis is selective among innate cell populations in the PV, and that there is a potential chemotaxic role for $CD163^{lo}$ Mϕs specifically. To determine if other CCR/ligand pairs were also reduced in the PV, we identified 19 CCR/ligands that were differentially expressed between PV, CP and decidua using bulk RNA-seq **(Fig 11D, Table 7)**. Expression of almost all of these was reduced in the PV.

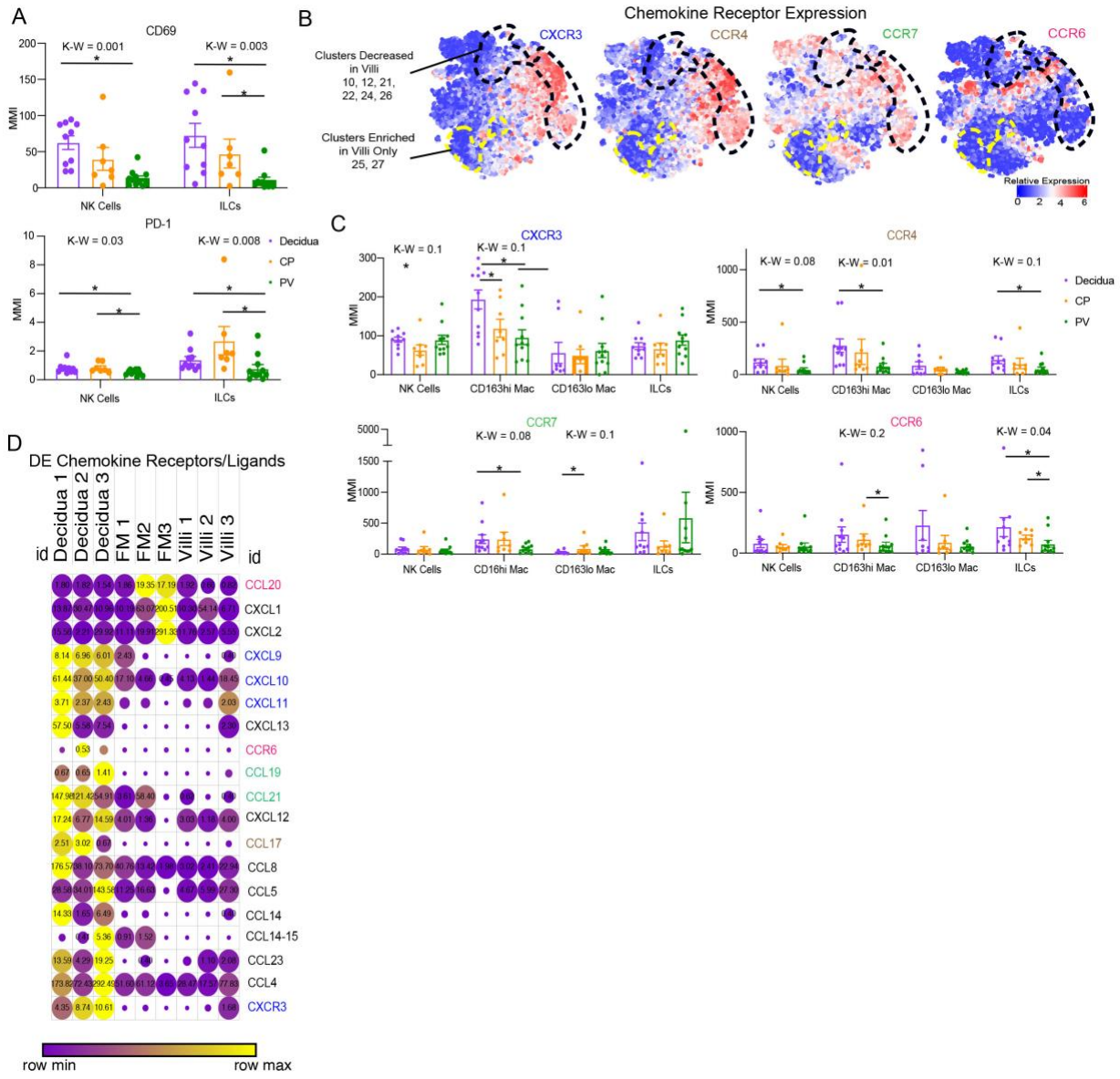

Figure 11 Activation and chemotaxis is limited in PV innate cells.
(A) Mean metal intensities (MMI) of CD69 (top) and PD-1 (bottom) for 2D gated NK and ILC populations. (B) Expression heatmaps for chemokine receptors mapped to cells from CyTOF tsne (Fig 10B). (C) MMIs of CCRs on innate cell subsets from 2D gating. (D) Expression from RNA-sequencing of differentially expressed chemokine ligand/receptor genes between tissues. Circle size indicative of expression value, circle color reflective of relative expression across row. Differentially expressed determined as: p value <0.05, false-discovery rate <20%, and fold change > absolute value 2. * = p value <0.05 upon post hoc analysis after Kruskal-Wallis(K-W) test.

These results validated the CyTOF findings of reduced expression of CCR6 and CXCR3 specifically, as well as at least one ligand for CCR7 and CCR4 and 9 other chemokine ligand/receptors implicated in different signaling pathways **(Fig 11D)**. These results suggest that

PV innate cells are either static or are migrating in a broad non-chemokine specific manner. This in combination with low expression of activation marker on PV immune cells, support a quiescent state of PV innate cells during mid-gestation.

Table 7 Differentially Expressed Chemokine Genes

Gene Name	Expression Values								
	Decidua 1	Decidua 2	Decidua 3	CP1	CP2	CP3	PV1	PV2	PV3
CCL20	1.8	1.82	1.54	1.86	19.35	17.19	1.92	0.6	0.82
CXCL1	13.87	30.47	10.96	10.19	63.07	200.51	10.3	54.14	6.71
CXCL2	15.56	2.21	29.92	11.11	19.91	291.33	11.76	2.57	5.55
CXCL9	8.14	6.96	6.01	2.43	0.11	0	0	0.05	0.4
CXCL10	61.44	37	50.4	17.1	4.66	0.45	4.13	1.44	18.45
CXCL11	3.71	2.37	2.43	0.37	0.31	0	0.25	0.32	2.03
CXCL13	57.5	5.58	7.54	0.08	0	0	0	0	2.3
CCR6	0.08	0.53	0.26	0.03	0	0.04	0	0	0.02
CCL19	0.67	0.65	1.41	0	0	0	0	0	0.19
CCL21	147.98	121.42	54.91	3.61	58.4	0.1	0.62	0.07	0.4
CXCL12	17.24	6.77	14.59	4.01	1.36	0.01	3.03	1.18	4
CCL17	2.51	3.02	0.67	0	0	0	0	0	0.12
CCL8	176.57	38.1	73.7	40.76	13.42	1.98	3.02	2.41	22.94
CCL5	28.58	34.01	143.58	11.25	16.63	0.12	4.67	5.99	27.3
CCL14	14.33	1.65	6.49	0.15	0.18	0	0	0.04	0.4
CCL14-15	0.17	0.41	5.36	0.91	1.52	0	0	0	0
CCL23	13.59	4.29	19.25	0	0.4	0	0.26	1.1	2.08
CCL4	173.82	72.43	292.49	51.6	61.12	3.65	28.47	17.57	77.83
CXCR3	4.35	8.74	10.61	0.06	0.11	0	0	0.14	1.68

2.3.3 PV Mϕs shuttle maternal IgG

As we observed reduced activation signals and chemokine receptor expression in PV innate cells, we hypothesized some of these cell populations may perform alternate functions. To investigate, we focused on the PV highly enriched population of cluster 25 Mϕ, that were both

CD16^{pos} and IgG^{pos} **(Fig 10C)**. CD16 (FcγRIII) binds to the Fc region of IgGs suggesting that this cluster of Mϕs potentially binds to IgG. It is well documented that maternal IgG is transported across the placenta to the fetal blood supply as a form of passive immunity[130]. However, the transport mechanism between the outer trophoblast layer of the PV to the fetal endothelium remains elusive.

Table 8 Imaging Mass Cytometry Panel

Metal	Target	Clone	Vendor
115In	CD44	IM7	BioLegend
142Nd	CD19	6OMP31	Fluidigm
143Nd	Vimentin	D21H3	Fluidigm
144Nd	CD14	EPR3653	Fluidigm
147Sm	CD163	EDHu-1	Fluidigm
148Nd	PanKeratin	C11	Fluidigm
151Eu	CD31	EPR3094	Fluidigm
152Sm	CD45	D8M81	Fluidigm
156Gd	CD4	EPR6855	Fluidigm
160Gd	IgG	MHK49	Fluidigm
161Dy	Ki67	8D5	BioLegend
162Dy	CD8a	C8/144B	Fluidigm
164Dy	pZAP70		Cell Signaling
165Ho	pCREB	87G3	Cell Signaling
166Er	CD45RA	HI100	Fluidigm
167Er	p44/42	D13.14.4E	Cell Signaling
169Tm	pSTAT3	A1600213	Cell Signaling
170Er	CD3	polyclonal	Fluidigm
171Yb	CD66a	CD66a-B1.1	Fluidigm
173Yb	CD45RO	UCHL1	Fluidigm
174Yb	HLA-DR	LN3	Fluidigm
175Lu	pS6	D57.2.2E	Cell Signaling
176Yb	pHistoneH3	HTA28	Fluidigm

To visualize IgG^{pos} Mf in the PV, we first used IF to detect IgG^{pos} Mϕs potentially accepting IgG from the trophoblast barrier **(Fig 12A)**. We next used IMC to document the localization of IgG on cells in the PV nestled between IgG^{pos} trophoblasts and fetal endothelial cells (CD31^{pos}) **(Fig 12B).** The detection of IgG^{pos} cells in between the PanKer^{pos} trophoblast cells (which

translocate IgG from the maternal blood to the stroma) and the fetal blood vessels is consistent with PV Mϕs potentially carrying IgG across the PV stroma to the fetal blood supply. As there is no evidence of a fetus producing its own supply of IgG and is dependent on the transfer of maternal IgG for passive immunity, we sought to verify the maternal origin of IgG in the PV. We used *in situ* hybridization against IgG mRNA and found no cells transcribing IgG in the PV **(Fig 12C)**. In contrast IgG transcripts were detected in cells from the matched maternal decidua **(Fig 12C)**. This finding confirms the IgG protein detected on Mϕs in the PV is likely of maternal origin needing to be transported to the fetal blood supply as a mechanism of passive immunity.

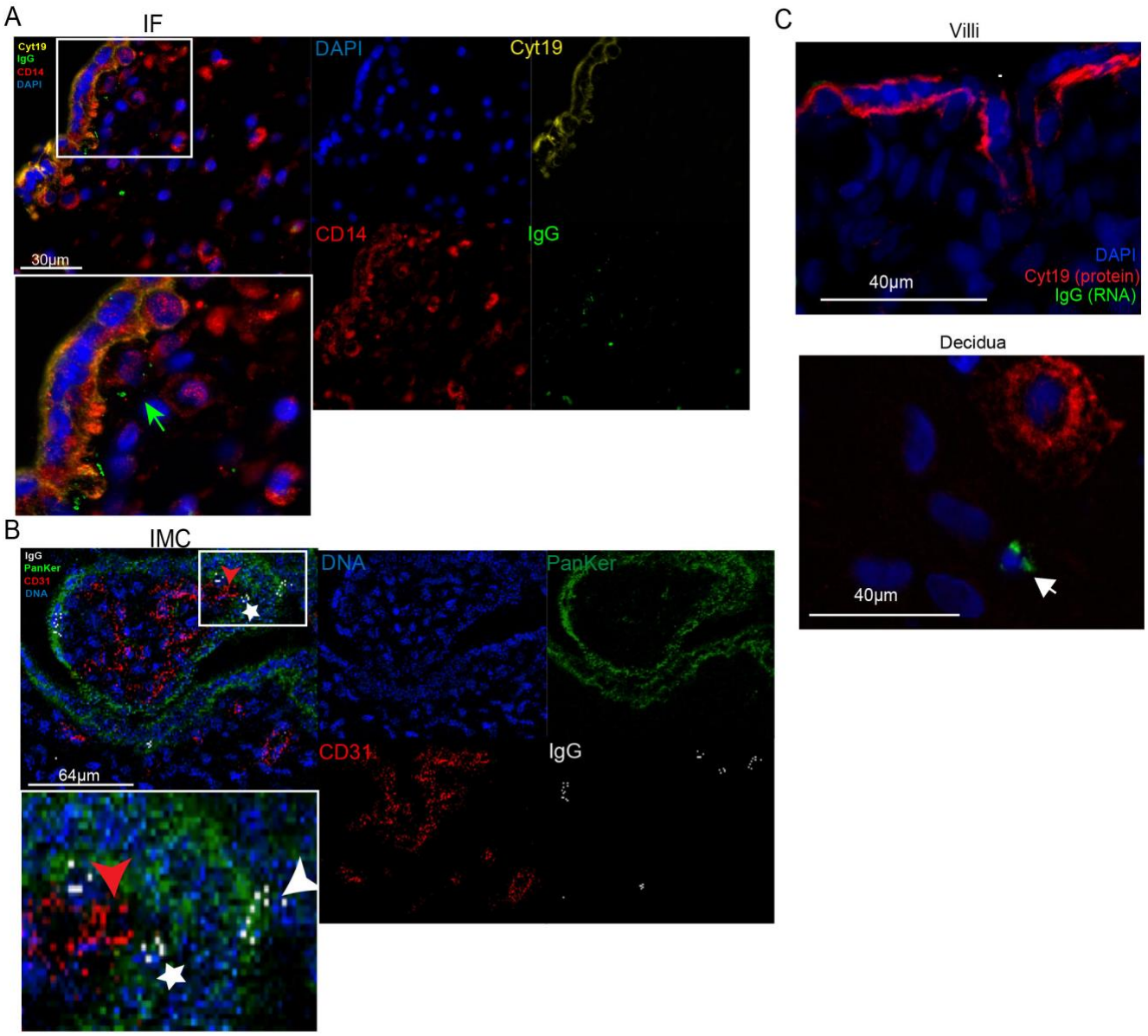

Figure 12 Imaging shows IgG^{pos} Mϕs intermediary to trophoblasts and fetal endothelium
(A) IF detection of IgG^{pos} Mϕ near trophoblast layer (green arrow). (B) Representative IMC image showing IgG^{pos} cell between trophoblast and fetal endothelium (indicated with star) (IgG identified with arrows). C) Dual in situ hybridization and IF for IF RNA in matched PV and decidua.

To further explore the potential of Mϕs as IgG transporters, we used automated imaging analysis to discern which cell populations closely neighbored IgG^{pos} Mϕs. Images were segmented into individual cells and then clustered based on marker expression intensity per cell. Cell identity was determined based on relative staining intensity per cell and individual cell populations

(clusters) were mapped back to the original image **(Fig 13A)**. Consistent with our hypothesis, IgG^{pos} Mϕs (cluster 10) neighbored both trophoblast (cluster 1) and endothelial cell types (clusters 13) at a frequency greater than by random chance indicating that these cell populations are likely interacting **(Fig 13B-C)**. Interestingly, we also saw IgG^{pos} Mϕs interacting with other neighboring Mϕs clusters 6 and 11 **(Fig 13B-C)** suggesting that IgG shuttling in the PV might involve communication from multiple Mϕ populations.

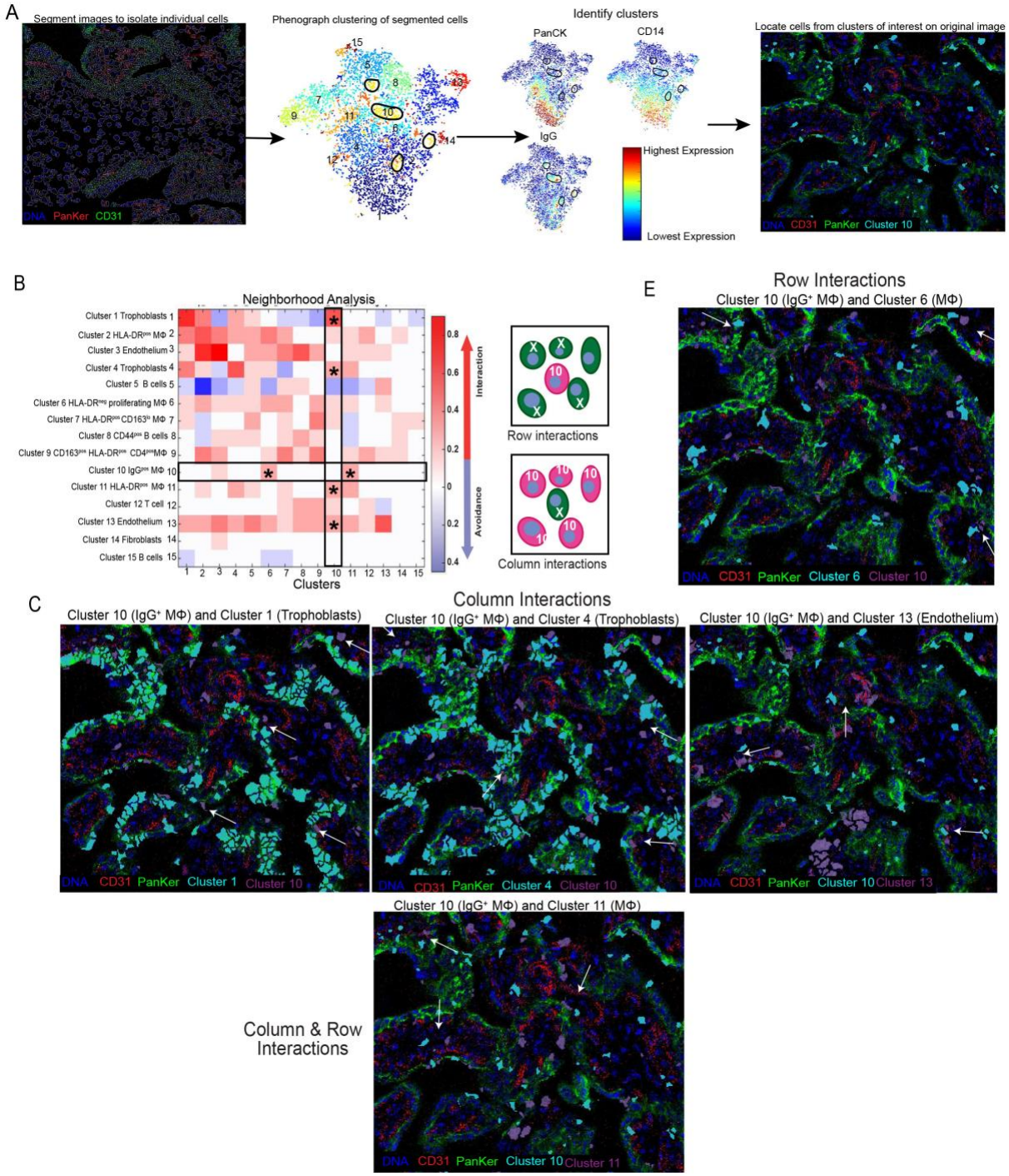

Figure 13 Neighborhood analysis confirms potential Mϕ IgG shuttle

(A) Pipeline for automated imaging analysis. (B) Cell-Cell interactions identified with neighborhood analysis. (C) Representative images of cell clusters identified in neighborhood analysis. Arrows pointing at designated clusters located close together.

2.3.4 PV antigen presenting cells are diverse and phenotypically immunosuppressive

Next, we examined antigen presenting cell (APC) populations within each placental layer by clustering on CD45^{pos} CD3^{neg} HLA-DR^{pos} cells **(Fig 14A)**. We identified seven types of APCs including: myeloid DCs (mDCs), plasmacytoid DCs (pDCs), CD163^{hi} Mϕ, CD163^{lo} Mϕ, B cells, NK cells and other cells that we could not identify based on the available markers **(Fig 14B-C)**. In confirmation of our previous findings **(Fig 8,10)**, NK cells were again more prevalent in the decidua compared to the PV **(Fig 14D)**. HLA-DR^{pos} NK cells that independently present antigens to CD4 T cells have been described[131]. In contrast to HLA-DR^{neg} innate cells **(Fig 10)**, numerous individual APC clusters were enriched in the PV **(Fig 14E-F)**. Of note, multiple populations were enriched in the decidua and CP as well **(Fig 14G)**. Specifically, B cell clusters 7 and 27, mDC clusters 16 and 20, and CD163^{lo} CD4^{neg} Mϕ clusters 6 and 22 were significantly more abundant in the PV than either decidua or CP **(Fig 14E-F)**. Complimenting this finding, CD4^{pos}CD163^{hi} Mϕs (cluster 26) was reduced in the PV compared to decidua and membranes **(Fig 14G)**. CD4^{pos} Mϕ have been shown to be tissue resident Mϕs in the intestine and perhaps they serve a similar role in the decidua[132]. The large number of APC clusters (11 in total) differentially abundant between the PV and decidua/CP suggests that antigen presentation in the PV may be functioning through alternate mechanisms or is inhibited compared to the decidua and CP in the healthy second trimester.

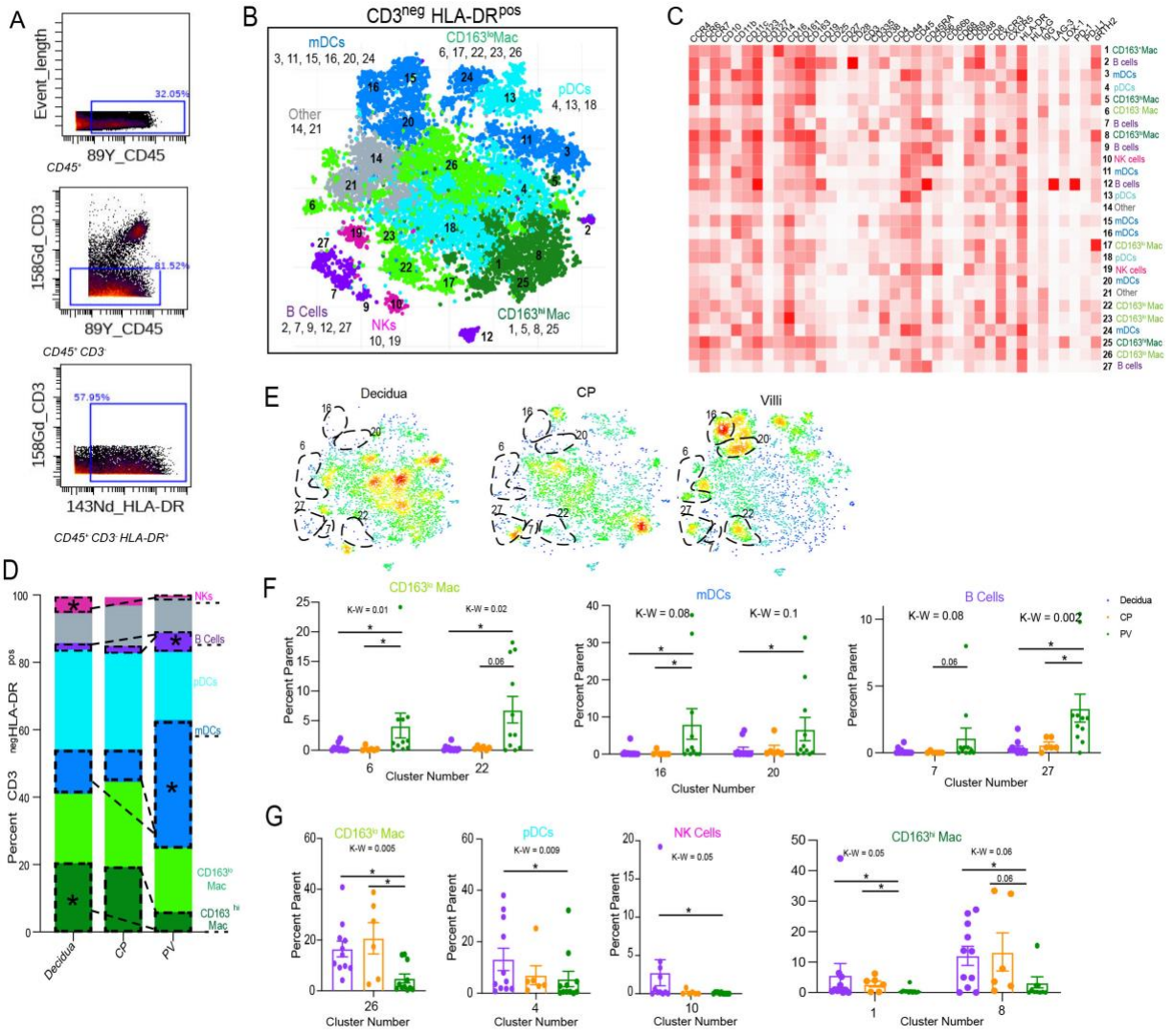

Figure 14 High diversity of PV antigen presenting cells

(A) Pre-gating strategy for APC population. (B) Cumulative CyTOF tsne for CD45^{pos} CD3^{neg} HLA-DR^{pos} cells. (C) Clustergrammer heatmap used for cluster identification. (D) Stacked bar graph of abundance of major immune subtypes. (E) Density plot separated by tissue of origin from (B). (F) Statistically significantly abundant clusters in PV outlined. Quantitative data of PV abundant clusters outlined in density plots. (G) Quantitative data on abundance of decidua and CP enriched clusters. * = p-value <0.05 for posthoc analysis after Kruskal-Wallis (K-W)

To investigate potential functional distinctions in PV APCs, we examined the expression of both activation and immunosuppressive markers on each APC subset identified in **Figure 14D**. In contrast to the hypothesis that PV APCs have altered function compared to decidua and CP, we found no difference in HLA-DR expression among classical APC subsets **(Fig 15A)**. However, consistent with PV APCs being more inhibited than decidua and CP counterparts, we identified

significantly reduced expression of the activation maker CD69 in PV CD163^{hi} Mϕ, HLA-DR^{pos} NK cells, pDCs and mDCs **(Fig 15B)**. Furthermore, when we examined the inhibitory ligand PD-L1, we saw increased expression on multiple APC subsets, significantly so on CD163^{lo} Mϕ and HLA-DR^{pos} NK cells **(Fig 15C)**.

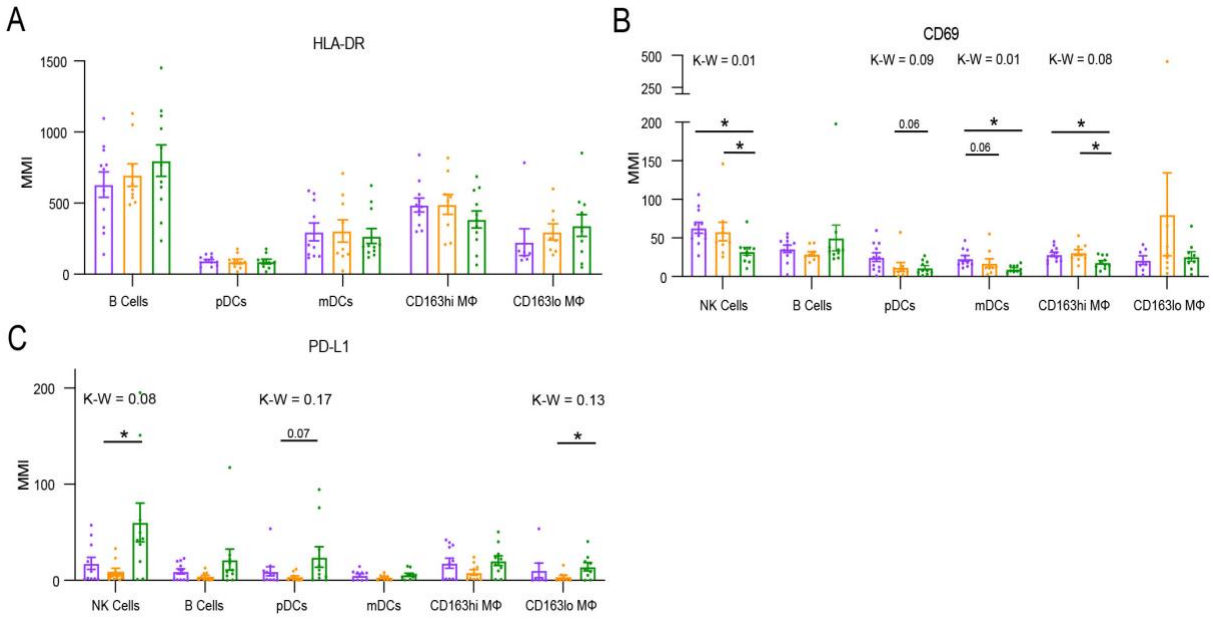

Figure 15 PV APCs have reduced activation and increased suppressive surface marker expression
Mean Metal Intensity (MMI) of HLA-DR (A), CD69 (B) and PD-L1 (C) for 2D gated populations. * = p value <0.05 upon post hoc analysis after Kruskal-Wallis (K-W) test.

The observation of high PD-L1 expression on PV APCs was confirmed by immunofluorescent staining, where almost every observable PV HLA-DR^{pos} cell co-expressed PD-L1 **(Fig 16A)**. The constitutive expression of PD-L1 on PV APCs may be resultant of preferential transcription of IFNγ (a regulator of PD-L1) over TNFα at baseline **(Fig 16B-C)**. Additionally, PV immune cells transcribe IFNγ in similar amounts, but transcribe much less TNFα than decidual immune cells **(Fig 16D)**. It is possible that PV immune cells transcribe IFNγ during homeostasis to drive expression of PD-L1 on APCs.

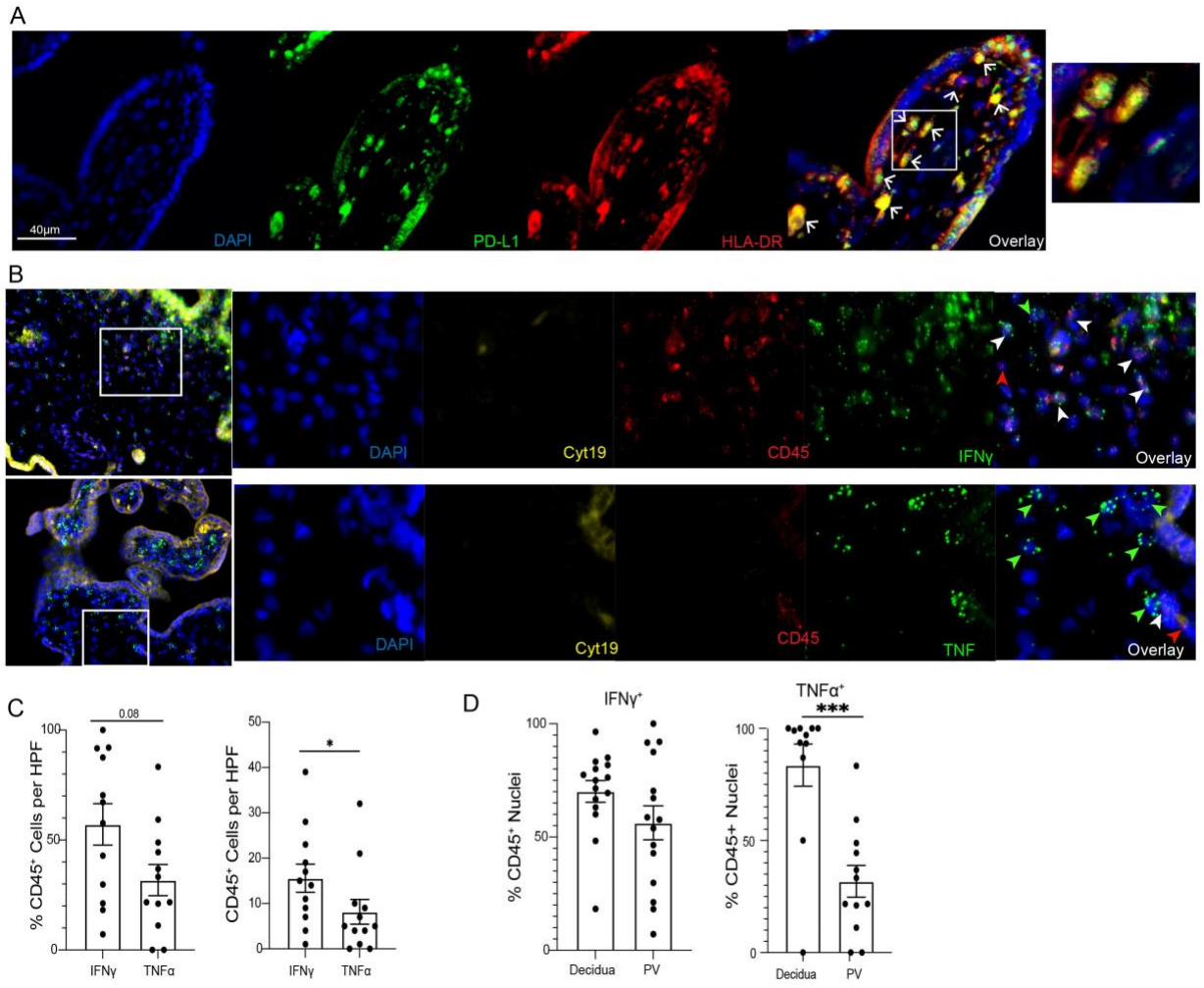

Figure 16 Elevated PD-L1 on PV APCs is congruent with IFNγ expression

(A) Representative image of PD-L1^{pos} APC populations in PV. (B) Representative images for dual RNA *in situ* hybridization and immunofluorescence for cytokines in PV. (C) Quantification of cytokines in PV from CellProfiler automated imaging analysis. (D) Quantification of cytokines comparing PV to decidua from CellProfiler automated imaging analysis. * = p-value <0.05 in Mann-Whitney two-tailed test. Green arrow heads = CD45^{neg} cytokine producing cell, white arrow heads = CD45pos cytokine producing cell, Red arrow heads = CD45^{pos} cytokine^{neg} cell.

2.3.5 The mid-gestation placenta is dominated by CD8 memory T cells

As we observed high PD-L1 expression on APCs, we next explored if there were T cells present in the PV that would be inhibited by immunosuppressive APCs. We identified both circulating (within blood vessel) and potentially tissue resident T cells in the PV **(Fig 17A)**.

Moreover, using IMC, we identified T cells of CD4, CD8 and double negative (DN) phenotypes that expressed CD45RO, a marker upregulated after antigen experience **(Fig 17B-C)**. To determine how abundance PV T cell populations were overall in the PV we stained quantified $CD3^{pos}$ nuclei as a percent of stromal nuclei (defined as non-multinucleated trophoblast cells on the outer edge of the villous) and all nuclei. We report PV T cell populations represent 1-3% of stromal nuclei per high power field and 0.5-1.5% of all nuclei **(Fig 17D)**.

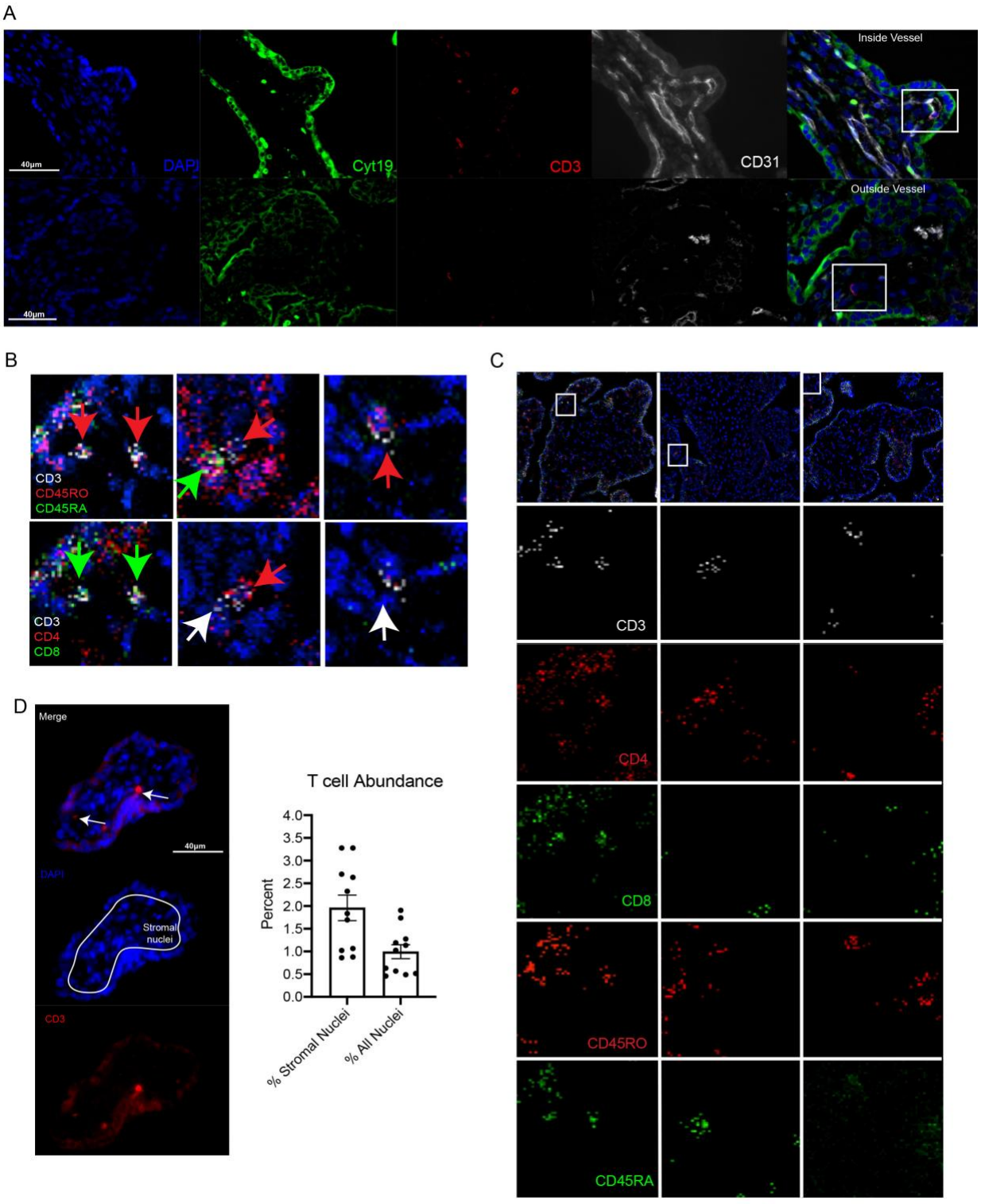

Figure 17 Intravillous localization of antigen experienced PV T cells.
(A) Representative images of T cells inside (top) and outside (bottom) fetal vasculature (CD31) in PV. (B) IMC images of T cell subtypes in PV. (C) Single color splits identifying region (white rectangle) of PV sections represented in (B). (D) Quantification of T cell abundance of nuclei per high power field.

Turning to our CyTOF data, when clustering specifically on T cells **(Fig 18A)**, we found that all three layers of the placenta had T cell profiles dominated by CD8 T cells **(Fig 18B-D)**. Building off the initial detection of CD45RO by IMC, we found that the majority of T cells in the PV were of memory phenotypes, delineated based on expression of CCR7 and CD45RA **(Fig 18E)**. Additionally, we found CD8 T cells with tissue-resident memory (TRM) phenotype in all three layers **(Fig 18E)** based on the expression of CD69, which is not expressed on vascular or lymphatic T cells[133]. CD8 and CD4 non-regulatory T cell subtypes were evenly distributed between all three layers **(Fig 18D)**. However, CD4 regulatory T cells (Tregs) were enriched in the decidua compared to the PV **(Fig 18D)**. The abundance and importance of Tregs throughout pregnancy in the decidua is well documented[52,134], but the role of Tregs in the membranes and the PV is unclear. Moreover, there was an enrichment of $CD4^{neg}$ $CD8^{neg}$ (DN) T cells in the PV **(Fig 18C-D)**. These were likely gamma-delta T cells and not NKT cells as they lacked CD56 or CD16 expression **(Fig 18C)**. The presence of gamma-delta T cells in the first trimester PV has been described[74].

The detection of PV T cells expressing memory markers in human second trimester PV is novel. To investigate T cell signatures unique to the PV, we next compared the abundance of individual T cell clusters. Cluster 9 $CD4^{neg}$ $CD8^{neg}$ DN T cells, cluster 4 CD8 T cells, and cluster 11 CD4 T cells were enriched in the PV **(Fig 18F-G)**, and two clusters were enriched in the decidua **(Fig 18H)**. Cluster 11 T cells were $CCR4^{pos}CXCR3^{neg}CCR6^{neg}$ **(Fig 18C,H)**. This surface marker expression pattern suggested a T helper 2 (TH2) phenotype, however further analysis for detection of TH2 specific transcription factors (GATA3) is needed for confirmation.

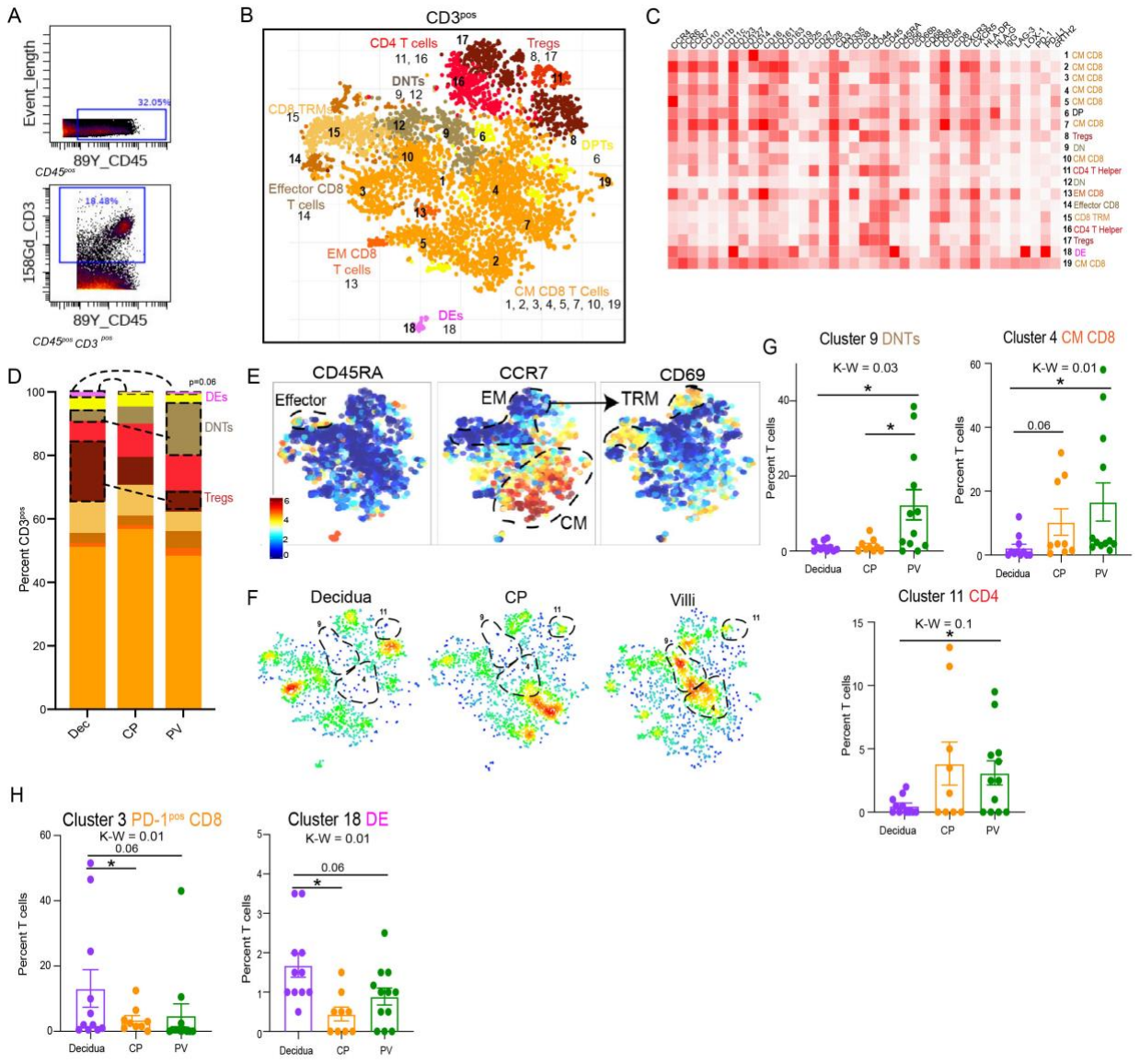

Figure 18 Mid-gestation placenta has distinct memory T cell populations

(A) Pre-gating strategy for T cell population. (B) Cumulative CyTOF tsne for $CD45^{pos}$ $CD3^{pos}$ cells. (C) Clustergrammer heatmap used for cluster identification. (D) Stacked bar graph of abundance of T cell subtypes. (E) Relative expression of memory T cell markers in cell populations from (B). (F) Density plot separated by tissue of origin, statistically significantly abundant clusters in PV outlined. (G) Quantitative data of PV abundant clusters outlined in density plots. (H) Quantitative data on abundance of decidua and CP enriched clusters. * = p value < 0.05 after posthoc analysis from Kruskal-Wallis (K-W) test.

2.3.6 Resting signatures define PV T cell subsets

As we detected a resting, homeostatic trend in PV innate cells **(Fig 11)** and a resting/coinhibitory profile among PV APCs **(Fig 15)**, we next explored if a resting phenotype was

consistent among PV T cell subsets identified **(Fig 18)**. Consistent with previous results, PV T cells exhibited reduced expression of CD69 **(Fig 19A)**, fewer PD-1^{pos} cells **(Fig 19B)** and reduced PD-1 per T cell compared to decidual counterparts **(Fig 19C-D)**. Though PD-1 is a marker of T cell exhaustion, it is also upregulated upon activation of the T cell receptor (summarized in[135]). We propose this is the more likely role of observed down-regulation of PD-1 in PV T cells as it is consistent with the downregulation of CD69. As CD69 is also indicative of TRM phenotypes and is not expressed on T cells in the blood[133], we only compared CD69 expression on non-TRM subsets to assess its dual role as an activation marker.

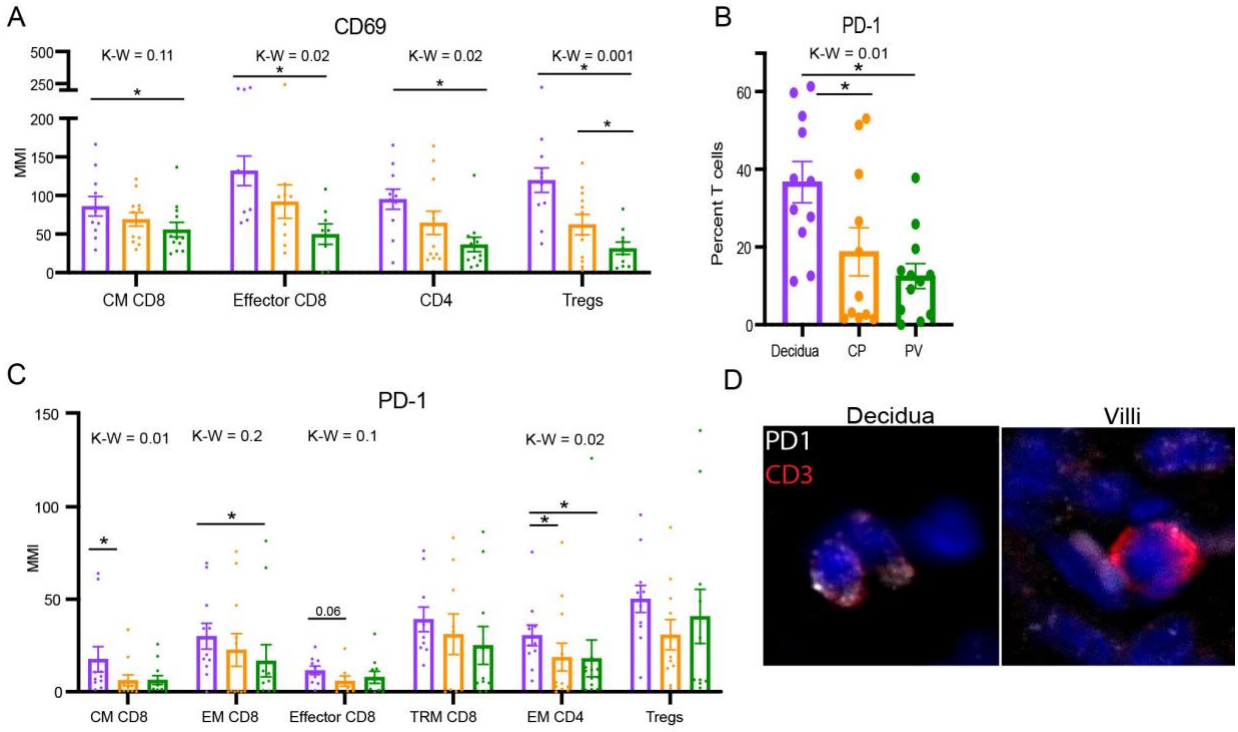

Figure 19 Resting signatures in PV T cells.

(A) Mean Metal Intensity (MMI) of CD69 from 2D gating of populations. (B) Abundance of PD-1^{pos} T cells by 2-D gating. (C) PD-1 MMI from 2D gated subsets. (D) Representative image of PD-1 on T cells in PV and decidua. * = p value <0.05 upon post hoc analysis after Kruskal-Wallis (K-W) test. CM = central memory, EM = effector memory, TRM = tissue-resident memory.

2.3.7 Maternal antigens can activate PV T cells

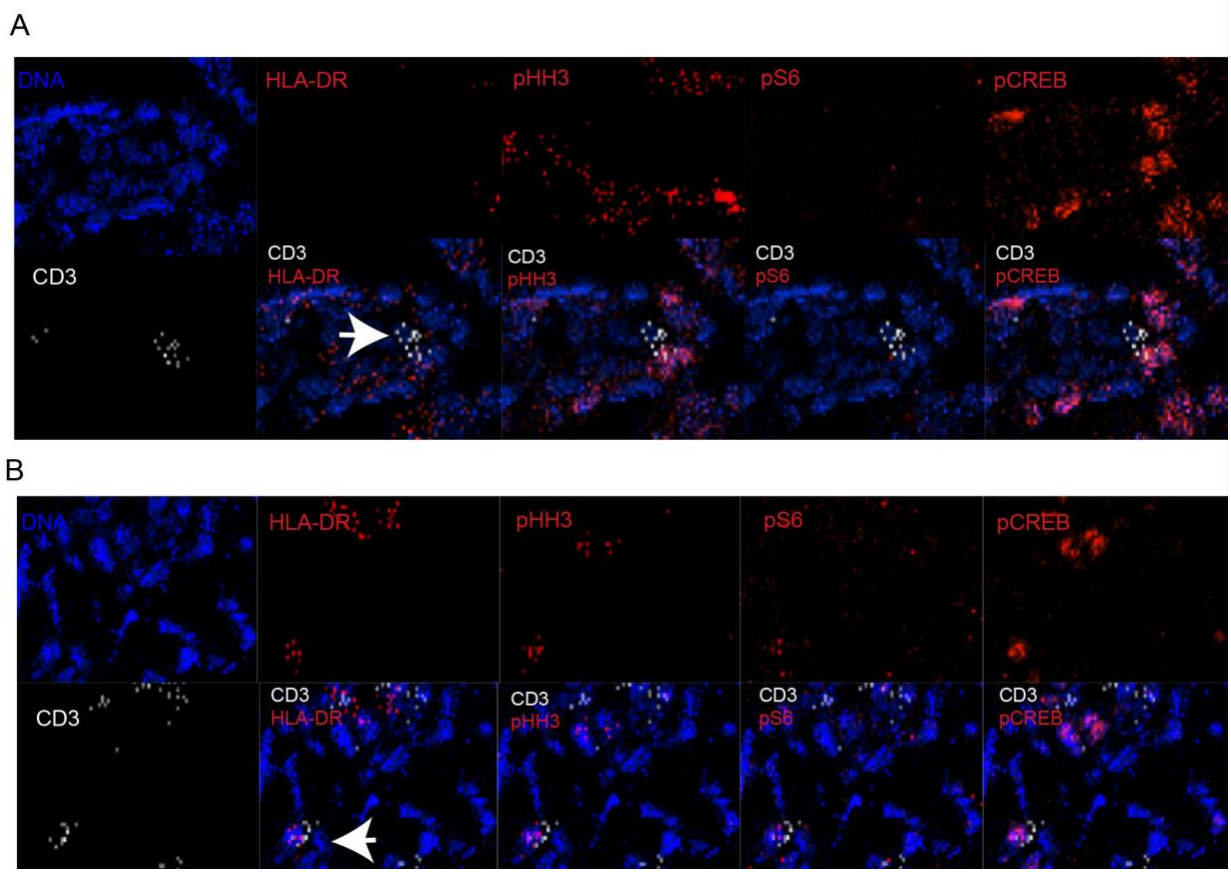

Figure 20 Resting and activated T cells detected at baseline in PV by IMC
(A) IMC images of inactive T cell in PV. (B) IMC images of activated T cell in PV.

To determine if PV T cells have a reduced activation profile **(Fig 19)** due to functional abnormalities, we scanned for activated T cells via the detection of HLA-DR, phosphorylated Histone H3, phosphorylated S6 and phosphorylated CREB in T cells using IMC. Based on these markers we identified both resting **(Fig 20A)** and active T cells in the PV **(Fig 20B)** at baseline. As such, we questioned if activated T cells seen with IMC could have been activated in a TCR dependent manner. To test the functionality of the TCR pathway in PV T cells, we stimulated live, single cells isolated from cryopreserved PV with soluble αCD3 and αCD28 antibodies for 72 hours. Consistent with normal TCR pathway functionality, we observed increased CD69

expression after stimulation **(Fig 21A)** and an increased proportion of cells proliferating **(Fig 21B)** with stimulation.

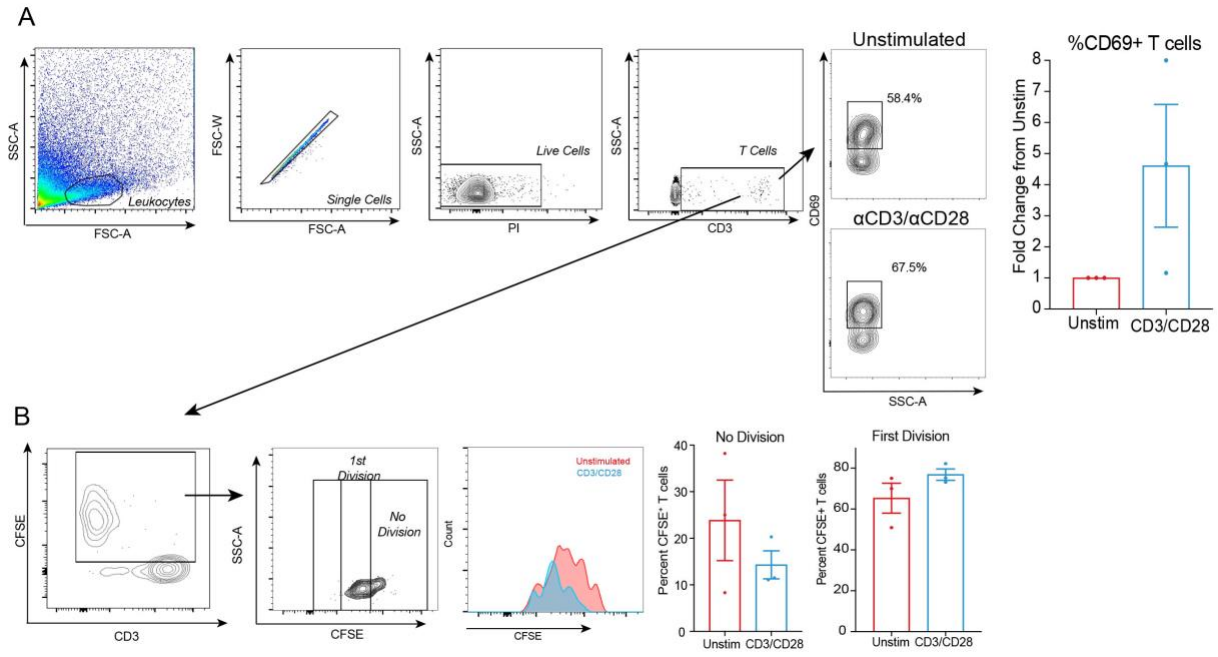

Figure 21 PV T cells can be activated through the TCR.
(A) Pre-gating to T cells from flow cytometry data with representative CD69^{pos} population and graphical abundance of CD69^{pos} T cells. (B) Representative images and quantification of CFSE staining for proliferative T cells.

To discern if PV T cells could be activated by antigens present on the maternal side of the placenta, we stimulated isolated PV cells with either PMA/Ionomycin as a positive control or lysed cellular components from either: pregnancy-matched decidua, unmatched decidua or unmatched pooled donor PBMCs. Consistent with activation of PV T cells, we saw elevated CD69 expression in the PMA/Ionomcyinand and both matched and unmatched decidual components conditions. Moreover, we observed reduced CD69 expression by PV T cells stimulated with unmatched PBMC components **(Fig 22A-B)**. Validating the activation of PV T cells by decidual antigens, we also observed increased production of TNFα in CD69^{pos} T cells **(Fig 22C-D)**. These functional assays show that PV T cells have the potential to be activated by PV APCs through the TCR pathway. Therefore, PV T cells could potentially become proinflammatory when stimulated in a

TCR-dependent manner if exposed to particular antigens present in the uterine environment of pregnant women but not in the periphery of non-pregnant individuals.

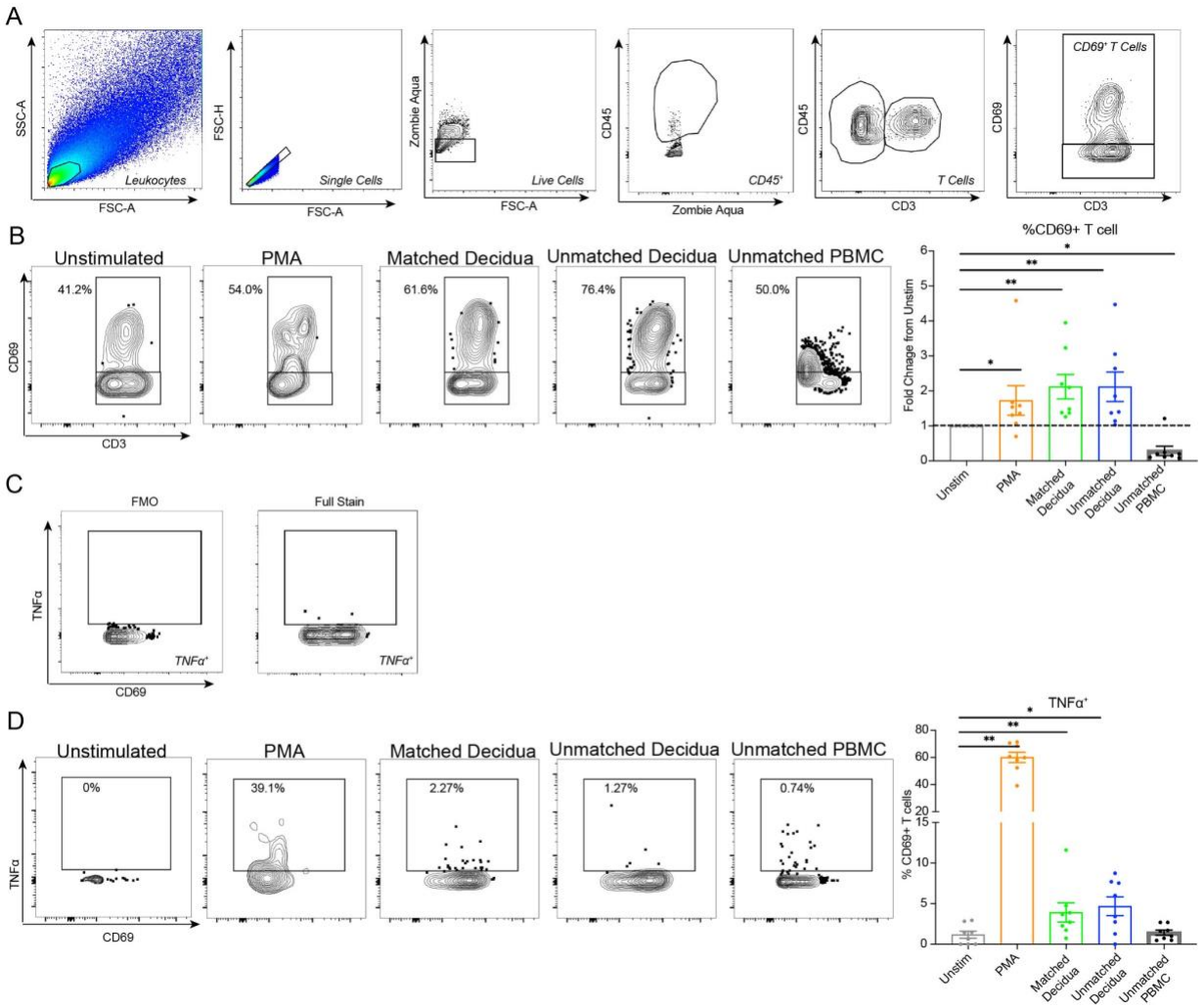

Figure 22 PV T cells respond to lysed decidual components
(A) Pre-gating to CD69^{pos} cells. (B) Representative flow plots and quantification of CD69^{pos} cells. (C) Representative plots of fluorescence minus one (FMO) and full stain for TNF staining. (D) Representative flow plots for CD69^{pos} TNF^{pos} cells. * = p-value <0.05 in Mann-Whitney test compared to Unstimulated condition.

2.3.8 Summary of Findings

In summation **(Fig 23)**, we demonstrate that the intravillous compartment of the healthy second trimester PV contains a diverse immune landscape comprised of Mϕ, NK cells, ILCs, Dcs,

B cells and noncanonically naïve T cells **(Fig 8)**. Moreover, we determined that the immune cells in the PV are likely capable of eliciting an inflammatory response but maintain immune homeostasis at baseline through a variety of mechanisms. The mechanisms described include limiting chemotaxis by reduced expression of chemokine receptors on innate cells and low transcription of chemokine ligands in the PV overall **(Fig 11)**. PV Mϕ also perform alternative functions such as the potential shuttling of IgG to the fetal blood vessels **(Fig 12-13)**. Moreover, PV APCs constitutively express PD-L1, possibly regulated by the high expression of IFNγ by PV immune cells **(Fig 16)**. This PD-L1 expression by APCs is potentially needed to prevent the activation of antigen-experienced PV T cells **(Fig 20-21)** that can be activated through the TCR pathway by antigens present in the uterine environment **(Fig 22)**.

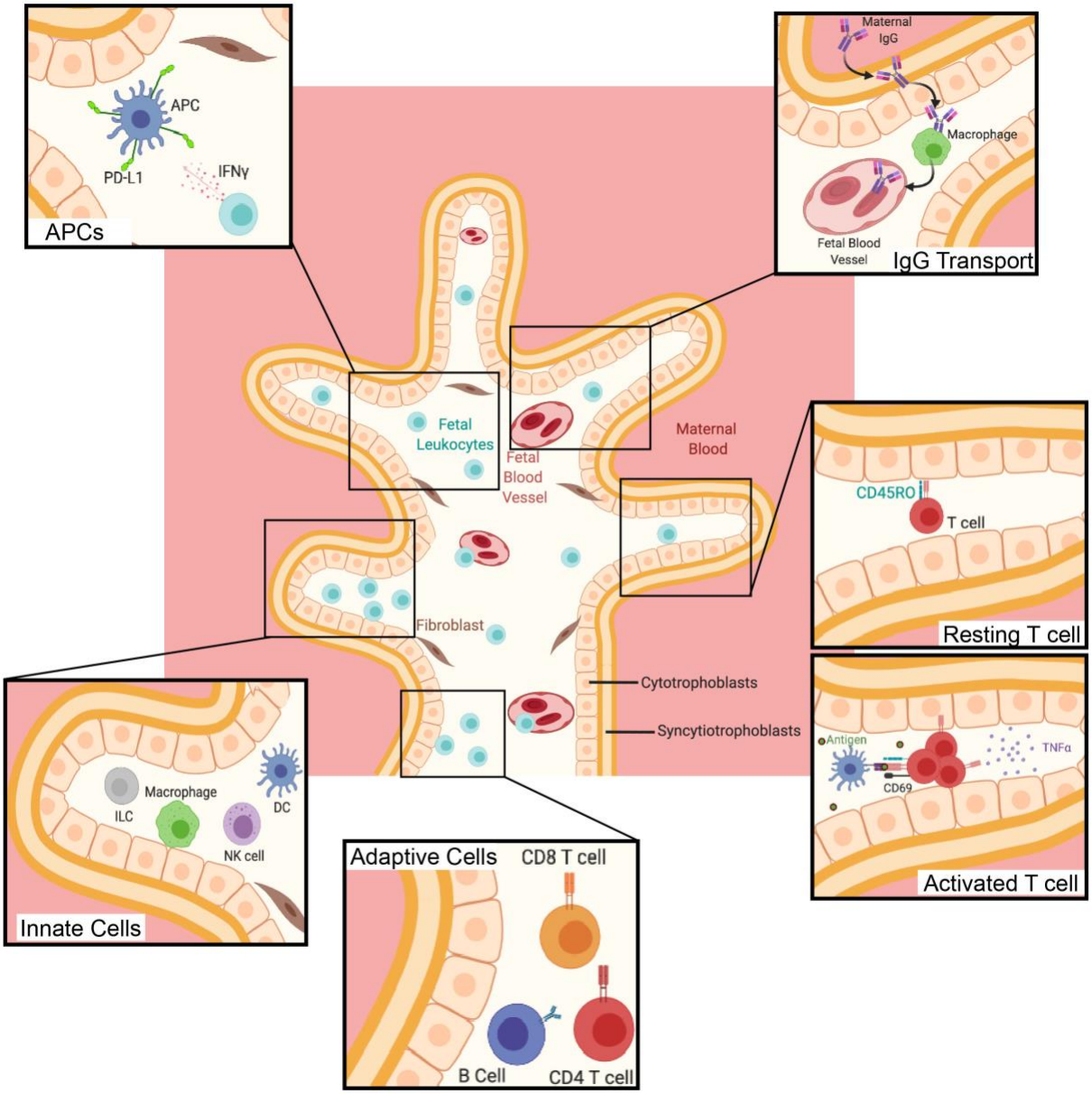

Figure 23 Summary of chapter 2 findings.
Image was generated with Biorender.com

2.4 Discussion

Preserving tolerance at the fetal-maternal interface is critical for maintaining a healthy pregnancy. Studies of the roles of maternal immunity within the decidua and maternal peripheral

blood have resulted in the discovery of important immunological tolerance mechanisms including: tolerogenic uterine NK cells[33], unique populations of Tregs[52] restriction of DC migration to the uterus[136] and suppressive B cells[54]. The contribution of leukocytes within the placental villi beyond Hofbauer cells (PV resident Mϕ) has been far less explored.

Single cell studies within the past three years of the first trimester[105,106] and full term[75,107] placenta highlighted the diversity of immune cells within the PV. Interestingly Pique-Rige and colleagues identified leukocyte signatures specific to the PV and highlighted a potential role for activated PV T cells in post-delivery placentas[75]. With these first and third trimester studies in mind, we hypothesized that the activated leukocytes detected by Pique-Regi[75] may be present and poised to be activated in the PV earlier in gestation. Congruently, we hypothesized that PV immune cells may be subject to immunosuppressive mechanisms which maintain homeostasis in utero.

To test these hypotheses, we analyzed placental tissue including decidua, placental villi and fetal membranes from the chorionic plate. We confirmed that there are diverse immune cells in second trimester PV samples not representative of maternal blood in the intervillous space by detecting the Y chromosome in the majority of PV cells via FISH and showing an enrichment of Y genes in PV male fetuses. Moreover, we detected signatures consistent with tissue-residency such as CD69 which is not expressed on any T cell populations in the blood[133]. Although it is still possible that our analysis of PV immune cells included a proportion of maternal cells, ethical limitations precluded us from collecting maternal peripheral blood in our study. Future studies employing dual HLA-haplotyping/Y chromosome detection with staining for various immune populations in the PV are needed to distinctly determine the origin of individual immune cell populations within the PV vasculature and stroma.

Previous studies have suggested that PV fetal immune cells are limited to Hofbauer cells[66]. However, the increased granularity provided by single cell methods, have allowed for the detection of T, B and NK cells of fetal origin in healthy term placentas[75]. Furthermore, a recent study identified infiltrating cells in the PV to be largely of fetal origin in cases of infectious villitis[116]. Moreover, Erbach et *al.* isolated T cells from single cell suspension of placentas at 18-24 weeks' gestation[137]. It is important to note that immune cells isolated by digesting tissue and creating single cell suspensions represent populations from both the PV vasculature and PV stroma. In the current study, by combining CyTOF (single cell suspension-based assay) and multiple imaging techniques, we identified a diverse immune landscape in the PV and have shown that many populations are present both in the PV vasculature and stromal compartments.

Focusing specifically on the innate non-APC population we identified NK cells, ILCs and Mϕ in the PV. Thomas et *al.* recently reported that Hofbauer cells in the first trimester are HLA-DR^{neg}[66], consistent with this we found an increased abundance of Mϕ in the PV compared to the decidua in the innate HLA-DR^{neg} compartment. Surprisingly, we report that many of these HLA-DR^{neg} Mϕ in the PV lacked the expression of CD163, a marker reported to be expressed in all Hofbauer cells[67,138]. It is possible that CD163^{lo} Mϕs reflect downregulation of CD163 by Hofbauer cells during cell isolation as has been reported in the presence of collagenase[139]. Though it is also possible that Hofbauer cell populations are more diverse than previously thought and CD163 should be used in combination with other Mϕ markers such as CD14, CD68 and DC-SIGN[140] in future studies. It is also possible that some of these cells represent non-Hofbauer Mϕ within the PV.

In addition to reporting novel immune cell phenotypes, we identified mechanisms of immunosuppression and nonclassical function for multiple subsets of PV immune cells likely

involved in preventing inflammation in utero. Specifically, we found that innate non-APCs expressed lower levels of multiple chemokine receptors including: CXCR3, CCR6, CCR4 and CCR7 compared to decidual counterparts. This finding is consistent with histologic evaluation of Hofbauer cells showing a lack of CCR7 and CX3CR1 staining[122]. This coupled with reduced expression of multiple chemokine ligands for these and other chemokine receptors we observed in bulk RNAseq data, could suggest that innate cells in the PV are either more static or are mobile in a non-targeted manner at baseline. Furthermore, we report that PV Mϕ may serve a previously undocumented role of shuttling IgG between the trophoblast and fetal endothelium. The transport of maternal IgG across the placenta has been documented for decades (reviewed in[130]). Recently it has been appreciated that IgE crosses the placenta as well[141]. While it is known that the neonatal Fc receptor (FcRn) shuttles IgG across the syncytiotrophoblast layer; the process by which IgG is transported across the stroma to the endothelium remains elusive[130]. We detected one cluster of IgG^{pos} Mϕ exclusively found in the PV and absent from the neighboring decidua and CP by CyTOF. In situ hybridization confirmed this IgG is likely maternally derived. Using IMC and automated imaging analysis we determined that IgG^{pos} Mϕs are closely associated with both trophoblast and endothelial cells and are physically located between the two populations suggesting a potential shuttling mechanism. Consistent with this, it has been documented that Hofbauer cells can express multiple Fc-receptors[142]. Fc-receptor expression by Mϕs could also be indicative of phagocytic activity, of which Hofbauer cells can participate in early in gestation[66].

We also report a diversity of HLA-DR^{pos} cells present in the PV, where we identified mDCs, pDCs, B cells, Mϕ and a population of HLA-DR^{pos} NK cells. The antigen-presentation potential for NK cells has been previously described[131]. The identification of fetal HLA-DR^{pos} Mϕ contrasts Thomas et *al's* recent findings showing no HLA-DR^{pos} cells in the villous core up to the

10^{th} week of gestation[66]. It should be noted that some of the HLA-DR^{pos} Mϕs in our study may reflect the presence of contaminate maternal Mϕs (termed PAMMs by Thomas et *al*) repairing breaks in the trophoblast layer[66]. However, the location of HLA-DR^{pos} cells in our study by both immunofluorescence and IMC show that some cells are located distant from the trophoblast layer and suggest that HLA-DR^{pos} Mϕ appear in the stroma after the time period studied by Thomas et al between 10-18 weeks' gestation. It would be interesting to determine the fetal versus maternal origin of these second trimester HLA-DR^{pos} Mϕ and evaluate if the Hofbauer cell population from 18-23 weeks is transcriptionally distinct from those detected in prior studies[105].

Similar to other innate populations in the PV, we detected immunosuppressive mechanisms in APC subsets observed within the PV. Irrespective of PV APC ontogeny, we determined that PV APCs express more PD-L1 per cell than decidual counterparts. PD-L1's function as a coinhibitory molecule has been extensively studied[143]. Moreover, PD-L1 expression is mediated through interferon gamma signaling (IFNγ)[144]. Interestingly we showed that PV immune cells produce IFNγ preferentially to TNFα, another proinflammatory cytokine. These findings insinuate that PV APCs mediate in utero homeostasis by controlling T cell activation through the expression of coinhibitory ligands.

The detection of memory T cells within the PV justifies the need for PV APCs to limit T cell activation. Memory T cells have been detected in multiple human fetal organs[97,101,102,145,146]. Additionally activated and resting T cells have been detected in PV samples post-delivery[75] and central memory T cell can be found in human cord blood from preterm infants[147]. Here we report that PV T cells are enriched for CD8 and DN T cells, both of these populations have been shown in placentas by IHC[137,148]. Moreover, we found that at baseline PV T cells express low activation signatures (decreased CD69 and PD-1 expression) potentially suggesting that PV T cells have been

previously educated (hence the memory marker expression) but remain quiescent due to either the lack of antigens or direct inhibition from PD-L1^{pos} APCs.

The presence of a placental and/or fetal microbiome as a source of potential antigens for PV T cells remains highly contested[149–154]. However, our group recently showed that xenobiotic metabolites including those derived likely from the maternal microbiome are present in the fetal intestine at 14 weeks' gestation[155]. As such, it is possible that maternal bacteria derived peptides similarly cross the placenta and educate fetal T cells. Fetal T cell activation by maternal antigens has also been implicated in preterm birth where T cells from cord blood exposed to maternal antigens delivered on fetal APCs showed increased proliferation and secretion of TNFα and IFNγ[147]. Our data indicates that T cells obtained from second trimester PV can be stimulated via the TCR pathway (αCD3/CD28 antibodies) and when exposed to decidual antigens but not to unmatched PBMC antigens. Of note, we found many more T cells upregulating CD69 compared to those secreting TNFα upon decidual stimulation. It is likely that there is a differential response to maternal antigens among PV T cells and future studies are needed to determine what other cytokines may be produced by activated PV T cells. Collectively, these findings suggest that antigens, could stimulate a proinflammatory PV T cell response upon crossing the placental barrier, however multiple immunosuppressive mechanisms are in place as early as 17 weeks within the placenta to prevent inappropriate T cell activation including: limited chemotaxis of innate sensor cells and high expression of coinhibitory molecules by PV APCs.

Our study had several limitations of note the lack of genetic information to segregate fetal from maternal cells. It would be very interesting for a future cohort to definitively determine the origin of each PV immune cell subset identified in this work using dual *in situ* hybridization and

immunodetection techniques. Furthermore, legal limitations prevented the collection of maternal and fetal blood to use for comparison.

The ability of fetal immune cells to execute mature functions has recently been discovered in multiple cell types and organs throughout the fetus[97,100,102,146,147,156]. As such the detection of immunosuppressive mechanisms to control this fetal immune response and prevent in utero inflammation is critical, particularly so at the point of contact and potential antigen exchange between mother and fetus. Throughout this study we have identified previously understudied immune cell populations within the mid-gestation PV. Moreover, we detected multiple mechanisms of immunosuppression utilized by these PV immune cells to help maintain homeostasis and prevent inflammation in utero. This work has implications for future studies to better understand the complex roles of fetal and maternal immune cells within the placenta and potentially contribute to improved understanding of immune tolerance in multiple disease contexts. In the next chapter, the consequences of improper PV immune cell activation is explored in the context of intra-amniotic inflammation.

3.0 Immune cells in the placental villi contribute to intra-amniotic inflammation

Text and figures in chapter 3 were modified from: Toothaker, J. M. *et al.* Immune Cells in the Placental Villi Contribute to Intra-amniotic Inflammation. *Front. Immunol.* **11,** 866 (2020), which was first published by Frontiers Media and copyright to © Toothaker, Presicce, Cappelletti, Stras, McCourt, Choughnet, Kallapur and Konnikova. Original article can be found at https://www.frontiersin.org/articles/10.3389/fimmu.2020.00866/full.

3.1 Study Goals

In chapter 2, we uncovered that the mid-gestation placental villi (PV) harbor mature and functional immune cells that maintain an immunosuppressive phenotype in utero. However, we also revealed that some PV T cells have the potential to become proinflammatory with appropriate stimulation. Inflammation in utero or intra-amniotic inflammation can lead to placental dysfunction, intrauterine growth restriction, preeclampsia, and spontaneous preterm labor. Therefore, we hypothesized that the PV immune cell subsets we identified in chapter 2, specifically APCs and T cells may contribute to inflammation in the intra-amniotic cavity in pathological pregnancies. As previously described in chapter 1, non-human primates are an appropriate model of human placentation and have many advantages to murine models for studying diseases of pregnancy. In this study, we used a rhesus macaque model of lipopolysaccharide (LPS) induced intra-amniotic inflammation to determine the contribution of PV immune cells in disease progression. Furthermore, we investigated if PV immune cell inflammation was dependent on

TNF. The goals of this study were to: (1) evaluate abundance, and dependence on TNF of immune cell populations during intra-amniotic inflammation in the choriodecidua and PV; (2) determine what signaling pathways were active in PV immune cells during intra-amniotic inflammation; and (3) investigate cytokine production by PV immune cells during intra-amniotic inflammation.

3.2 Materials and Methods

Animals: Adult multiparous female rhesus macaques (*Macaca mulatta*) (n=14) were time mated at the California Primate Center, UC Davis. At ~130 days (~80%) gestation the pregnant dam received either 1 ml saline solution (n=4) or 1 mg LPS (Sigma-Aldrich, St. Louis, MO, n=5) in 1 ml saline solution by ultrasound-guided intra-amniotic (IA) injection. Two of the four monkeys received intramuscular saline instead of IA, however no LPS was administered intramuscularly. TNF blocker Adalimumab (Humira, AbbVie Inc. North Chicago, IL) alone was administered to Blockade group by IA (40 mg) + maternal subcutaneous (40 mg) at 1 and 3 h before LPS (n=5) to inhibit TNF signaling in the amniotic and systemic compartments **(Fig 24).**

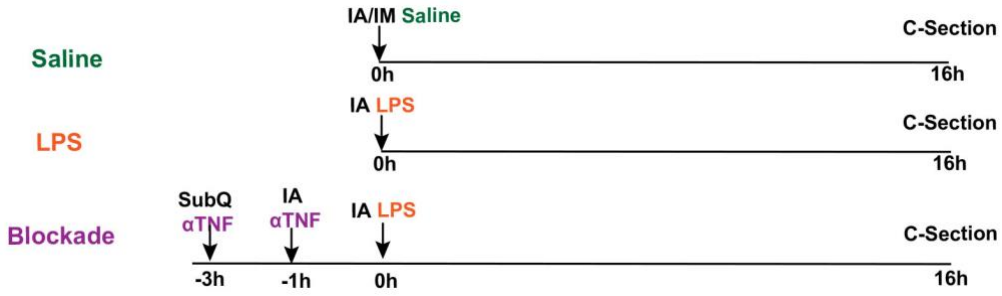

Figure 24 Rhesus model of intra-amniotic inflammation

Pregnant rhesus monkeys at 80% gestation were divided into three groups. Saline grouped animals received either intra-amniotic (IA) (n=2) or intra-muscular (IM) (n=2) saline solution and then were delivered via Cesarean-section (C-section) 16 hours later. LPS (n=5) grouped animals received IA LPS and were delivered via C-section 16 hours later. Blockade (n=5) grouped animals received subcutaneous (SubQ) anti-TNF (αTNF) antibody at -3 hours then IA aTNF at -1 hours prior to IA LPS at 0 hours and were delivered via C-section 16 hours later.

The concentration of LPS was determined based on prior experiments using a sheep model of LPS-induced intra-amniotic inflammation[157]. 1mg was then calculated as an allometric derivation, proportional to the average rhesus weight compared to what was used for the average weight of sheep. Fetuses were delivered via C-section 16 hours after LPS injection. 16-hour duration was determined to be optimal in prior studies using the same method of LPS-driven inflammation in pregnant rhesus macaques[87]. The maternal macaques and their fetuses were similar in clinical variables **(Table 9)**. After delivery, fetuses were euthanized with pentobarbital, and fetal tissues were collected. There were no spontaneous deaths or preterm labor in each animal group. As the experimental window was started at 80% gestation, the delivered fetuses were still premature neonates, though there was no preterm labor.

Table 9 Demographics of animals included in study

Animal ID	Maternal Age (years)	Maternal Weight (kg)	Gestational Age at Birth (days)	Fetal Weight (kg)	Fetal Gender
Saline IA					
423	10	8.14	132	.351	M
427	5	6.42	131	.223	M
Saline IM					
430	14	9.95	130	.282	M
432	15	9.96	129	.299	M
LPS					
429	16	11.18	132	.374	F
436	8	10.56	136	.420	F
437	13	11.31	136	.308	F
440	8	11.35	129	.281	M
442	8	6.78	130	.244	M
Blockade					
431	10	10.43	130	.389	F
438	11	12.58	134	.452	M
439	10	10.89	131	.339	F
441	14	10.7	131	.322	M
443	10	10.44	127	.183	F

Placental dissection: Placental membranes were dissected away from the placenta as previously described[86,87]. Decidua parietalis cells and the attached chorion were separated from the placenta. The rest of the chorionic tissue was then peeled away from the amnion and decidua

with forceps. After full separation of membranes from decidua, portions of PV tissue were isolated and shipped overnight on ice to the University of Pittsburgh. Choriodecidual cells representing decidua parietalis with attached chorion were washed, and digested with Dispase II (Life Technologies) plus collagenase A (Roche) followed by DNase I (Roche) treatment, as previously described[86,87]. PV samples were digested identically to choriodecidua with the substitution of Accutase (Millipore) in place of Dispase II at the same concentration and timing.

CyTOF (Phospho-panel): Single cell suspensions were divided evenly among groups. Phospho-stained samples were incubated for 20 minutes under 37ºC and 5% CO_2 conditions with no ex vivo stimulation. Post 20-minute incubation, cells were stabilized through fixation using 0.2% paraformaldehyde and then washed with cell staining buffer (CSB), which consists of Dulbecco's PBS with 0.5% bovine serum albumin (Sigma) and 0.02% sodium azide. After washing, cells were incubated with Human TruStain FcX (Biolegend). Metal-coupled surface staining antibodies were then applied to each sample (0.5uL of each antibody per tube). Cells were then washed twice with CSB and fixed with 1.6% paraformaldehyde. Ice cold methanol was used to permeabilize the cells and washed with CSB. Metal-coupled intracellular staining antibodies were added, and the cells were washed twice with CSB. (Cytokine-staining):Cells were incubated with equivalent concentrations GolgiStop/GolgiPlug as in Phospho-staining but for 4 hours at 37ºC and 5% CO_2 with no ex-vivo stimulation. Cells were washed in CSB after surface staining (as above), incubated in FOXP3 fixation and permeabilization solution (Invitrogen), washed with 1X FOXP3 wash buffer (Invitrogen) and stained with an intracellular antibody cocktail. CyTOF panels listed in **Table 10**.

Table 10 Mass cytometry panels used. Antibodies in black were used in all panels. Antibodies in green were used in phospho-panel only. Antibodies in blue were used in cytokine panel only.

Metal Tag	Marker	Clone	Vendor
113In	CD88	P12/1	Bio Rad
115In	CD11c	IM7	Bio Rad
141Pr	CD86	37301	Novus Biologicals
142Nd	CD19	HIB19	BioLegend
143Nd	HLA-DR	L243	Fluidigm
145Nd	CD16	3G8	BioLegend
146Nd	CD8a	RPA.T8	BioLegend
147Sm	CD10	HI10a	BioLegend
148Nd	CD45	D058-1283	BD Biosciences
149Sm	CD25	2A3	Fluidigm
150Nd	IL-22	22URTI	Fluidigm
151Eu	CD56	NCAM16.2	BD Biosciences
152Sm	CD14	M5E2	BioLegend
153Eu	CD45RA	HI100	BioLegend
154Sm	CD38	HIT2	BioLegend
155Gd	CD27	L128	Fluidigm
156Gd	IL-6	MQ2-13A5	BioLegend
158Gd	CD20	2H7	BD Biosciences
159Tb	CCR7	G043H7	Fluidigm
160Gd	pSTAT1 IFNγ	58D6 4S.B3	Cell Signaling Technologies Biolegend
161Dy	IL-23p19	23dcdp	Fluidigm
162Dy	IL-1B	H1b-27	BioLegend
163Dy	CD183	G043H7	Fluidigm
164Dy	pZAP70 IL-13	Y319 JES10-5A2	Cell Signaling Technologies BioLegend
165Ho	pCREB FOXP3	87G3 PCH101	Fluidigm eBiosciences
166Er	pp38	D3F9	Cell Signaling Technologies
167Er	p44/42MAPK (ERK1/2) GranzymeB	D13.14.4E GB11	Cell Signaling Technologies BioLegend
168Er	CD127	A019D5	Fluidigm
169Tm	pSTAT3 IL-17a	D3A7 XP R BL168	Cell Signaling Technologies BioLegend
170Er	IL-8	6217	R&D Systems
171Yb	CD68	Y1/82A	Fluidigm
172Yb	IL-21	3A3-N2	BioLegend
173Yb	pIRAK4 IFNα	D6D7 MAR1-583	Cell Signaling Technologies BioLegend
174Yb	CD4	OKT4	eBiosciences
175Lu	pS6 TNFα	D57.2.2E XP R Mab11	Cell Signaling Technologies BioLegend
176Yb	pSTAT6 IL-10	D8S9Y JES3-19F1	Cell Signaling Technologies BioLegend
209Bi	CD3	Sp34.2	BD Biosciences

(All staining): Following intracellular staining, cells were resuspended in 1.6% paraformaldehyde and washed with CSB. Samples were stored in Freezing Media (FBS + 10% DMSO) until day of CyTOF run. Freezing media was spun out and cells were washed with CSB. Cells were labeled with intercalator-Ir (Fluidigm). Intercalator solution was spun out and cells were washed twice with CSB. PV: samples were then shipped overnight with refrigeration to the Longwood Medical Area CyTOF Core of the Dana-Farber Cancer Institute. Choriodecidual samples were run on site at the University of California, Los Angeles Flow Cytometry Facility. Prior to being run on the Helios (Fluidigm) CyTOF machine, PV samples were resuspended in MilliQ water with a 1:10 dilution of EQ beads for normalization.

Data analysis: Bead normalized FCS files were uploaded to Premium Cytobank® where they were pre-gated on DNA^{pos}, live ($Rh103^{neg}$), $bead^{neg}$ prior to subsequent analysis. Percent positive and mean metal intensity (MMI) parameters were exported from 2D gated populations within Premium Cytobank® software. Samples with insufficient intracellular staining were omitted from individual analyses **(Table 11)**. Data was then uploaded to either R or GraphPad Prism software for analysis and graph generation. For automatic clustering, parent populations as indicated in figures were 2D gated and exported from Premium Cytobank®, and then uploaded to the cytofkit R package DOI: 10.18129/B9.bioc.cytofkit[120,158,159]. Samples with insufficient cell number were omitted from analysis **(Table 11)**. Data was transformed with cytofAsinh and merged with ceil. t-Distributed Stochastic Neighbor Embedding (tSNE) was used for dimensionality reduction. Phenograph was selected from clustering for all data using the preset k=30. All data was visualized using the https://cytofkit.shinyapps.io/shiny/ platform. All abundance data displayed in manuscript was extracted from Phenograph clustering output. Cluster identification

was achieved using generated heatmaps for antibody intensity. Any antibodies that showed insufficient staining across all samples were omitted from heatmaps.

Table 11 Samples ommitted from individual experiments

Sample	Figure	Omittance Justification
Decidua		
431	34	Insufficient intracellular staining
432	34	Insufficient intracellular staining
436	34	Insufficient intracellular staining
437	34	Insufficient intracellular staining
Villi - Phospho		
427	24-28, 35-37	Insufficient parent cell number
440	24-28, 35-37	Insufficient parent cell number
437	35-37	Insufficient intracellular staining
439	35-37	Insufficient intracellular staining
Villi Cytokine		
427	38-41	Insufficient parent cell number
440	38-41	Insufficient parent cell number
436	39-41	Insufficient parent cell number
437	39-41	Insufficient parent cell number (7D FOXP3$^-$ T cells)
438	39-41	Insufficient parent cell number (S4D HLA-DR+ CD4/CD8, HLA-DR- CD8)
439	38-41	Insufficient intracellular staining
442	41	Insufficient parent cell number (FOXP3+ T cells)

Statistical analysis and plot generation: R version 3.5.1 was used to perform statistical analysis between treatments using the Kruskal-Wallis test and post-hoc analysis with Dunn's multiple comparison test due to the non-parametric nature of primate data using PMCMR and data.table packages; p-values < 0.05 were considered significant. Plots were generated in Prism GraphPad 7. Each data point represents one monkey unless otherwise indicated.

Data availability: The data analyzed in this study is stored in accordance to institutional and IACUC guidelines. CyTOF data is publicly available on Premium Cytobank®.

3.3 Results

3.3.1 The rhesus PV has a diverse and distinct immune profile

To determine what effects inflammation has on the PV, we investigated the immunophenotype and activation states of immune cells based on the impact of prenatal exposures. PV cells were isolated using previously established protocols[86] from pregnant rhesus dams exposed to 16 hours of either intra-amniotic (IA) saline or intramuscular (IM) saline (n=4), LPS (n=5) or pretreatment with TNF inhibitors followed by LPS (n=5), referred to as blockade group throughout the manuscript (**Fig 24, Table 9**). To determine the immune landscape of PV, we performed CyTOF using a panel of 22 surface antibodies (**Table 11**). To determine the global immune profile, we first clustered on all leukocytes ($CD45^{pos}$), and identified populations based on surface marker expression (**Fig 25A**). We observed a complex immune landscape and identified cells as following: including monocytes/Mϕs ($CD14^{pos}$) that will be referred to as Mϕs in this manuscript, NK cells ($CD14^{neg}CD19^{neg}CD4^{neg}CD8^{neg}$HLA-$DR^{neg}CD56^{pos}$), dendritic cells (DCs) ($CD14^{neg}CD19^{neg}CD4^{neg}CD8^{neg}$HLA-$DR^{pos}$), B cells($CD14^{neg}CD19/CD20^{pos}$), T cells ($CD14^{neg}CD19^{neg}CD4/CD8^{pos}$), innate lymphoid cells (ILCs) ($CD14^{neg}CD19^{neg}CD4^{neg}$ $CD8^{neg}$ HLA-$DR^{neg}CD56^{neg}CD127^{pos}$), and presumptive neutrophils or presumptive hematopoietic stem cells ($CD14^{neg}CD19^{neg}CD4^{neg}CD8^{neg}$ HLA-$DR^{neg}CD56^{neg}CD10^{pos}$) (**Fig 25A**).

When examining the $CD45^{pos}$ population, we found a complex and highly diverse immune landscape in the non-human primate PV that has not been previously appreciated (**Fig 25A-B**). Notably, the PV was comprised not only of Mϕs, presumably Hofbauer Cells, whose presence and role during pregnancy has been previously described[140,160,161] but also numerous other cell types. Unfortunately, we could not further characterize Mϕs by CD163 expression as we could with our

human cohort (Chapter 2). The PV also contained DCs (10-40%), indicating multiple antigen presenting populations within the tissue, consistent with our human findings **(Fig 14)**. Moreover, we observed a group of clusters that were lineage^{neg} and CD10^{pos} **(Fig 25B).** These cells likely represent hematopoietic stem cells[70,162]. Unfortunately, we were unable to further phenotype these cells with our current panel. We observed no changes in population abundance between the various conditions when all clusters of each major immune subtype were grouped together **(Fig 25C)**.

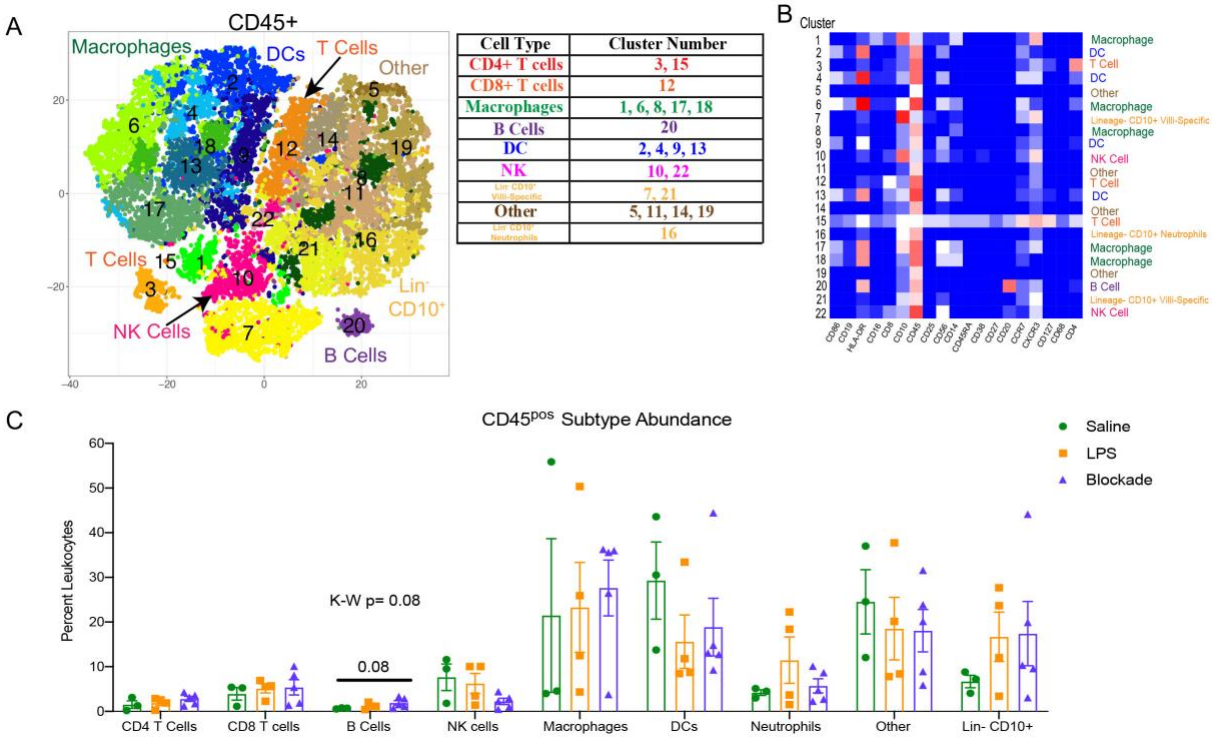

Figure 25 Immune landscape of healthy and inflammed PV
(A) Automated clustering of CD45^{pos} cells isolated from the PV. Tsne of all monkeys [saline (n=3), LPS (n=4), blockade (n=5)] analyzed. (B) Clusters were identified by relative intensity of each antibody in the heatmap. Red = highest relative expression, Blue = lowest relative expression. (C) Abundance of each major subtype listed in table from **A**. Kruskal-Wallis values are listed at the top of each graph. Post-hoc p values are listed as lines connecting respective comparisons. * = p-value <0.05.

We did observe a trend towards increase in the blockade group (p=0.08) of cluster 20, the only B cell population found in the PV **(Fig 26A-B)**. B cells were also a minor population in the healthy human PV **(Fig 8)**, consistent with our findings in saline monkeys. We also observed a

trend (p=0.08) towards a higher abundance of cluster 6 (CD86^{pos}CD10^{pos}CCR7^{pos}) macrophages in LPS exposed monkeys that was TNF-independent **(Fig 26A-B)**.

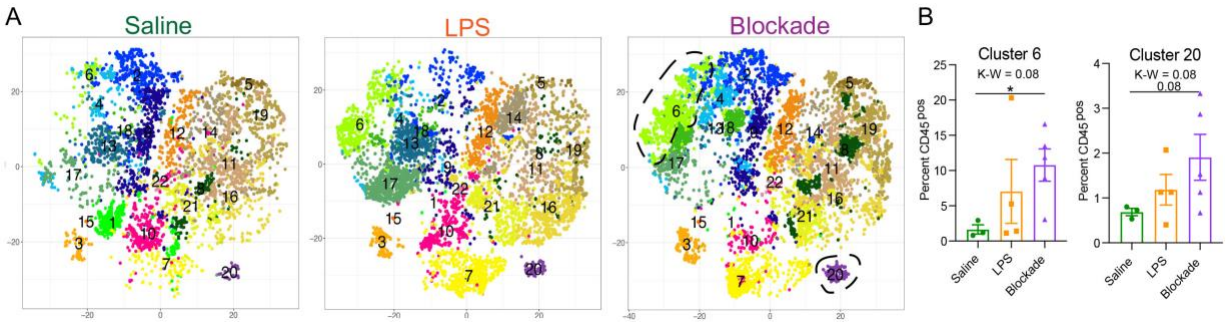

Figure 26 Blocking TNFα increases individual monocyte and B cell populations in the PV
(A) tsnes separated by treatment group. Outlined populations are those that are altered between treatment groups. (B) Graphical representation of two clusters outlines in A. Kruskal-wallis (K-W) values are listed at the top of each graph. Post-hoc p values are listed as lines connecting respective comparisons. * = p-value <0.05.

To determine if there were immune differences at a more granular level, we examined major immune populations separately. To assess APCs and activated T cells in the PV, we clustered on HLA-DR^{pos} CD45^{pos} cells (**Fig 27A**). We detected Mϕs, DCs, B cells and T cells (**Fig 27B**). The presence of both APCs and HLA-DR^{pos} T cells in the saline group indicated the potential for antigen presentation within the PV in healthy pregnancies, consistent with the human mid-gestation PV **(Fig 15,20)**. However, these HLA-DR^{pos} immune populations remained stable in abundance when exposed to IA LPS (data not shown).

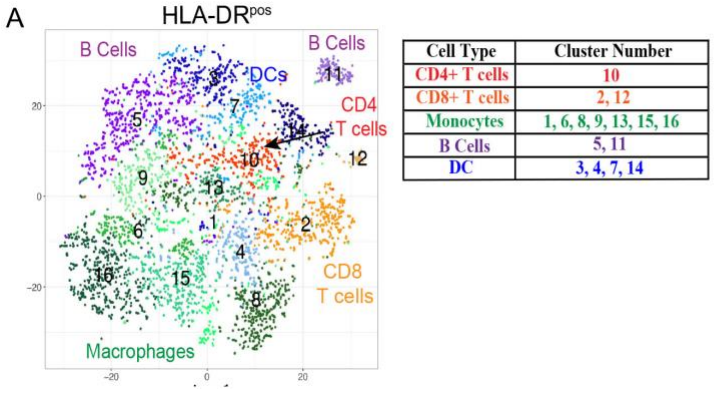

Cell Type	Cluster Number
CD4+ T cells	10
CD8+ T cells	2, 12
Monocytes	1, 6, 8, 9, 13, 15, 16
B Cells	5, 11
DC	3, 4, 7, 14

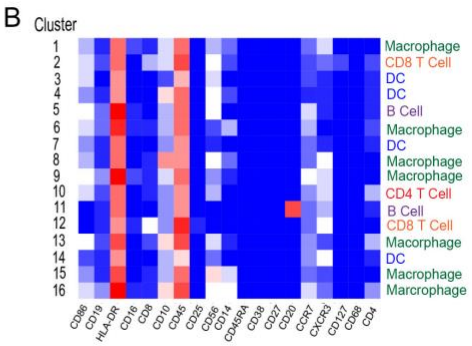

Figure 27 HLA-DR^{pos} populations are stable with IA LPS treatment

(A) Automated clustering of HLA-DR^{pos} cells in the PV, merged tsne of saline (n=3), LPS (n=4), blockade (n=5). (B) Clusters were identified by relative intensity of each antibody in the heatmap. Red = highest relative expression, Blue = lowest relative expression.

3.3.2 PV T cells show predominately memory phenotypes

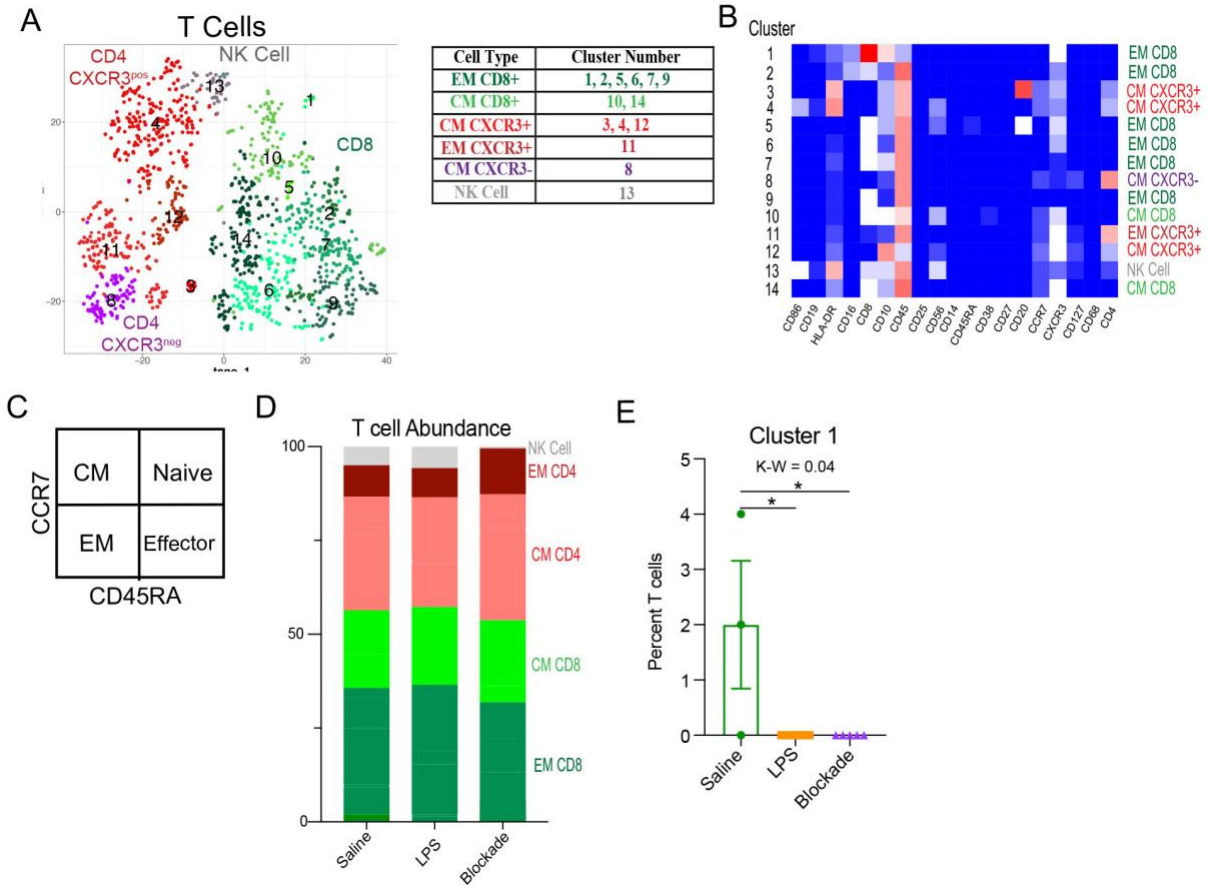

Cell Type	Cluster Number
EM CD8+	1, 2, 5, 6, 7, 9
CM CD8+	10, 14
CM CXCR3+	3, 4, 12
EM CXCR3+	11
CM CXCR3-	8
NK Cell	13

Figure 28 Memory T cell subsets are present and mostly stable with IA LPS treatments
(A) tSNE of T cells within the PV. Saline (n=3), LPS (n=4), blockade (n=5). CD4 T cells were categorized and labeled on tsne by CXCR3 expression. (B) Clusters were identified by relative intensity of each antibody in the heatmap. Red = highest relative expression, Blue = lowest relative expression. (C) Designation of memory phenotypes was determined by CCR7 and CD45RA expression. (D) Stacked bar graph showing abundance of clusters belonging to each memory T cell subset. (E) Graph of abundance of statistically significantly altered T cell cluster with IA LPS treatment. K-W = Kruskal-Wallis. * = post-hoc p-value < 0.05.

When clustering on T cells specifically, we detected both CD4 and CD8 populations, consistent with prior reports[73,163] (**Fig 28A-C**). However, we were able to greatly expand upon these findings and deeply phenotype the T cells within the villous tissue. We showed that in saline

treated placentas, the T cell compartment was made up of 56% CD8, 38% CD4 and 6% NK/NKT cells. Additionally, within the CD4 populations we report most clusters were CXCR3^{pos} suggesting a T_{H1} phenotype (**Fig 28B**). This is notably different from the human PV **(Fig 18)**. Using expression of CCR7 and CD45RA, we have found that in all treatment groups there were no clusters segregated as naïve (CCR7^{pos} CD45RA^{pos}) T cells of either CD4 or CD8 phenotype (**Fig 28B-C**). Furthermore, we report that while the majority of CD4 cells (58%) were of central memory (CM) phenotype (CCR7^{pos}CD45RA^{neg}), the majority (64%) of CD8 cells were of effector memory (EM) phenotype (CCR7^{neg} CD45RA^{neg}) (**Fig 28D**). These findings suggest that CD4 T cells were predominately being educated in the vasculature, while CD8 T cells were educated within the tissues. IA LPS had no effect on the relative proportions of T cell populations except for a decrease in cluster 1 (CD8^{pos}CXCR3^{pos}CD10^{pos}CD16^{pos}) EM CD8 T cells in a TNF-dependent manner (**Fig 28E**). HLA-DR expression within two CD4 T cell clusters was upregulated with LPS in a TNF-independent manner [cluster 4 (CM CXCR3^{pos}) and cluster 11 (EM CXCR3^{pos})] suggesting that the IA LPS leads to downstream activation of PV CD4 T cells **(Fig 29A).**

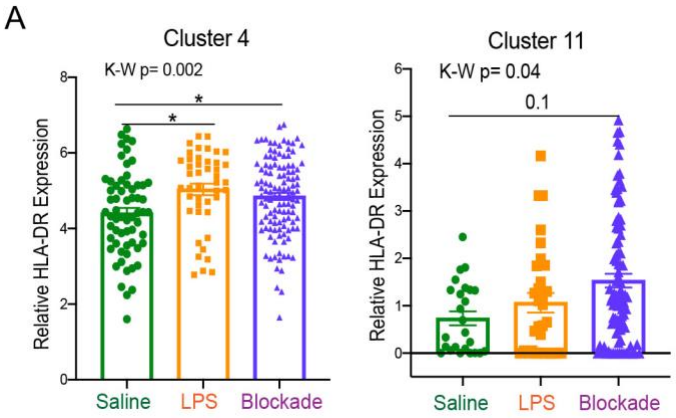

Figure 29 Upregulation of T cell HLA-DR Expression with IA LPS
(A) HLA-DR expression in two clusters of T cells (Fig 27), each dot represents a single cell within a treatment group. Kruskal-Wallis values are listed at the top of each graph. Post-hoc P-values are listed as lines connecting respective comparisons. * = p-value <0.05.

3.3.3 The PV immune landscape is distinct from the choriodecidua

We next examined the immune compartment in the choriodecidua to determine if the immune landscape reported above was PV-specific. When looking at the choriodecidual CD45^{pos} population, we observed many immune cells that were either absent from the PV, such as ILCs, or present in greatly different abundances. For example, while the saline choriodecidua contained 25-30% T cells (**Fig 30A**), the PV in contrast were only 10-15% T cells (**Fig 25)**. In the choriodecidua, we observed one population of neutrophils with the phenotype of major lineage marker^{-} CD10^{pos}, cluster 10 **(Fig 30B-C).** In the PV, cluster 16 **(Fig 25)** is probably also neutrophils as we saw a similar trend of an increased abundance in LPS animals that is corrected with the blockade **(Fig 25).** However, two PV clusters 7 and 21 with similar surface marker expression (major lineage marker^{neg} CD10^{pos}) were not detected in the choriodecidua **(Fig 30B-C)**. These findings suggest that the diverse immune landscape we found in the PV is tissue-specific and unique from the neighboring choriodecidua.

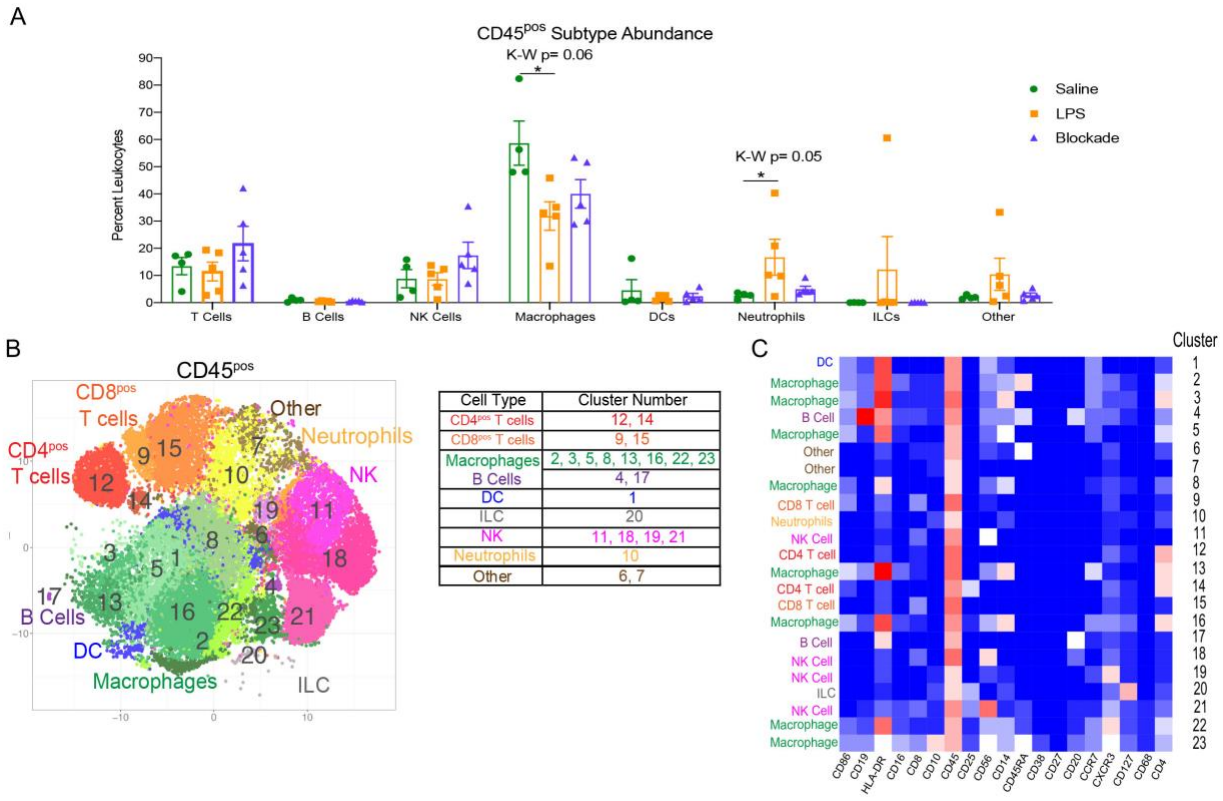

Cell Type	Cluster Number
CD4pos T cells	12, 14
CD8pos T cells	9, 15
Macrophages	2, 3, 5, 8, 13, 16, 22, 23
B Cells	4, 17
DC	1
ILC	20
NK	11, 18, 19, 21
Neutrophils	10
Other	6, 7

Figure 30 Global immune subtypes in the healthy and inflammed choriodecidua
(A) Abundance of each major immune subtype as a percent of CD45^{pos} cells. Kruskal-wallis values are listed at the top of each graph. Post-hoc p values are listed as lines connecting respective comparisons. * = p-value <0.05. (B) Automated clustering of CD45^{pos} cells isolated from the choriodecidua. Tsne is a merged image of all monkeys analyzed saline (n=4), LPS (n=5), blockade (n=5). (C) Clusters were identified as one of nine major immune subtypes based on intensity of antibody staining represented by the heatmap. Blue = lowest relative expression. Red = highest relative expression

3.3.4 Choriodecidual immune cells are sensitive to IA LPS in a TNF dependent manner

To compare major populations in the choriodecidua i.e. Mϕs, DCs, T cells etc., we combined clusters of the same subtype together (**Fig 30A**) and saw no differences between treatment groups except for Mϕs and neutrophils. However, when looking at individual clusters of immune cells, we observed that there was a significant decrease in abundance of cluster 2 Mϕs (CD14^{pos} HLA-DR^{pos} CD16^{pos} CD4^{pos} CD45RA^{pos}) in LPS animals, which was partially restored with the blockade **(Fig 31)**. Moreover, there was an influx of cluster 21 NK cells (CD56^{pos} CD25^{pos}

CD8^{pos}), observed specifically with the blockade treatment (**Fig 31**). Furthermore, cluster 10, presumptive neutrophils, which also represents the entire neutrophil population **(Fig 30)**, was increased significantly with LPS treatment, and restored back down to normal levels with the blockade (**Fig 31**) consistent with previously published work[86,87]. This result suggests that IA LPS results in alterations of the frequency of specific immune populations (i.e., individual clusters). Moreover, TNF blockade prior to IA LPS restores some, such as neutrophils, but not all the LPS induced immune dysregulation.

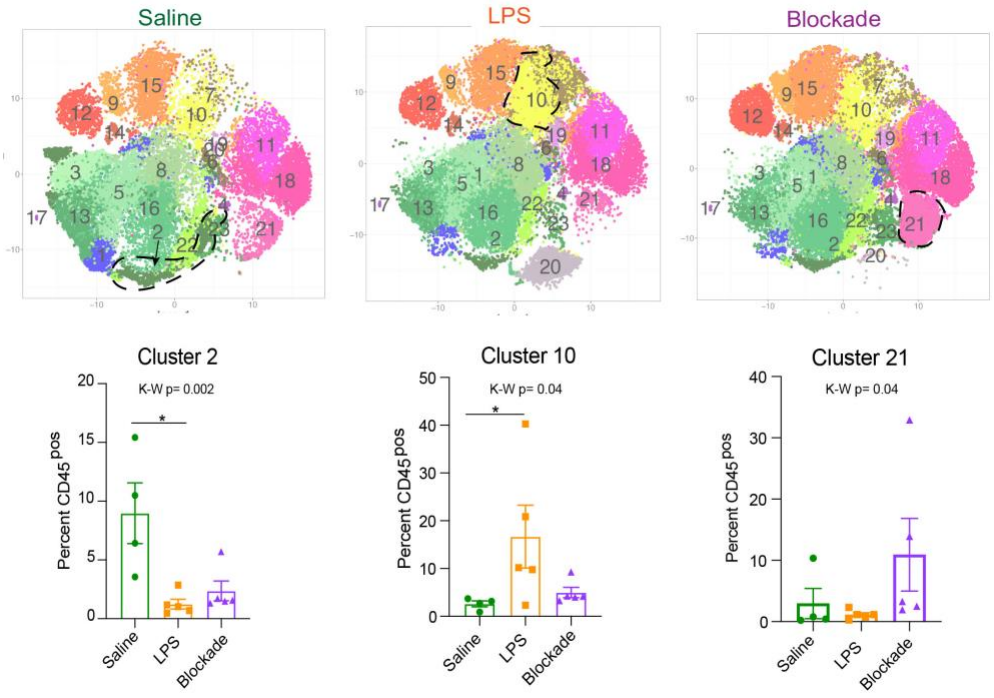

Figure 31 Specific populations sensitive to IA LPS treatment in the choriodecidua
Tsnes separated by treatment group. Outlined populations are those that are altered between treatment groups. Outlined populations are shown graphically below. Kruskal-wallis values are listed at the top of each graph. Post-hoc P values are listed as lines connecting respective comparisons. * = p-value <0.05

3.3.5 LPS induced IA alters CD56^{hi} NK cells in the choriodecidua

Decidual natural killer cells (dNK) are a specialized subset of NK cells that are phenotypically distinct from peripheral blood NK cells and marked CD56^{superbright} [121,164]. dNK cells

have been implicated as critical cells in healthy and diseased pregnancies that play diverse roles from implantation to parturition (summarized in[165]). To assess the NK cell compartment in the choriodecidua, we clustered on NK cells (**Fig 32A**). Clusters were classified as CD56^{lo}, CD56^{mid} or CD56^{hi} (likely canonical dNK) **(Fig 32B-C)**. We found cluster 20 (CD56^{hi}CD16^{pos}CXCR3^{pos}) was trending towards increase in blockade animals alone, while cluster 11 (CD56^{hi}CXCR3^{pos}) was reduced in IA LPS-exposed monkeys, and partially corrected in blockade (**Fig 32D**). This finding is consistent with reports in mice that show administration of LPS at 9.5 days post-coitum leads to decrease in NK cells in the uterus[166].

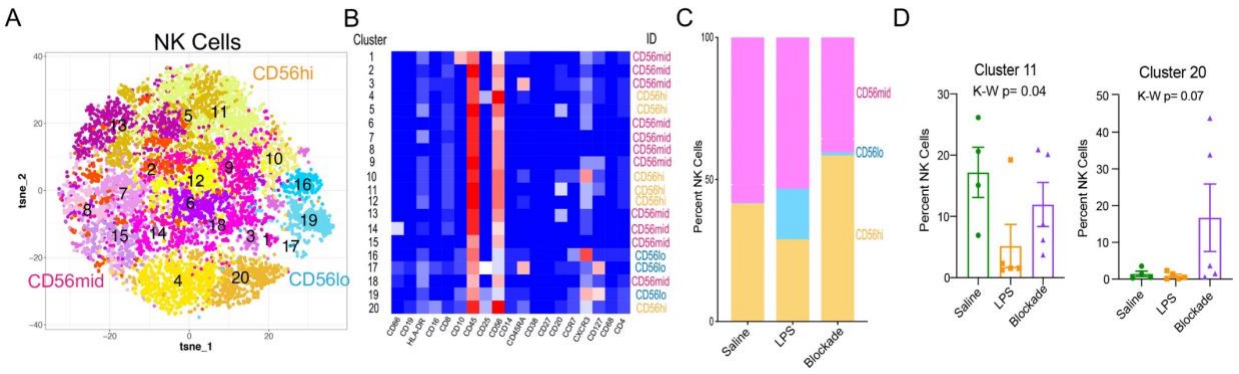

Figure 32 NK cell abundance fluctuates with IA LPS in the choriodecidua

(A) Automated clustering of NK cells in the choriodecidua, merged tsne of saline (n=4), LPS (n=5), blockade (n=5). (B) Clusters were identified by relative intensity of each antibody in the heatmap. Red = highest expression. Blue = lowest expression. (C) Stacked bar graph comparing abundances of all NK cell clusters segregated by CD56 expression. (D) Quantification of two clusters most statistically different in abundance between groups. K-W = Kruskal-Wallis test. No significant p-values were present in post hoc analysis.

3.3.6 Antigen presenting cells in the choriodecidua increase in abundance with LPS treatment independent of TNF

Next, we analyzed choriodecidual HLA-DR^{pos} cells (**Fig 33A**), representing APCs. HLA-DR is upregulated on activated T cells[167,168] and thus these cells were detected in the HLA-DR^{pos} compartment as well **(Fig 33B-C)**. IA LPS treatment significantly altered the HLA-DR^{pos} non-T

cell landscape with one population of Mϕs (cluster 9) being increased with LPS in a TNF dependent manner **(Fig 33D)**. Furthermore, two populations of Mϕs (clusters 18 & 20); one population of DCs (cluster 10); and one population of B cells (cluster 7) were elevated in a TNF-independent fashion (**Fig 33E**). This contrasts our findings from the $CD45^{pos}$ clustering in which cluster 2 Mϕs (HLA-DR^{pos} $CD4^{pos}$ $CD45RA^{pos}$ $CXCR3^{pos}$) were depleted with LPS (**Fig 31)**. We determined that this cluster 2 population of Mϕs is two distinct clusters when only HLA-DR^{pos} cells are analyzed (clusters 3&4) and confirm our observations with a trend towards a decrease of these Mϕs in LPS animals (**Fig 33F**). The two Mϕ populations that expanded the most with LPS treatment were $CXCR3^{pos}$ while the Mϕ populations that were reduced after LPS exposure were $CXCR3^{neg}$ **(Fig 33E).** CXCR3 on Mϕs has been shown to be upregulated during infection and inflammation[169] suggesting that either the endogenous decidual Mϕs already present upregulated their CXCR3 expression or there was an influx of new $CXCR3^{pos}$ Mϕs upon LPS treatment.

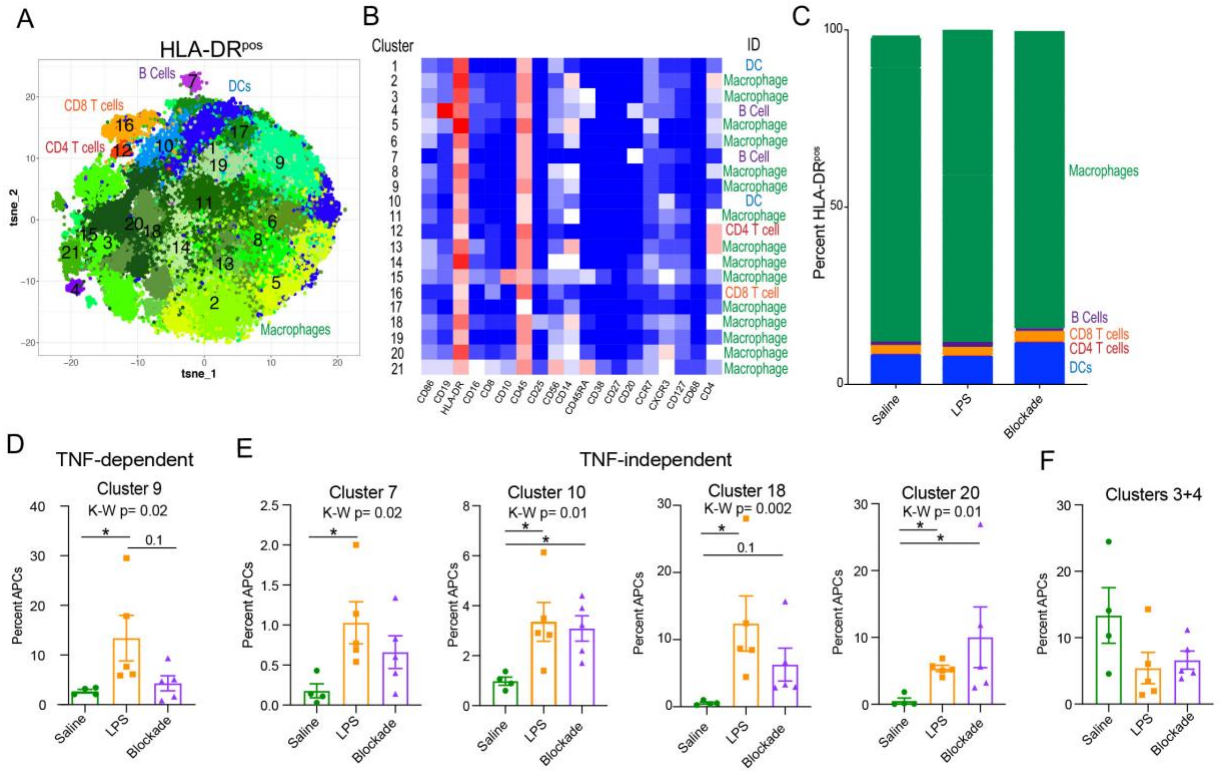

Figure 33 LPS significantly alters APC landscape in the choriodecidua

(A) Automated clustering of HLA-DR^{pos} cells in the choriodecidua, merged tsne of saline (n=4), LPS (n=5), blockade (n=5). (B) Clusters were identified by relative intensity of each antibody in the heatmap. Red = highest expression. Blue = lowest expression. (C) Stacked bar graph comparing abundances of all HLA-DR^{pos} clusters segregated by cell type. (D) Quantification of TNF-dependent clusters. (E) Quantification of TNF-independent clusters. (F) Quantification of CXCR3^{neg} monocyte clusters. Kruskal-Wallis (K-W) values are listed at the top of each graph. Post-hoc p-values are listed as lines connecting respective comparisons. * = p-value <0.05.

3.3.7 Diverse memory T cell populations are present, but not altered with IA LPS in the choriodecidua

We next clustered on T cells specifically within the choriodecidua (**Fig 34A**) and found 18 unique populations. CD4^{pos} clusters were separated based on CXCR3 expression and Treg phenotypes (CD25^{pos} CD127^{lo}) (**Fig 34B**). Based on the expression of CCR7 and CD45RA (**Fig 34C**) we observed naïve (cluster 2); central memory (CM) (clusters 1,16,18); and effector memory (EM) (clusters 2,4,7,9,15) clusters to be present in the choriodecidua. In contrast, only EM

phenotype was detected within the 7 clusters of CD8 cells identified. We report no alterations in T cell frequencies between the three treatment groups (**Fig 34D**).

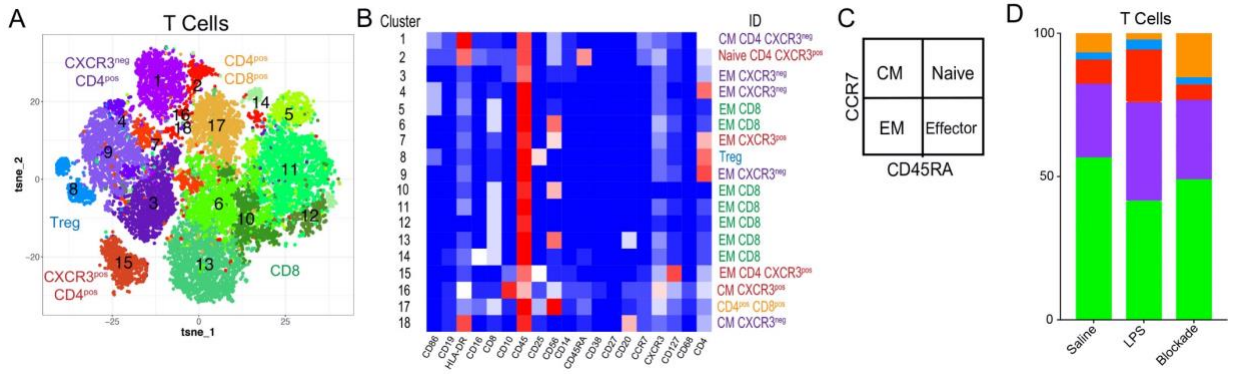

Figure 34 T cell populations in the choriodecidua are stable across treatments
(A) Automated clustering of T cells in the choriodecidua, merged tsne of saline (n=4), LPS (n=5), blockade (n=5). (B) Clusters were identified by relative intensity of each antibody in the heatmap. Red = highest expression. Blue = lowest expression. (C) Classification of T cell memory phenotypes. (D) Stacked bar graph comparing abundances of all T cell clusters segregated by cell type.

3.3.8 Signaling in choriodecidua immune cells is not altered in the experimental window

To evaluate what signaling pathways are altered with IA LPS in the choriodecidua, we used intracellular antibodies against phosphorylated(p) proteins as a surrogate of STAT/MAP kinase/TCR/mTOR/CREB/IRAK signaling families (**Table 10**). Overall, at baseline we observed high phosphorylation of CREB in all $CD45^{pos}$ cells (**Fig 35A**). Additionally, we observed moderate levels of phosphorylation in the MAP kinases (ERK and p38), mTOR (S6) and IRAK4 pathways (**Fig 35A**) all critical to cell regulation. Moreover, we detected low levels of phosphorylation of STATs 1, 3 and 6. However, in the time analyzed, we report no significant change in any phosphorylation levels between the three treatment groups within total $CD45^{pos}$ cells (**Fig 35A**) and individual subtypes (**Fig 35B-F**).

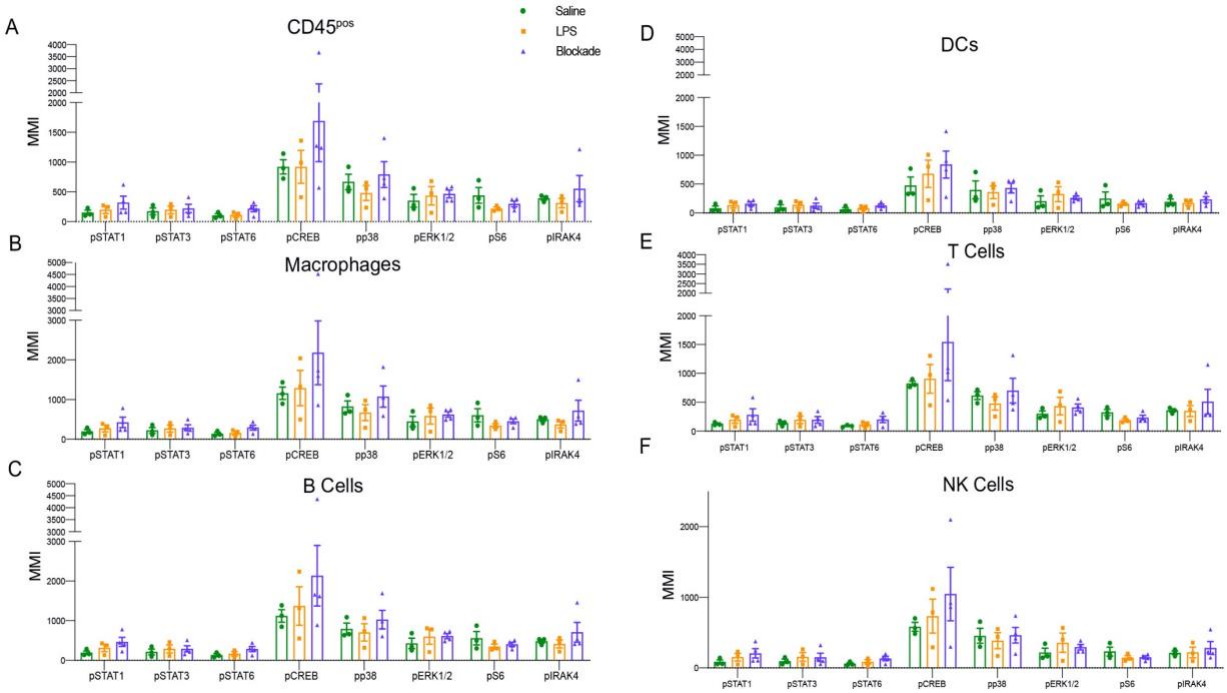

Figure 35 Signaling in choriodecidual immune cells is unaltered with treatment

Antibodies against phosphorylated proteins were used to evaluate signaling pathways in choriodecidual immune cells. (A-F) Total immune cells (A) and specific immune subsets (B-F) were 2D gated and Mean Metal Intensities (MMIs) were calculated and compared among treatment groups. Saline (n=3), LPS (n=3) blockade (n=4). No significant differences were detected among any groups when all three groups were compared (Kruskal-Wallis values) or when individual treatments were compared among each other using post-hoc testing. P value > 0.05 was used as significant.

3.3.9 LPS induces phosphorylation of multiple signaling pathways in the PV in a TNF-dependent manner

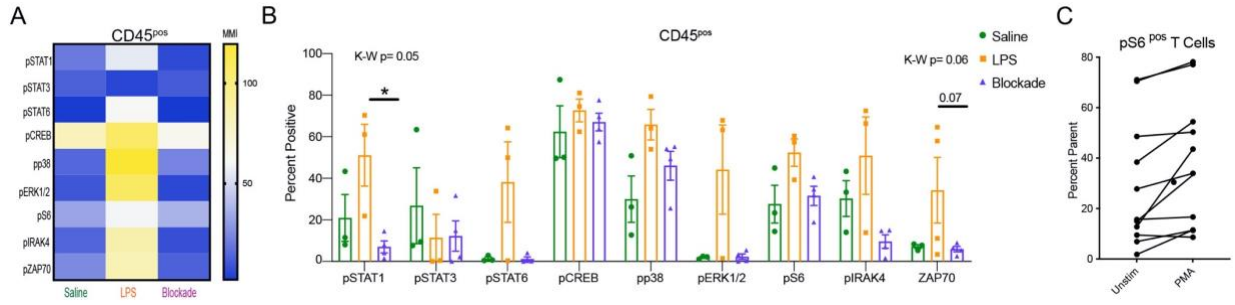

Figure 36 PV immune cells signal through STAT1 and ZAP70
(A) Mean Metal Intensities (MMIs) for nine signaling proteins in 2D-gated CD45^{pos} cells across treatment groups. (B) Percentages for nine signaling proteins in 2D-gated CD45^{pos} cells across treatment groups. Kruskal-Wallis comparisons of all three groups are listed at the top of each group of comparisons, individual post hoc comparisons between each individual group are marked with lines. * = p-value <0.05. (C) Validation that PV immune cells were still functional post transport. Percent of all T cells expressing pS6 in unstimulated and PMA/ionomycin stimulated conditions. Lines connect matched unstimulated-PMA stimulated samples from the same monkey.

When we analyzed protein phosphorylation of all CD45^{pos} cells in the PV, we detected an upregulation of phosphorylated proteins upon IA LPS treatment **(Fig 36A-B)**. We also confirmed transport between collection and staining of our samples did not significantly alter signaling capacity of our cells by showing that PV T cells signaled through pS6 as expected[170] after PMA/Ionomycin stimulation **(Fig 36C)**. In saline animals, we observed high levels of pCREB and moderate levels of pS6 and pZAP70 with little baseline phosphorylation of other proteins **(Fig 36B).** When exposed to LPS, all proteins had a TNF dependent increase in phosphorylation except for STAT3. The two proteins that were statistically the most sensitive to prenatal exposures when looking at MMI were pSTAT1 and pZAP70 (p=0.09). Upon LPS treatment, there was an increase in both pSTAT1 MMI in CD45^{pos} cells **(Fig 36A)** and an increase in the percent of cells with pSTAT1 (**Fig 36B**) which was TNF-dependent. Moreover, the steady state pSTAT1 phosphorylation in the saline treated animals was also TNF-dependent as the blockade treatment

reduced the overall pSTAT1 level below saline (**Fig 36A-B**). Additionally, we detected an increase of pZAP70 in CD45^{pos} cells in LPS treated monkeys which was reduced in the blockade group. Similar to pSTAT1 levels, the blockade group also had significantly reduced pZAP70 levels compared to the saline controls **(Fig 36A)**. ZAP70 is phosphorylated upon activation of the T, NK, and B cell receptors[171,172]. LPS's effect on ZAP70 is likely indirect given that LPS cannot directly activate the TCR. To further investigate if phosphorylated ZAP70 may be the result of TCR activation, we examined if antigen-presenting cells and activated (HLA-DR^{pos}) T cells specifically were responding to prenatal exposure of LPS.

To uncover which populations the pSTAT1 and pZAP70 signatures were originating from, we began analyzing immune subtypes individually. When looking at APCs, we report that IA LPS-exposure results in a higher frequency of cells that have pSTAT1 in all three of the APC subsets (MPCs, DCs and B cells) **(Fig 37A).** This was also seen by MMI in DCs **(Fig 37B).** This finding further supports that the STAT1 pathway is activated in the PV, and that TNFα signaling is required for its activation. In addition to STAT1, we also detected a trend towards increased phosphorylation of IRAK4 in the LPS compared to blockade groups in B cells (**Fig 37C**). IRAK4 becomes phosphorylated upon activation of TLR4. LPS is sensed through TLR4 on the surface of immune cells, and thus the trend of increased pIRAK4 in LPS-treated animals may be due to direct recognition of LPS by PV B cells.

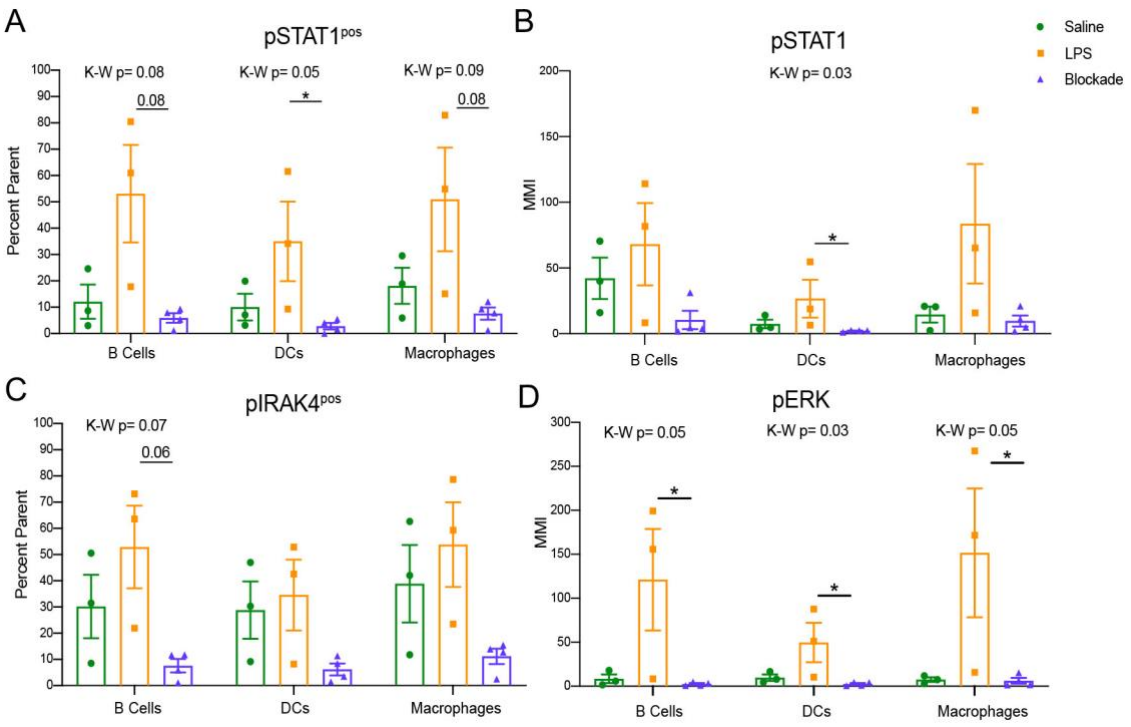

Figure 37 Signaling in PV APCs

(A) Quantification of abundance of pSTAT1^{pos} cells identified with 2D gating across APC subsets. (B) Quantification of pSTAT Mean Metal Intensity (MMI) across APC subsets. (C) Quantification of abundance of pIRAK4^{pos} cells across APC subsets. (D) Quantification of pERK MMI across APC subsets. Kruskal-Wallis comparisons of all three groups are listed at the top of each group of comparisons, individual post hoc comparisons between each individual group are marked with lines. * = p-value <0.05.

Further supporting activation of APCs with IA LPS, we detected alterations in MAP kinase signaling (**Fig 37D).** Specifically, within B cells, DCs and Mϕs we report an increase in ERK1/2 phosphorylation by MMI that was TNF dependent (**Fig 37D**). ERK1/2 is downstream of the IRAK4 signaling pathway, and its phosphorylation indicates that in addition to having inducible STAT1 signaling, PV APCs may be directly detecting LPS via TLR4/IRAK4 and then activating further downstream pathways.

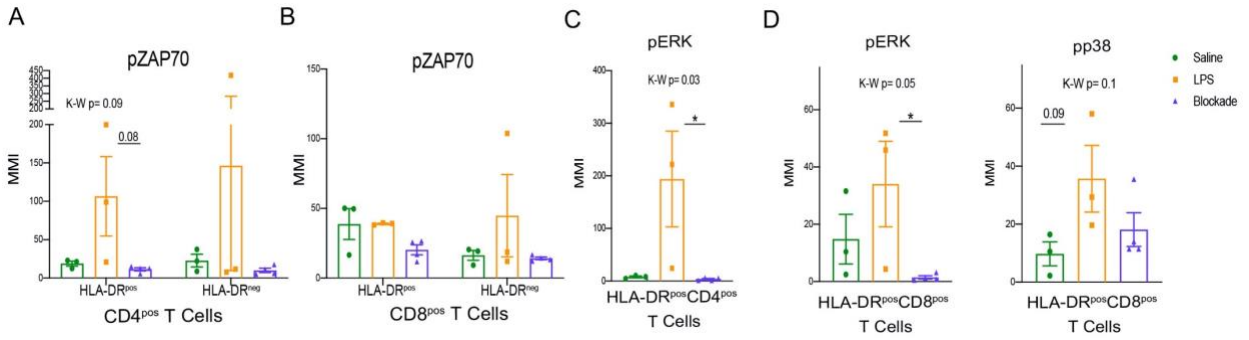

Figure 38 Signaling in PV T cells

(A) Quantification of pZAP70 Mean Metal Intensity (MMI) in CD4 T cells. (B) Quantification of pZAP70 MMI in CD8 T cells (C) Quantification of pERK MMI in HLA-DR^{pos} CD4 T cells. (D) Quantification of pERK and pp38 MMI in HLA-DR^{pos} CD8 T cells. Kruskal-Wallis comparisons of all three groups are listed at the top of each group of comparisons, individual post hoc comparisons between each individual group are marked with lines. * = p-value <0.05.

After we found that APCs were the source of the pSTAT1 signature that we observed in **Figure 36**, we next investigated what cells were phosphorylating ZAP70. As ZAP70 is phosphorylated downstream of TCR activation by APCs, we began looking at pZAP70 in activated T cell populations. We report that in CD4 HLA-DR^{pos} T cells, there was a reduction in pZAP70 in blockade versus LPS groups, but no changes in the HLA-DR^{neg} population (**Fig 38A).** These results are consistent with our observations of higher pZAP70 in LPS and lower pZAP70 in blockade in the total CD45^{pos} population (**Fig 36A**). CD8 T cells in contrast did not have any alterations in pZAP70 between treatments, but higher pZAP70 MMI was detected in saline animals in HLA-DR^{pos} versus HLA-DR^{neg} subsets **(Fig 38B).** Additionally, we observed an increase in the map kinases: pERK in CD4 **(Fig 37C)** and pERK and pp38 in CD8 **(Fig 38D)**, which are down-stream targets in multiple pathways including TCR activation. These findings suggest that T cells in the PV respond to antigens through the TCR, and that this response is inhibited when TNF signaling is blocked.

3.3.10 PV Immune cells alter cytokine production with IA LPS

Once we determined that leukocytes in the placental villi had differential signaling during our experimental window, we sought to determine if their cytokine profiles also fluctuated with LPS injection. As such, we used a cytokine CyTOF panel **(Table 10)** to evaluate differences in cytokine production between saline and IA LPS treated monkeys, and to determine if cytokine production was TNF-dependent. We report that CD45^{pos} cells from the PV produce high amounts of IL-17A and IFNα under homeostatic conditions (saline animals) **(Fig 39A)**. After *in utero* exposures we observed alterations in production of multiple cytokines, particularly granzymeB (GRNZB), IFNγ, IL-8 and IL-17 that were not statistically significant **(Fig 39A)**. However, we observed a decrease in both MMI and percent positive cells for IFNα in the blockade group when compared to saline (**Fig 39B**).

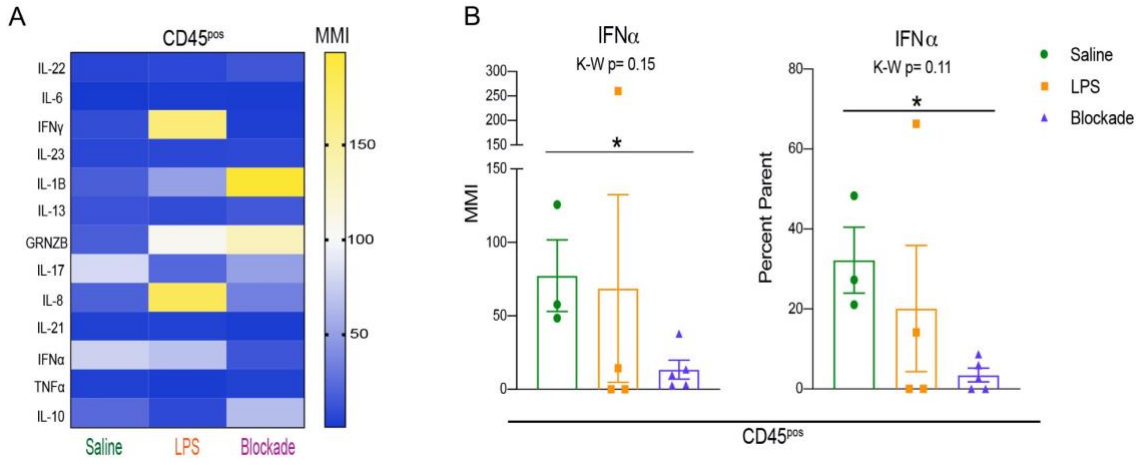

Figure 39 Cytokine production is altered in PV immune cells
(A) MMIs of cytokines in all CD45^{pos} cells from the PV as a heatmap. **(B)** IFNα MMI comparisons between treatment groups. Kruskal-Wallis values are listed at the top of each graph. Post-hoc p values are listed as lines connecting respective comparisons. * = p-value <0.05.

Similar to our approach to uncovering signaling pathways within APC subtypes **(Fig 37),** we assessed cytokine production by APCs. Although we saw no differences when all three

treatment groups were compared together, represented by the non-significant Kruskal Wallis value, we found multiple cytokines altered between the homeostatic condition (saline) and or LPS treatment and the blockade group when each treatment was compared individually **(Fig 40)**. In B cells, we report an increase in IL-1β in blockade compared to LPS **(Fig 40A)** indicating that with TNF blocked in vivo, B cells produced higher amounts of IL-1β. DCs had a significant increase in IL-22 and a decrease in IFNα in an LPS-independent, but TNF-dependent manner **(Fig 40B)**. Additionally, DCs had an increase in TNFα production in blockade treated animals compared to LPS animals **(Fig 40B)**. Blockade treatment also significantly reduced IL-10 production in Mϕs **(Fig 40C)**.

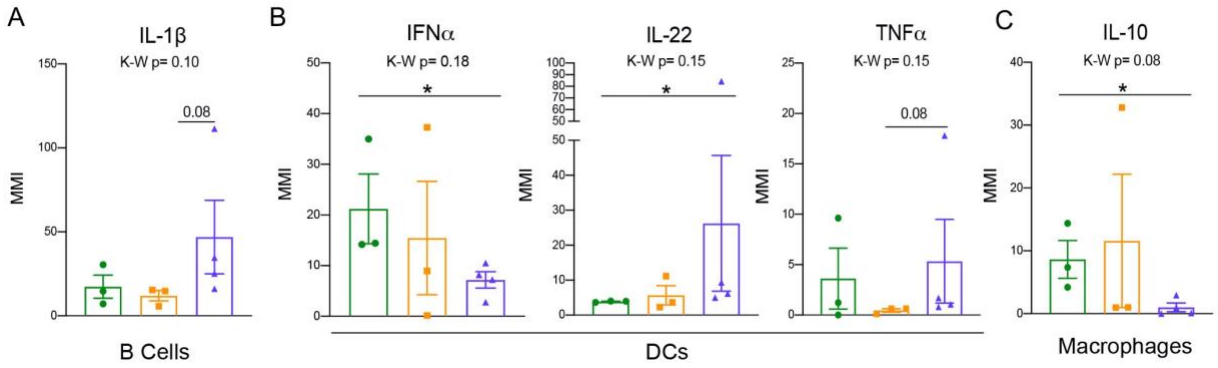

Figure 40 Cytokine alterations in PV APCs are TNF-dependent
(A) Quantification of IL-1β Mean Metal Intensity (MMI) in B cells. (B) Quantification of IFNα, IL-22 and TNFα MMIs in DCs. (C) Quantification of IL-10 MMI in monocytes. Kruskal-Wallis values are listed at the top of each graph. Post-hoc p values are listed as lines connecting respective comparisons. * = p-value <0.05.

As previously noted, we observed evidence of activation of T cells via increased HLA-DR expression **(Fig 29)** and phosphorylation of the TCR pathway **(Fig 38)**. We examined cytokine production in the HLA-DR^{pos} T cells to determine which cytokines were produced by activated T cells. In CD8 T cells, we report that only IL-22 production was reduced (p=0.08) in IA LPS treated animals compared to saline controls that was reversed with TNF blockade (**Fig 41A).** In contrast, cytokine production by activated CD4 T cells was more affected by the treatments where six

cytokines: IL-13, IL-23, IL-6, TNFα, GNZB and IL17A were altered by LPS/blockade treatment (**Fig 41B**). These findings are congruent with recent work showing alterations of multiple cytokines in amniotic fluid of pregnant mice injected with anti-CD3 antibody[173]. Overall, we have shown that activated (HLA-DR^{pos}) T cells have multiple phosphorylated components of the TCR pathway and change their cytokine profile in inflamed *in utero* environments suggesting that antigen-specific activation of T cells may contribute to IA inflammation.

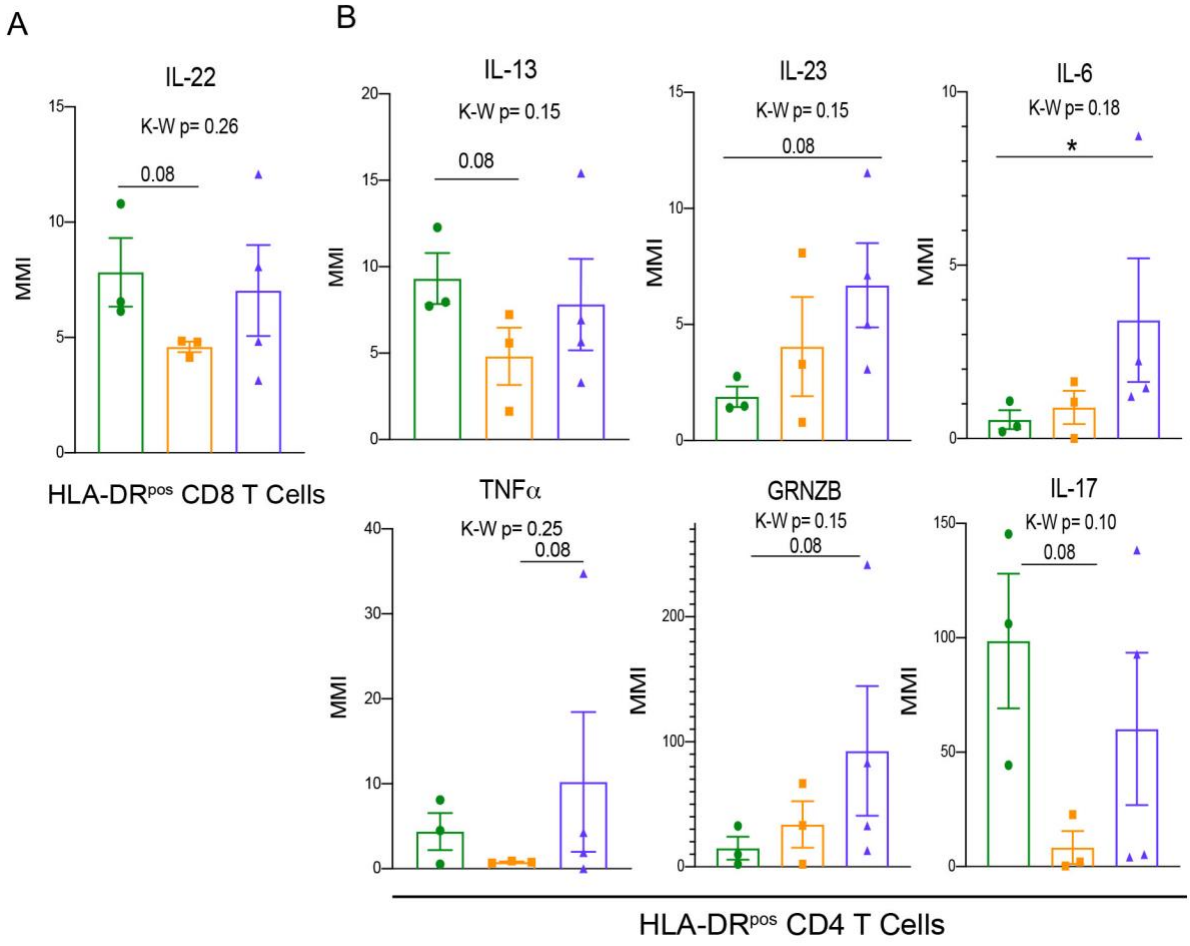

Figure 41 Cytokine production is LPS sensitive in activated PV T cells
(A) Quantification of IL-22 Mean Metal Intensity (MMI) in HLA-DR^{pos} CD8 T cells. (B) Quantification of IL-13, IL-23, IL-6, TNFα, GRNZB, and IL17 MMIs in HLA-DR^{pos} CD4 T cells. Kruskal-Wallis values are listed at the top of each graph. Post-hoc P values are listed as lines connecting respective comparisons. * = p-value <0.05.

3.3.11 PV T regulatory cells are depleted and have an altered cytokine profile with IA LPS

We next investigated if Tregs were affected by IA LPS treatment. To do this, we clustered T cells using our cytokine panel based on surface marker and FOXP3 expression (**Fig 42A**) and identified clusters that were $CD25^{pos}FOXP3^{pos}$. We found that both CD4 (cluster 5) and CD8 (clusters 1&4) populations contained $FOXP3^{pos}$ cells **(Fig 42A-B).** There was a trend towards a reduction in the overall number of $FOXP3^{pos}$ cells in both LPS and blockade groups **(Fig 42C)**. When stratifying between T cell subtypes, it appeared that the abundance of CD8 Tregs was more sensitive to treatment than CD4 Tregs (**Fig 42B**). We next examined cytokine production in Tregs ($FOXP3^{pos}$ CD4 or CD8 T cells) compared to effector T cells ($FOXP3^{neg}$ CD4 or CD8 T cells) **(Fig 42C**. In confirmation of our phenotypic cluster identification **(Fig 42A)**, we observed higher IL-10 MMI in saline animals in both CD4 and CD8 Tregs compared to effectors **(Fig 42C).** In CD8 Tregs, we saw LPS-independent, TNF-dependent production of IL-22 (**Fig 42C**). CD8 Tregs also suppressed IL-17 in a TNF-dependent manner when given IA LPS (**Fig 42C**). Moreover, we saw a rise in IL-23 production in IA LPS that was corrected and restored in blockade **(Fig 42C).** CD4 Tregs were also sensitive to LPS/ TNF inhibition as we saw varying alterations of IL-6 and IL-23 in blockade (**Fig 42C)**. In summation, we showed a loss of $CD8^{pos}$ $FOXP3^{pos}$ cells in both LPS and blockade animals and a more proinflammatory cytokine profile in both $CD4^{pos}$ and $CD8^{pos}$ Tregs that were exposed to intra-amniotic inflammation which is exacerbated with TNF inhibition.

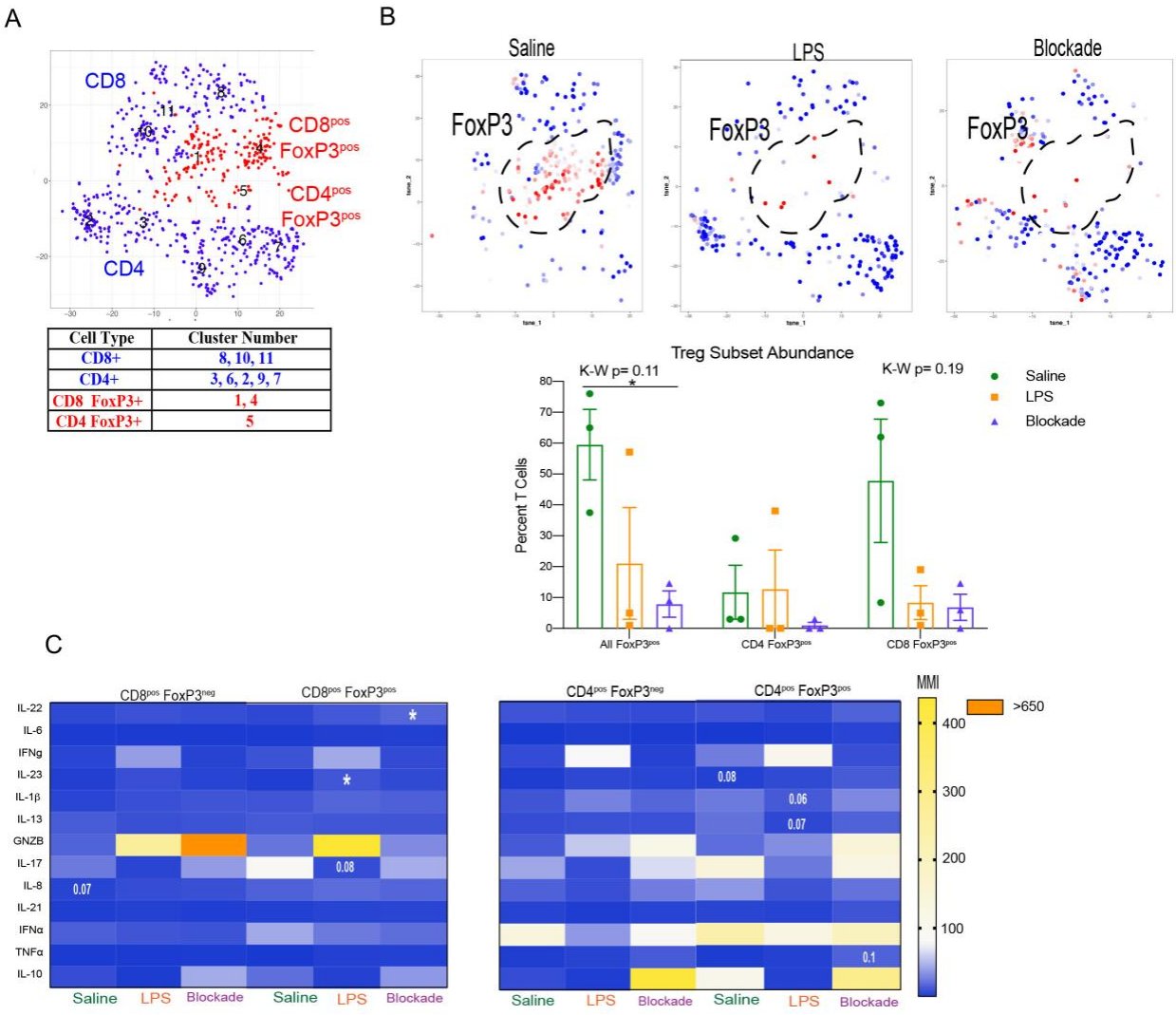

Cell Type	Cluster Number
CD8+	8, 10, 11
CD4+	3, 6, 2, 9, 7
CD8 FoxP3+	1, 4
CD4 FoxP3+	5

Figure 42 PV T regulatory cells are highly sensitive to IA LPS exposure independent of TNF

(A) Automated clustering of T cells from cytokine panel (n=3 per group). (B) Populations were identified based on antibody intensity. Red = strongest expression. FOXP3 expression on CD4 and CD8 T cells, FOXP3^{pos} cells are outlined in black and quantified as a percent of all T cells. Kruskal-wallis values are listed at the top of each graph. Post-hoc p values are listed as lines connecting respective comparisons. * = p-value <0.05. (C) Heatmap of MMIs of cytokines in FOXP3^{pos} and FOXP3^{neg} T cells. Comparisons are made between treatment groups within each subset of T cells. Significance was determined using Kruskal-Wallis comparisons. Comparisons listed on heatmaps are those with an overall K-W p value of less than 0.1 and are placed on the box of the group with the most different value from other treatments.

In summary, we have shown that the choriodecidua and PV contain diverse and distinct immunological profiles under homeostatic conditions. Within each tissue there are changes in individual immune cell populations with IA LPS that were not universally corrected with blockade

(**Fig 43)**. Moreover, PV immune cells were able to signal in a TNF-dependent manner when exposed to IA LPS. Specifically, we have revealed that PV APCs sense LPS through IRAK4 and activate the STAT1 pathway, which subsequently may activate T cells through the TCR pathway and ZAP70. These activated T cells then alter cytokine production, and this dysregulation of cytokines may be the resultant of a reduction and abnormal cytokine production by Tregs, possibly making these Tregs more inflammatory and less suppressive.

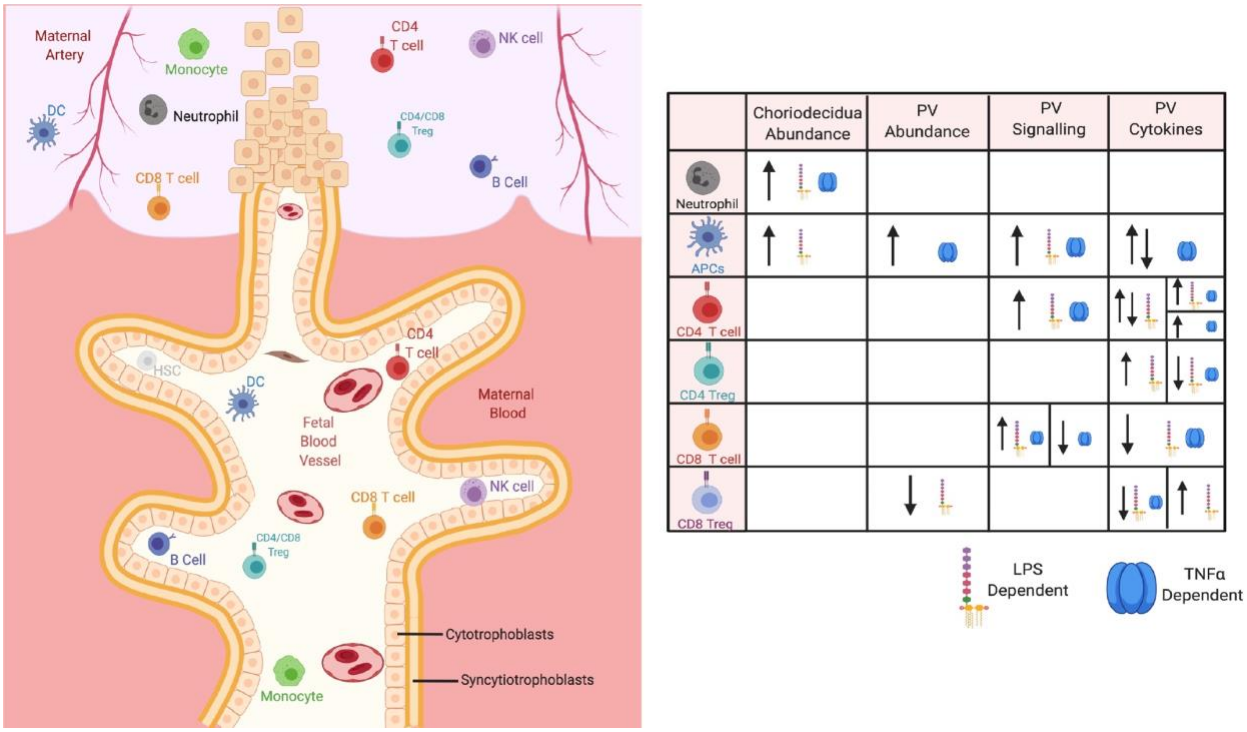

Figure 43 Summary of findings in chapter 3
Summary of cell types presenting in the rhesus choriodecidua and PV during homeostasis (left). Chart showing sensitivity of cell types to experimental treatments (right). This figure was generated with biorender.com.

3.4 Discussion

There is a need for a better understanding of the mechanisms driving intra-amniotic inflammation as these signals have residual long lasting maternal[83] and fetal[84,85] effects. Controlling inflammation at the fetal-maternal interface, is critical to preventing multiple obstetric complications not limited to placental dysfunction, preeclampsia, and spontaneous preterm labor. However, to date, most of the work involving inflammatory processes at the fetal-maternal interface have focused on the decidua and fetal membranes with sparse data available on the role of PV in this process. We aimed to investigate what the immune landscape was in both the choriodecidua and the fetal PV, and whether these cells contribute to inflammation in a rhesus macaque model of LPS-induced intra-amniotic inflammation. Additionally, we aimed to understand if LPS induced inflammation is TNF-dependent and can be alleviated with TNF blockade, as a potential therapeutic.

Using mass cytometry, we uncovered a complex immune landscape within the choriodecidua and PV. Moreover, we found that these two landscapes were distinct from one another, consistent with our human studies in chapter 2. Both the rhesus choriodecidua and the PV house phenotypically diverse innate and adaptive immune cells. Furthermore, using panels targeting phosphorylated proteins and cytokines, we show that cells within the PV respond to LPS in the TLR4 and STAT1 pathways during our experimental window and produce a wide variety of cytokines without ex vivo stimulation. We also conclude that some but not all of these effects are TNF-dependent. When looking at the choriodecidua, we were unable to detect the same changes in phospho-signaling we observed in the PV, however this is most likely reflective of a suboptimal time window.

Consistent with prior studies we detected a diverse population of immune cells in the choriodecidua (reviewed in[34]). Moreover, as previously described[87], we saw an elevation of presumptive neutrophils upon IA LPS treatment that was corrected with TNF blockade. Furthermore, IA LPS induced an increase in CXCR3^{pos} Mϕs in the HLA-DR^{pos} compartment, consistent with prior work showing that CXCR3 upregulation on Mϕs is beneficial in the context of inflammation[169]. Collectively, our results suggest that inflammation within the choriodecidua upon IA LPS injection is a tightly regulated response that involves individual immune cell population changes rather than global immune shifts.

Looking at nine signaling proteins, we found no differences in phosphorylation between any of our treatment groups in the choriodecidua. This is in contrast with previous work showing that immune cells in the choriodecidua are highly active in this model[86,87]. In our model, LPS is administered and then tissues are harvested 16 hours later. Alterations in cytokine production in the decidua were previously observed at this time point, but these are likely downstream of alterations in the signaling cascades we were specifically focusing on in this manuscript. As such, the lack of changes in the phosphorylation status in choriodecidual immune cells may be secondary to: (1) alterations in signaling cascades occurs prior to the time point of tissue collection in our experiments (2) high baseline level of protein phosphorylation making it challenging to detect any differences or (3) other signaling pathways mediate inflammation in our model. Future experiments are needed to address these possibilities.

When turning to the PV, we found a diverse immune landscape that was distinct from the choriodecidua. We report a robust population of Mϕs within the PV, consistent with our previous work (chapter 2), and likely reflective of the previously documented Hofbauer cell population. Furthermore, our results significantly build upon existing data by reporting diversity of immune

cell populations including: T cells[73–75], Mϕs[105,161], DCs, NK cells[75], and B cells[75] within the PV of the third trimester primate placenta. As these cell populations were also detected in the mid-gestation human placenta, we have confirmed the validity of using the rhesus macaque in this and future studies of PV-specific immune cells.

The detection of B cells in the PV is of particular interest. B cell populations within the decidua are rare, reportedly only encompassing 1-2% of $CD45^{pos}$ cells at term, and can acquire pathologic phenotypes in cases of preterm labor [54]. The greater abundance B cells in the PV within the control saline group suggests that B cells may play a PV-specific function in maintaining pregnancy and should be further investigated. Furthermore, we identified a group of $CD45^{pos}$ clusters that were major $lineage^{neg}$ $CD10^{pos}$ and not present in the choriodecidua. CD10 has been shown to be expressed on hematopoietic stem cells[174] additionally, the placenta is a site of hematopoiesis in utero[162], based on these observations we propose that this niche of cells represents hematopoietic stem cells. As CD10 was not included in the panel for our human studies, we could not evaluate the abundance of these potential hematopoietic stem cells earlier in gestation. Similar to the trends we observed in the choriodecidua, LPS treatment did not alter the relative composition of major immune subtypes in the PV, and instead caused alterations of specific immune populations. As such, studies should focus on investigating the role of specific immune populations such as $CD45RA^{pos}$ $CXCR3^{neg}$ Mϕs, rather than investigating all Mϕs together. This concept, particularly in regards to Hofbauer cells was recently validated in the first trimester[66].

Immune cells in the PV upregulated phosphorylation of multiple proteins including STAT1 in a TNF-dependent manner. Our data show that the source of pSTAT1 upregulation could be PV immune cell derived IFNα. However, there are other sources of IFNs in the placenta[175,176] that we did not directly assess. When we studied APCs specifically, we observed the same trends in

pSTAT1 that we observed at a global CD45^{pos} level, showing that this was an APC-associated signature. It would be interesting to study the impacts of trophoblast versus APC-secreted interferons on pSTAT1 signaling on all PV CD45^{pos} cells.

Additionally, we saw alterations in pIRAK4 levels, a critical component in the sensing of LPS. The lack of significance we reported in saline versus LPS groups is most likely attributed to our small number of animals in each group. However, we did detect a significant reduction in pIRAK4 in the blockade animals. This finding supports the hypothesis that TNF is required for PV APCs to sense LPS. Interestingly, it is reported that the amniotic fluid contains inhibitors to LPS mediated TLR4 signaling in the fetal mouse intestine[177]. It is plausible that addition of TNF blocking antibodies into the amniotic fluid is acting in a similar manner as these suppressive factors.

In our PV T cell analysis, we report only T cells with central or effector memory surface markers in the PV. These findings are consistent with our human work (chapter 2); studies in other human fetal organs[100–102]; and the detection activated T cells within the PV of term and preterm deliveries[75]. Additionally, we saw upregulation of HLA-DR and increased pZAP70 among specific T cell clusters in T cell subsets indicating activation of T cells through the TCR, consistent with the successful stimulation of human PV T cells via αCD3/αCD28 antibodies **(Fig 20**). One interesting finding was that HLA-DR^{pos}CD4^{pos} T cells in the blockade group produced cytokines not commonly made by T helper cells such as granzyme B. However, GRNZB^{pos} CD4 T cells have also been reported in the fetal small intestine[101] and in the decidua of mothers with preterm labor[173]. These findings suggest that TNF signaling in the PV is required to keep T cells from secreting proinflammatory cytokines in healthy pregnancies, reflective of our findings that human PV immune cells help maintain homeostasis *in utero*.

Similar to effectors, we saw abnormal expression of cytokines in Tregs in both of our treatment groups. Our findings are similar Rueda and colleagues' report of proinflammatory FOXP3^{pos} CD4 T cells in fetal blood, spleen, thymus and lung using a similar model of rhesus intra-amniotic inflammation. These inflammatory Tregs also could not be corrected with prior administration of anti-IL-1 antibody, congruent with our findings using TNF blocking antibody[178]. Our findings of FOXP3^{pos} CD8 T cells add to the growing body of literature supporting the importance of CD8 Tregs as critical players under both homeostatic and proinflammatory environments[179]. Furthermore, the presence of CD8 T cells with an anti-inflammatory cytokine profile have been shown to be present in the decidua and contribute to maintain healthy pregnancies[180]. It is possible the Tregs detected by our study and by Rueda and colleagues were generated at the same time in the fetus and then have trafficked to the blood, spleen, thymus, lung and PV. Our findings add to this field and confirm that these abnormal Tregs are at the fetal-maternal interface during intra-amniotic inflammation and potentially orchestrate an inflammatory response throughout the amniotic cavity.

As previously stated, we observed that some, but not all LPS-induced modulations in immune cell abundance and signaling were reversed with TNF blockade. These findings suggest that some phenotypes of intra-amniotic inflammation within the PV such as phosphorylation of the TCR pathway proteins are dependent on TNF signaling, while other phenotypes like depletion of the Treg population are mediated through alternative cytokine pathways. Moreover, it is known that other cytokines in addition to TNF are elevated with intra-amniotic inflammation[79], and future studies investigating the role of inhibition of these may uncover the mechanisms behind the TNF-independent phenotypes reported in this study.

The main limitations of our study were the relatively small sample size of each treatment group. Including more animals per treatment group would be helpful in determining if many of the trends we report were significant, but this was not feasible in the current experiment. However, the use of primate models is imperative to furthering our understanding of the etiologies of preterm birth. Another limitation is that our samples were exposed to unavoidable overnight transport between facilities. However, we did observe that cells could be stimulated with PMA as expected, suggesting that signaling cascades could still be initiated post-transport. A larger cohort of animals as well as the addition of a group that received just the TNF blockade without LPS exposure would be valuable to answer further questions about the effects of TNF signaling on the immune landscape of both the choriodecidua and PV, unfortunately these tests were not feasible for this experiment.

In conclusion, we report there is a complex and distinct immune landscape at the fetal maternal interface during homeostasis and intra-amniotic inflammation in both the choriodecidua and PV of rhesus macaques. Our data confirms our findings from mid-gestation human placentas, that the immune profile of these two tissues is distinct from one another and the PV should be considered in future immunological studies at the fetal-maternal interface. This study has broad implications for increasing our knowledge of primate placental biology and immunological drivers of intra-amniotic inflammation.

4.0 Synopsis and future directions

The goal of this dissertation was to investigate contributions of fetal immune cells within the PV in maintaining immunological tolerance at mid-gestation in healthy pregnancies. Additionally, this investigation highlighted the potential role for pathogenic immune responses by fetal cells during intra-amniotic inflammation. This dissertation is a culmination of immunophenotyping and functional analyses of leukocytes within placental tissues *in utero.* Furthermore, this work used a variety of cutting-edge techniques to examine both the transcriptional and translational properties of placental immune cells. Moreover, the studies in chapters 2 and 3 reflect the first uses of mass cytometry using CyTOF (chapter 2&3) and imaging mass cytometry (chapter 3) of primate placental tissues to date.

4.1 Limitations of study

There are notable limitations to the experiments described in this study specifically related to quantification of cell populations. Unlike traditional flow cytometry, quantification by cell number in CyTOF is difficult. This is attributed to the greater cell loss with mass cytometry with a return rate of only 20-30% of input cells. Therefore, common practice in CyTOF analysis is to quantify cell abundance as opposed to gross cell number. Furthermore, because the PV float in maternal blood in vivo, it is difficult to embed all of the individual villous trees per biopsy of PV tissue in the same orientation for FFPE sectioning. As a result, sections often contain multiple villous trees at various orientations (i.e., cross-sections of stroma of one villous next to the

circumferential section of the top of the trophoblast layer a second villous). Unfortunately, this study, did not embed singular villous trees, and thus quantification of specific immune cell populations per villous was not feasible.

Important considerations must be addressed when comparing the specimens analyzed between chapters 2 and 3. Chapter 2 studied placentas from human mid-gestation (45-57.5% of gestation) while chapter 3 used non-human primate placentas at 80% gestation. Additionally, when discussing decidual samples specifically, it must be noted that human decidual samples reflected the decidual basalis and non-human primate choriodecidual samples were taken from the decidua parietalis **(Fig 1)**. As such, it is difficult to determine if inconsistencies in placental immune populations between chapters are attributed to gestational or species-specific differences. For example, the human mid-gestation PV harbored a greater abundance of central memory rather than effector memory CD8 T cells **(Fig 18)**. In contrast, the non-human primate placenta at 80% gestation under homeostasis (Saline treated animals) contained a more evenly split combination of central memory and effector memory CD8 T cells based on the surface expression of the same two markers CCR7 and CD45RA in each study **(Fig 28)**. This inconsistency of T cell memory phenotypes could be attributed to a fundamental difference in non-human primate and human placental biology or could represent a shift towards tissue-generated memory responses (effector memory) of PV T cells with increasing gestation. Future studies comparing both non-human primate and human placentas throughout gestation would be integral to uncovering species-specific PV T cell function in maintaining immunological tolerance.

4.2 Conserved findings in human and non-human primate placentas

Implementing studies in both humans and primates at varying points in gestation however allowed for the identification of potential evolutionarily and gestationally conserved signatures of placental immunity. Such signatures included the presence of Mϕs, NK cells, DCs, B cells and activated T cell phenotypes in the PV in both human and non-human primates. Moreover, the dual species and gestational timeline approach uncovered the potential importance of T cell activation during intra-amniotic inflammation. Though the human mid-gestation placentas studied were collected from normal uninflamed placentas, this investigation uncovered that healthy mid-gestation PV harbor T cells capable of eliciting a proinflammatory response when exposed to optimal stimuli. The non-human primate investigation complemented these findings by identifying upregulation of the TCR pathway and skewed inflammatory cytokine production by T cells in PV collected from pregnancies with intra-amniotic inflammation. Finally, the dual species/gestational investigation generated potential hypotheses for mechanisms of immunosuppression in healthy pregnancy by drawing on data from both human and non-human primate studies. Specifically, both studies independently identified a role for IFN production by PV immune cells. Human work showed PV immune cells preferentially transcribe IFNγ over TNFα under homeostasis **(Fig 16)**, and non-human primate PV immune cells had elevated IFNγ levels in inflamed PV though this observation was not statistically significant in this potentially due to the limited number of monkeys per group **(Fig 39)**. Interestingly, non-human primate PV APCs had elevated pSTAT1 under inflammatory conditions **(Fig 37)** a signaling pathway downstream of IFNγ. One potential outcome of IFNγ signaling in APCs is upregulation of PD-L1. Strikingly, human PV APCs expressed high levels of PD-L1 at baseline **(Fig 15&16)**. Collectively, this data provides support

in favor of the hypothesis that the IFNγ, pSTAT1, PD-L1 signaling pathway is critical for promoting immunological tolerance in both human and non-human primate placenta and is potentially upregulated during intra-amniotic inflammation to control activated T cell responses in the PV. It would be interesting to study the role of check-point inhibitors in future studies of the role of IFNs on APC-T cell interactions during normal and pathogenic pregnancies.

In summation, this dissertation has identified the role for fetal immune cells in the PV in promoting immunological tolerance during healthy pregnancy. Additionally, this study revealed PV T cell activation as a potential contributor to intra-amniotic inflammation, a common symptom of pathogen pregnancies. The findings from this work not only implicate the importance of PV immune cells as potential therapeutic targets for obstetric complications, but also are applicable to other immunological tolerance settings such as autoimmunity and transplantation biology.

Bibliography

1. *The Placenta*. (Wiley-Blackwell, 2011). doi:10.1002/9781444393927
2. Okada, H., Tsuzuki, T. & Murata, H. Decidualization of the human endometrium. *Reprod Med Biol* **17,** 220–227 (2018).
3. Sharma, S., Godbole, G. & Modi, D. Decidual control of trophoblast invasion. *Am J Reprod Immunol* **75,** 341–350 (2016).
4. Kajihara, T. *et al.* Differential expression of FOXO1 and FOXO3a confers resistance to oxidative cell death upon endometrial decidualization. *Mol. Endocrinol.* **20,** 2444–2455 (2006).
5. Bourne, G. The foetal membranes. A review of the anatomy of normal amnion and chorion and some aspects of their function. *Postgrad. Med. J.* **38,** 193–201 (1962).
6. Cheung, P. Y. & Challis, J. R. Prostaglandin E2 metabolism in the human fetal membranes. *Am. J. Obstet. Gynecol.* **161,** 1580–1585 (1989).
7. Challis, J. R. & Vaughan, M. Steroid synthetic and prostaglandin metabolizing activity is present in different cell populations from human fetal membranes and decidua. *Am. J. Obstet. Gynecol.* **157,** 1474–1481 (1987).
8. Strauss, J. F. Extracellular matrix dynamics and fetal membrane rupture. *Reprod Sci* **20,** 140–153 (2013).
9. Gomez-Lopez, N., Estrada-Gutierrez, G., Jimenez-Zamudio, L., Vega-Sanchez, R. & Vadillo-Ortega, F. Fetal membranes exhibit selective leukocyte chemotaxic activity during human labor. *J Reprod Immunol* **80,** 122–131 (2009).
10. Arechavaleta-Velasco, F., Ogando, D., Parry, S. & Vadillo-Ortega, F. Production of matrix

metalloproteinase-9 in lipopolysaccharide-stimulated human amnion occurs through an autocrine and paracrine proinflammatory cytokine-dependent system. *Biol. Reprod.* **67,** 1952–1958 (2002).

11. Jacobs, S. O. *et al.* Characterizing the immune cell population in the human fetal membrane. *Am J Reprod Immunol* e13368 (2020). doi:10.1111/aji.13368
12. Evain-Brion, D. & Malassine, A. Human placenta as an endocrine organ. *Growth Horm IGF Res* **13 Suppl A,** S34-7 (2003).
13. Wei, J. *et al.* Trophoblastic debris modifies endothelial cell transcriptome in vitro: a mechanism by which fetal cells might control maternal responses to pregnancy. *Sci. Rep.* **6,** 30632 (2016).
14. Bayer, A. *et al.* Human trophoblasts confer resistance to viruses implicated in perinatal infection. *Am. J. Obstet. Gynecol.* **212,** 71.e1-71.e8 (2015).
15. Pollheimer, J., Vondra, S., Baltayeva, J., Beristain, A. G. & Knöfler, M. Regulation of placental extravillous trophoblasts by the maternal uterine environment. *Front. Immunol.* **9,** 2597 (2018).
16. de Rijk, E. P. C. T. & Van Esch, E. The Macaque Placenta—A Mini-Review. *Toxicol. Pathol.* **36,** 108S–118S (2008).
17. Furukawa, S., Kuroda, Y. & Sugiyama, A. A comparison of the histological structure of the placenta in experimental animals. *J Toxicol Pathol* **27,** 11–18 (2014).
18. Malassiné, A., Frendo, J. L. & Evain-Brion, D. A comparison of placental development and endocrine functions between the human and mouse model. *Hum. Reprod. Update* **9,** 531–539 (2003).
19. Maltepe, E., Bakardjiev, A. I. & Fisher, S. J. The placenta: transcriptional, epigenetic, and

physiological integration during development. *J. Clin. Invest.* **120,** 1016–1025 (2010).

20. Menon, R., Bonney, E. A., Condon, J., Mesiano, S. & Taylor, R. N. Novel concepts on pregnancy clocks and alarms: redundancy and synergy in human parturition. *Hum. Reprod. Update* **22,** 535–560 (2016).
21. Silk, J., Short, J., Roberts, J. & Kusnitz, J. Gestation length in rhesus macaques (Macaca mulatta). *Int J Primatol* **14,** 95–104 (1993).
22. Bercovitch, F. B. *et al.* Multiple sirehood in free-ranging twin rhesus macaques (Macaca mulatta). *Am. J. Primatol.* **57,** 31–34 (2002).
23. Bechard, A., Nicholson, A. & Mason, G. Litter size predicts adult stereotypic behavior in female laboratory mice. *J. Am. Assoc. Lab. Anim. Sci.* **51,** 407–411 (2012).
24. PrabhuDas, M. *et al.* Immune mechanisms at the maternal-fetal interface: perspectives and challenges. *Nat. Immunol.* **16,** 328–334 (2015).
25. Aghaeepour, N. *et al.* An immune clock of human pregnancy. *Sci. Immunol.* **2,** (2017).
26. Fragiadakis, G. K. *et al.* Mapping the fetomaternal peripheral immune system at term pregnancy. *J. Immunol.* **197,** 4482–4492 (2016).
27. Le Gars, M. *et al.* Increased proinflammatory responses of monocytes and plasmacytoid dendritic cells to influenza A virus infection during pregnancy. *J. Infect. Dis.* **214,** 1666–1671 (2016).
28. Richani, K. *et al.* Normal pregnancy is characterized by systemic activation of the complement system. *J. Matern. Fetal Neonatal Med.* **17,** 239–245 (2005).
29. Fettke, F. *et al.* Maternal and Fetal Mechanisms of B Cell Regulation during Pregnancy: Human Chorionic Gonadotropin Stimulates B Cells to Produce IL-10 While Alpha-Fetoprotein Drives Them into Apoptosis. *Front. Immunol.* **7,** 495 (2016).

30. Sasaki, Y. *et al.* Decidual and peripheral blood CD4+CD25+ regulatory T cells in early pregnancy subjects and spontaneous abortion cases. *Mol. Hum. Reprod.* **10,** 347–353 (2004).

31. Dieppe, P., Wollheim, F. A., Schumacher, H. R., Wollheim, F. A. & Schumacher, H. R. *The ameliorating effect of pregnancy on chronic atrophic (infectious rheumatoid) arthritis, fibrositis, and intermittent hydrarthrosis : Hench PS*. (CRC Press, 2001).

32. Munoz-Suano, A., Kallikourdis, M., Sarris, M. & Betz, A. G. Regulatory T cells protect from autoimmune arthritis during pregnancy. *J. Autoimmun.* **38,** J103-8 (2012).

33. Erlebacher, A. Immunology of the maternal-fetal interface. *Annu. Rev. Immunol.* **31,** 387–411 (2013).

34. Liu, S. *et al.* The role of decidual immune cells on human pregnancy. *J Reprod Immunol* **124,** 44–53 (2017).

35. Vargas, M. L. *et al.* Comparison of the proportions of leukocytes in early and term human decidua. *Am J Reprod Immunol* **29,** 135–140 (1993).

36. Bulmer, J. N., Morrison, L., Longfellow, M., Ritson, A. & Pace, D. Granulated lymphocytes in human endometrium: histochemical and immunohistochemical studies. *Hum. Reprod.* **6,** 791–798 (1991).

37. Koopman, L. A. *et al.* Human decidual natural killer cells are a unique NK cell subset with immunomodulatory potential. *J. Exp. Med.* **198,** 1201–1212 (2003).

38. Heikkinen, J., Möttönen, M., Komi, J., Alanen, A. & Lassila, O. Phenotypic characterization of human decidual macrophages. *Clin. Exp. Immunol.* **131,** 498–505 (2003).

39. Mincheva-Nilsson, L. & Baranov, V. in *Immunology of Pregnancy* (ed. Mor, G.) 195–214 (Springer New York, 2006). doi:10.1007/0-387-34944-8_18

40. Gardner, L. & Moffett, A. Dendritic cells in the human decidua. *Biol. Reprod.* **69,** 1438–

1446 (2003).

41. Kämmerer, U. *et al.* Human decidua contains potent immunostimulatory CD83(+) dendritic cells. *Am. J. Pathol.* **157,** 159–169 (2000).

42. Feyaerts, D. *et al.* Human uterine lymphocytes acquire a more experienced and tolerogenic phenotype during pregnancy. *Sci. Rep.* **7,** 2884 (2017).

43. Boyson, J. E. *et al.* CD1d and invariant NKT cells at the human maternal-fetal interface. *Proc. Natl. Acad. Sci. USA* **99,** 13741–13746 (2002).

44. Ditzian-Kadanoff, R., Garon, J., Verp, M. S. & Zilberstein, M. Gamma delta T cells in human decidua. *Am. J. Obstet. Gynecol.* **168,** 831–836 (1993).

45. Le Bouteiller, P. Human decidual NK cells: unique and tightly regulated effector functions in healthy and pathogen-infected pregnancies. *Front. Immunol.* **4,** 404 (2013).

46. Le Bouteiller, P. *et al.* Engagement of CD160 receptor by HLA-C is a triggering mechanism used by circulating natural killer (NK) cells to mediate cytotoxicity. *Proc. Natl. Acad. Sci. USA* **99,** 16963–16968 (2002).

47. Kalkunte, S. S. *et al.* Vascular endothelial growth factor C facilitates immune tolerance and endovascular activity of human uterine NK cells at the maternal-fetal interface. *J. Immunol.* **182,** 4085–4092 (2009).

48. Male, V. *et al.* The effect of pregnancy on the uterine NK cell KIR repertoire. *Eur. J. Immunol.* **41,** 3017–3027 (2011).

49. Crespo, Â. C. *et al.* Decidual NK cells transfer granulysin to selectively kill bacteria in trophoblasts. *Cell* **182,** 1125–1139.e18 (2020).

50. Shima, T. *et al.* Regulatory T cells are necessary for implantation and maintenance of early pregnancy but not late pregnancy in allogeneic mice. *J Reprod Immunol* **85,** 121–129 (2010).

51. Jasper, M. J., Tremellen, K. P. & Robertson, S. A. Primary unexplained infertility is associated with reduced expression of the T-regulatory cell transcription factor Foxp3 in endometrial tissue. *Mol. Hum. Reprod.* **12,** 301–308 (2006).

52. Salvany-Celades, M. *et al.* Three Types of Functional Regulatory T Cells Control T Cell Responses at the Human Maternal-Fetal Interface. *Cell Rep.* **27,** 2537–2547.e5 (2019).

53. Miyazaki, S. *et al.* Predominance of Th2-promoting dendritic cells in early human pregnancy decidua. *J. Leukoc. Biol.* **74,** 514–522 (2003).

54. Huang, B. *et al.* Interleukin-33-induced expression of PIBF1 by decidual B cells protects against preterm labor. *Nat. Med.* **23,** 128–135 (2017).

55. Ander, S. E., Diamond, M. S. & Coyne, C. B. Immune responses at the maternal-fetal interface. *Sci. Immunol.* **4,** (2019).

56. Ander, S. E. *et al.* Human Placental Syncytiotrophoblasts Restrict Toxoplasma gondii Attachment and Replication and Respond to Infection by Producing Immunomodulatory Chemokines. *MBio* **9,** (2018).

57. Delorme-Axford, E. *et al.* Human placental trophoblasts confer viral resistance to recipient cells. *Proc. Natl. Acad. Sci. USA* **110,** 12048–12053 (2013).

58. Pudney, J. *et al.* Differential expression of toll-like receptors in the human placenta across early gestation. *Placenta* **46,** 1–10 (2016).

59. Bryant, A. H. *et al.* Human gestation-associated tissues express functional cytosolic nucleic acid sensing pattern recognition receptors. *Clin. Exp. Immunol.* **189,** 36–46 (2017).

60. Huang, Y., Zhu, X.-Y., Du, M.-R. & Li, D.-J. Human trophoblasts recruited T lymphocytes and monocytes into decidua by secretion of chemokine CXCL16 and interaction with CXCR6 in the first-trimester pregnancy. *J. Immunol.* **180,** 2367–2375 (2008).

61. Lissauer, D., Piper, K., Goodyear, O., Kilby, M. D. & Moss, P. A. H. Fetal-specific CD8+ cytotoxic T cell responses develop during normal human pregnancy and exhibit broad functional capacity. *J. Immunol.* **189,** 1072–1080 (2012).

62. Kahn, D. A. & Baltimore, D. Pregnancy induces a fetal antigen-specific maternal T regulatory cell response that contributes to tolerance. *Proc. Natl. Acad. Sci. USA* **107,** 9299–9304 (2010).

63. Rowe, J. H., Ertelt, J. M., Xin, L. & Way, S. S. Pregnancy imprints regulatory memory that sustains anergy to fetal antigen. *Nature* **490,** 102–106 (2012).

64. Liu, F. *et al.* Placental trophoblasts shifted Th1/Th2 balance toward Th2 and inhibited Th17 immunity at fetomaternal interface. *APMIS* **119,** 597–604 (2011).

65. Murphy, S. P. & Tomasi, T. B. Absence of MHC class II antigen expression in trophoblast cells results from a lack of class II transactivator (CIITA) gene expression. *Mol. Reprod. Dev.* **51,** 1–12 (1998).

66. Thomas, J. R. *et al.* Phenotypic and functional characterization of first-trimester human placental macrophages, Hofbauer cells. *J. Exp. Med.* **218,** (2021).

67. Reyes, L. & Golos, T. G. Hofbauer cells: their role in healthy and complicated pregnancy. *Front. Immunol.* **9,** 2628 (2018).

68. Kim, S. Y. *et al.* Methylome of fetal and maternal monocytes and macrophages at the feto-maternal interface. *Am J Reprod Immunol* **68,** 8–27 (2012).

69. Seval, Y., Korgun, E. T. & Demir, R. Hofbauer cells in early human placenta: possible implications in vasculogenesis and angiogenesis. *Placenta* **28,** 841–845 (2007).

70. Alvarez-Silva, M., Belo-Diabangouaya, P., Salaün, J. & Dieterlen-Lièvre, F. Mouse placenta is a major hematopoietic organ. *Development* **130,** 5437–5444 (2003).

71. Gekas, C., Dieterlen-Lièvre, F., Orkin, S. H. & Mikkola, H. K. A. The placenta is a niche for hematopoietic stem cells. *Dev. Cell* **8,** 365–375 (2005).

72. Melchers, F. Murine embryonic B lymphocyte development in the placenta. *Nature* **277,** 219–221 (1979).

73. Goldsobel, A., Ank, B., Spina, C., Giorgi, J. & Stiehm, E. R. Phenotypic and cytotoxic characteristics of the immune cells of the human placenta. *Cell Immunol.* **97,** 335–343 (1986).

74. Bonney, E. A., Pudney, J., Anderson, D. J. & Hill, J. A. Gamma-delta T cells in midgestation human placental villi. *Gynecol Obstet Invest* **50,** 153–157 (2000).

75. Pique-Regi, R. *et al.* Single cell transcriptional signatures of the human placenta in term and preterm parturition. *Elife* **8,** (2019).

76. Nadeau-Vallée, M. *et al.* Sterile inflammation and pregnancy complications: a review. *Reproduction* **152,** R277–R292 (2016).

77. Liu, L. *et al.* Global, regional, and national causes of under-5 mortality in 2000-15: an updated systematic analysis with implications for the Sustainable Development Goals. *Lancet* **388,** 3027–3035 (2016).

78. Bukowski, R. *et al.* Onset of human preterm and term birth is related to unique inflammatory transcriptome profiles at the maternal fetal interface. *PeerJ* **5,** e3685 (2017).

79. Bhatti, G. *et al.* Compartmentalized profiling of amniotic fluid cytokines in women with preterm labor. *PLoS One* **15,** e0227881 (2020).

80. Gomez-Lopez, N. *et al.* Cellular immune responses in amniotic fluid of women with preterm labor and intra-amniotic infection or intra-amniotic inflammation. *Am J Reprod Immunol* e13171 (2019). doi:10.1111/aji.13171

81. Gomez-Lopez, N. *et al.* The immunophenotype of amniotic fluid leukocytes in normal and complicated pregnancies. *Am J Reprod Immunol* **79,** e12827 (2018).

82. Hamilton, S. *et al.* Macrophages infiltrate the human and rat decidua during term and preterm labor: evidence that decidual inflammation precedes labor. *Biol. Reprod.* **86,** 39 (2012).

83. Gaudillière, B. *et al.* Implementing Mass Cytometry at the Bedside to Study the Immunological Basis of Human Diseases: Distinctive Immune Features in Patients with a History of Term or Preterm Birth. *Cytometry A* **87,** 817–829 (2015).

84. Boonkasidecha, S., Kannan, P. S., Kallapur, S. G., Jobe, A. H. & Kemp, M. W. Fetal skin as a pro-inflammatory organ: Evidence from a primate model of chorioamnionitis. *PLoS One* **12,** e0184938 (2017).

85. Kallapur, S. G., Presicce, P., Rueda, C. M., Jobe, A. H. & Chougnet, C. A. Fetal immune response to chorioamnionitis. *Semin Reprod Med* **32,** 56–67 (2014).

86. Presicce, P. *et al.* Neutrophil recruitment and activation in decidua with intra-amniotic IL-1beta in the preterm rhesus macaque. *Biol. Reprod.* **92,** 56 (2015).

87. Presicce, P. *et al.* IL-1 signaling mediates intrauterine inflammation and chorio-decidua neutrophil recruitment and activation. *JCI Insight* **3,** (2018).

88. Park, C.-W. *et al.* The involvement of human amnion in histologic chorioamnionitis is an indicator that a fetal and an intra-amniotic inflammatory response is more likely and severe: clinical implications. *Placenta* **30,** 56–61 (2009).

89. Hudalla, H. *et al.* LPS-induced maternal inflammation promotes fetal leukocyte recruitment and prenatal organ infiltration in mice. *Pediatr. Res.* **84,** (2018).

90. Gomez-Lopez, N., Vadillo-Perez, L., Nessim, S., Olson, D. M. & Vadillo-Ortega, F. Choriodecidua and amnion exhibit selective leukocyte chemotaxis during term human labor.

Am. J. Obstet. Gynecol. **204,** 364.e9-16 (2011).

91. Catov, J. M. *et al.* Neonatal outcomes following preterm birth classified according to placental features. *Am. J. Obstet. Gynecol.* **216,** 411.e1-411.e14 (2017).
92. Tamblyn, J. A., Lissauer, D. M., Powell, R., Cox, P. & Kilby, M. D. The immunological basis of villitis of unknown etiology - review. *Placenta* **34,** 846–855 (2013).
93. Saso, A. & Kampmann, B. Vaccine responses in newborns. *Semin Immunopathol* **39,** 627–642 (2017).
94. Simonsen, K. A., Anderson-Berry, A. L., Delair, S. F. & Davies, H. D. Early-onset neonatal sepsis. *Clin. Microbiol. Rev.* **27,** 21–47 (2014).
95. Paloczi, K. Immunophenotypic and functional characterization of human umbilical cord blood mononuclear cells. *Leukemia* **13 Suppl 1,** S87-9 (1999).
96. Mold, J. E. *et al.* Maternal alloantigens promote the development of tolerogenic fetal regulatory T cells in utero. *Science* **322,** 1562–1565 (2008).
97. Halkias, J. *et al.* CD161 contributes to prenatal immune suppression of IFNγ-producing PLZF+ T cells. *J. Clin. Invest.* **129,** 3562–3577 (2019).
98. Miller, D. *et al.* CD71+ erythroid cells from neonates born to women with preterm labor regulate cytokine and cellular responses. *J. Leukoc. Biol.* **103,** 761–775 (2018).
99. Elahi, S. *et al.* Immunosuppressive CD71+ erythroid cells compromise neonatal host defence against infection. *Nature* **504,** 158–162 (2013).
100. Stras, S. F. *et al.* Maturation of the human intestinal immune system occurs early in fetal development. *Dev. Cell* **51,** 357–373.e5 (2019).
101. Li, N. *et al.* Memory CD4+ T cells are generated in the human fetal intestine. *Nat. Immunol.* **20,** 301–312 (2019).

102. Schreurs, R. R. C. E. *et al.* Human Fetal TNF-α-Cytokine-Producing CD4+ Effector Memory T Cells Promote Intestinal Development and Mediate Inflammation Early in Life. *Immunity* **50,** 462–476.e8 (2019).

103. Zhang, X. *et al.* CD4 T cells with effector memory phenotype and function develop in the sterile environment of the fetus. *Sci. Transl. Med.* **6,** 238ra72 (2014).

104. Odorizzi, P. M. *et al.* In utero priming of highly functional effector T cell responses to human malaria. *Sci. Transl. Med.* **10,** (2018).

105. Vento-Tormo, R. *et al.* Single-cell reconstruction of the early maternal-fetal interface in humans. *Nature* **563,** 347–353 (2018).

106. Suryawanshi, H. *et al.* A single-cell survey of the human first-trimester placenta and decidua. *Sci. Adv.* **4,** eaau4788 (2018).

107. Pavličev, M. *et al.* Single-cell transcriptomics of the human placenta: inferring the cell communication network of the maternal-fetal interface. *Genome Res.* **27,** 349–361 (2017).

108. Popescu, D.-M. *et al.* Decoding human fetal liver haematopoiesis. *Nature* **574,** 365–371 (2019).

109. Bunis, D. G. *et al.* Single-Cell Mapping of Progressive Fetal-to-Adult Transition in Human Naive T Cells. *Cell Rep.* **34,** 108573 (2021).

110. Fawkner-Corbett, D. *et al.* Spatiotemporal analysis of human intestinal development at single-cell resolution. *Cell* **184,** 810–826.e23 (2021).

111. Spitzer, M. H. & Nolan, G. P. Mass cytometry: single cells, many features. *Cell* **165,** 780–791 (2016).

112. Schwanhäusser, B. *et al.* Global quantification of mammalian gene expression control. *Nature* **473,** 337–342 (2011).

113. Konnikova, L. *et al.* High-dimensional immune phenotyping and transcriptional analyses reveal robust recovery of viable human immune and epithelial cells from frozen gastrointestinal tissue. *Mucosal Immunol.* **11,** 1684–1693 (2018).

114. Schindelin, J. *et al.* Fiji: an open-source platform for biological-image analysis. *Nat. Methods* **9,** 676–682 (2012).

115. McQuin, C. *et al.* CellProfiler 3.0: Next-generation image processing for biology. *PLoS Biol.* **16,** e2005970 (2018).

116. Enninga, E. A. L. *et al.* Maternal T Cells in the Human Placental Villi Support an Allograft Response during Noninfectious Villitis. *J. Immunol.* **204,** 2931–2939 (2020).

117. Catena, R., Montuenga, L. M. & Bodenmiller, B. Ruthenium counterstaining for imaging mass cytometry. *J. Pathol.* **244,** 479–484 (2018).

118. Damond, N. *et al.* A map of human type 1 diabetes progression by imaging mass cytometry. *Cell Metab.* **29,** 755–768.e5 (2019).

119. Schapiro, D. *et al.* histoCAT: analysis of cell phenotypes and interactions in multiplex image cytometry data. *Nat. Methods* **14,** 873–876 (2017).

120. Chen, H. *et al.* Cytofkit: A bioconductor package for an integrated mass cytometry data analysis pipeline. *PLoS Comput. Biol.* **12,** e1005112 (2016).

121. King, A., Balendran, N., Wooding, P., Carter, N. P. & Loke, Y. W. $CD3^-$ Leukocytes Present in the Human Uterus During Early Placentation: Phenotypic and Morphologic Characterization of the $CD56^{++}$ Population. *Dev. Immunol.* **1,** 169–190 (1991).

122. Joerink, M., Rindsjö, E., van Riel, B., Alm, J. & Papadogiannakis, N. Placental macrophage (Hofbauer cell) polarization is independent of maternal allergen-sensitization and presence of chorioamnionitis. *Placenta* **32,** 380–385 (2011).

123. Ohl, L. *et al.* CCR7 governs skin dendritic cell migration under inflammatory and steady-state conditions. *Immunity* **21,** 279–288 (2004).

124. Cibrián, D. & Sánchez-Madrid, F. CD69: from activation marker to metabolic gatekeeper. *Eur. J. Immunol.* **47,** 946–953 (2017).

125. Kumar, B. V. *et al.* Human Tissue-Resident Memory T Cells Are Defined by Core Transcriptional and Functional Signatures in Lymphoid and Mucosal Sites. *Cell Rep.* **20,** 2921–2934 (2017).

126. Borrego, F., Robertson, M. J., Ritz, J., Peña, J. & Solana, R. CD69 is a stimulatory receptor for natural killer cell and its cytotoxic effect is blocked by CD94 inhibitory receptor. *Immunology* **97,** 159–165 (1999).

127. Salimi, M. *et al.* Activated innate lymphoid cell populations accumulate in human tumour tissues. *BMC Cancer* **18,** 341 (2018).

128. Yu, Y. *et al.* Single-cell RNA-seq identifies a PD-1hi ILC progenitor and defines its development pathway. *Nature* **539,** 102–106 (2016).

129. Concha-Benavente, F. *et al.* PD-L1 Mediates Dysfunction in Activated PD-1+ NK Cells in Head and Neck Cancer Patients. *Cancer Immunol Res* **6,** 1548–1560 (2018).

130. Simister, N. E. Placental transport of immunoglobulin G. *Vaccine* **21,** 3365–3369 (2003).

131. Roncarolo, M. G. *et al.* Natural killer cell clones can efficiently process and present protein antigens. *J. Immunol.* **147,** 781–787 (1991).

132. Shaw, T. N. *et al.* Tissue-resident macrophages in the intestine are long lived and defined by Tim-4 and CD4 expression. *J. Exp. Med.* **215,** 1507–1518 (2018).

133. Buggert, M. *et al.* The Identity of Human Tissue-Emigrant CD8+ T Cells. *Cell* **183,** 1946–1961.e15 (2020).

134. Mjösberg, J., Berg, G., Jenmalm, M. C. & Ernerudh, J. FOXP3+ regulatory T cells and T helper 1, T helper 2, and T helper 17 cells in human early pregnancy decidua. *Biol. Reprod.* **82,** 698–705 (2010).

135. Xu-Monette, Z. Y., Zhang, M., Li, J. & Young, K. H. PD-1/PD-L1 Blockade: Have We Found the Key to Unleash the Antitumor Immune Response? *Front. Immunol.* **8,** 1597 (2017).

136. Tagliani, E. & Erlebacher, A. Dendritic cell function at the maternal-fetal interface. *Expert Rev Clin Immunol* **7,** 593–602 (2011).

137. Erbach, G. T. *et al.* Phenotypic characteristics of lymphocyte populations isolated from middle gestation human placenta. *J Reprod Immunol* **25,** 1–13 (1993).

138. Schliefsteiner, C. *et al.* Human Placental Hofbauer Cells Maintain an Anti-inflammatory M2 Phenotype despite the Presence of Gestational Diabetes Mellitus. *Front. Immunol.* **8,** 888 (2017).

139. Tang, Z. *et al.* Isolation of hofbauer cells from human term placentas with high yield and purity. *Am J Reprod Immunol* **66,** 336–348 (2011).

140. Yang, S. W. *et al.* DC-SIGN expression in Hofbauer cells may play an important role in immune tolerance in fetal chorionic villi during the development of preeclampsia. *J Reprod Immunol* **124,** 30–37 (2017).

141. Msallam, R. *et al.* Fetal mast cells mediate postnatal allergic responses dependent on maternal IgE. *Science* **370,** 941–950 (2020).

142. Bright, N. A., Ockleford, C. D. & Anwar, M. Ontogeny and distribution of Fc gamma receptors in the human placenta. Transport or immune surveillance? *J. Anat.* **184 (Pt 2),** 297–308 (1994).

143. Sun, C., Mezzadra, R. & Schumacher, T. N. Regulation and Function of the PD-L1 Checkpoint. *Immunity* **48,** 434–452 (2018).

144. Garcia-Diaz, A. *et al.* Interferon Receptor Signaling Pathways Regulating PD-L1 and PD-L2 Expression. *Cell Rep.* **19,** 1189–1201 (2017).

145. Stras, S. F. *et al.* Maturation of the Human Intestinal Immune System Occures Early During Fetal Development. *Dev. Cell* (2019).

146. Angelo, L. S., Bimler, L. H., Nikzad, R., Aviles-Padilla, K. & Paust, S. CXCR6+ NK cells in human fetal liver and spleen possess unique phenotypic and functional capabilities. *Front. Immunol.* **10,** 469 (2019).

147. Frascoli, M. *et al.* Alloreactive fetal T cells promote uterine contractility in preterm labor via IFN-γ and TNF-α. *Sci. Transl. Med.* **10,** (2018).

148. Kim, J. S. *et al.* Involvement of Hofbauer cells and maternal T cells in villitis of unknown aetiology. *Histopathology* **52,** 457–464 (2008).

149. Theis, K. R. *et al.* No consistent evidence for microbiota in murine placental and fetal tissues. *mSphere* **5,** (2020).

150. Kuperman, A. A. *et al.* Deep microbial analysis of multiple placentas shows no evidence for a placental microbiome. *BJOG* **127,** 159–169 (2020).

151. de Goffau, M. C. *et al.* Human placenta has no microbiome but can contain potential pathogens. *Nature* **572,** 329–334 (2019).

152. Rackaityte, E. *et al.* Viable bacterial colonization is highly limited in the human intestine in utero. *Nat. Med.* **26,** 599–607 (2020).

153. Aagaard, K. *et al.* The placenta harbors a unique microbiome. *Sci. Transl. Med.* **6,** 237ra65 (2014).

154. Leiby, J. S. *et al.* Lack of detection of a human placenta microbiome in samples from preterm and term deliveries. *Microbiome* **6,** 196 (2018).

155. Li, Y. *et al.* In utero human intestine harbors unique metabolome, including bacterial metabolites. *JCI Insight* (2020).

156. McGovern, N. *et al.* Human fetal dendritic cells promote prenatal T-cell immune suppression through arginase-2. *Nature* **546,** 662–666 (2017).

157. Kramer, B. W. *et al.* Dose and time response after intraamniotic endotoxin in preterm lambs. *Am. J. Respir. Crit. Care Med.* **164,** 982–988 (2001).

158. Becher, B. *et al.* High-dimensional analysis of the murine myeloid cell system. *Nat. Immunol.* **15,** 1181–1189 (2014).

159. Wong, M. T. *et al.* Mapping the Diversity of Follicular Helper T Cells in Human Blood and Tonsils Using High-Dimensional Mass Cytometry Analysis. *Cell Rep.* **11,** 1822–1833 (2015).

160. Tang, Z., Abrahams, V. M., Mor, G. & Guller, S. Placental Hofbauer cells and complications of pregnancy. *Ann. N. Y. Acad. Sci.* **1221,** 103–108 (2011).

161. Reyes, L., Wolfe, B. & Golos, T. Hofbauer cells: placental macrophages of fetal origin. *Results Probl Cell Differ* **62,** 45–60 (2017).

162. Bárcena, A., Muench, M. O., Kapidzic, M. & Fisher, S. J. A new role for the human placenta as a hematopoietic site throughout gestation. *Reprod Sci* **16,** 178–187 (2009).

163. Vega-Sanchez, R. *et al.* Placental blood leukocytes are functional and phenotypically different than peripheral leukocytes during human labor. *J Reprod Immunol* **84,** 100–110 (2010).

164. King, A., Wellings, V., Gardner, L. & Loke, Y. W. Immunocytochemical characterization

of the unusual large granular lymphocytes in human endometrium throughout the menstrual cycle. *Hum. Immunol.* **24,** 195–205 (1989).

165. Gaynor, L. M. & Colucci, F. Uterine natural killer cells: functional distinctions and influence on pregnancy in humans and mice. *Front. Immunol.* **8,** 467 (2017).
166. Qi, X. *et al.* Endogenous TWEAK is critical for regulating the function of mouse uterine natural killer cells in an immunological model of pregnancy loss. *Immunology* **148,** 70–82 (2016).
167. Tatsumi, E. *et al.* T lymphocytes expressing human Ia-like antigens in infectious mononucleosis (IM). *Blood* **56,** 383–387 (1980).
168. Tomkinson, Wagner, Nelson & Sullivan. Epstein-Barr virus infection.Activated lymphocytes during acute.
169. Cuenca, A. G. *et al.* Critical role for CXC ligand 10/CXC receptor 3 signaling in the murine neonatal response to sepsis. *Infect. Immun.* **79,** 2746–2754 (2011).
170. Salerno, F., Paolini, N. A., Stark, R., von Lindern, M. & Wolkers, M. C. Distinct PKC-mediated posttranscriptional events set cytokine production kinetics in CD8+ T cells. *Proc. Natl. Acad. Sci. USA* **114,** 9677–9682 (2017).
171. Chen, L. *et al.* Expression of ZAP-70 is associated with increased B-cell receptor signaling in chronic lymphocytic leukemia. *Blood* **100,** 4609–4614 (2002).
172. Au-Yeung, B. B. *et al.* The structure, regulation, and function of ZAP-70. *Immunol. Rev.* **228,** 41–57 (2009).
173. Arenas-Hernandez, M. *et al.* Effector and Activated T Cells Induce Preterm Labor and Birth That Is Prevented by Treatment with Progesterone. *J. Immunol.* **202,** 2585–2608 (2019).
174. Galy, A., Travis, M., Cen, D. & Chen, B. Human T, B, natural killer, and dendritic cells arise

from a common bone marrow progenitor cell subset. *Immunity* **3,** 459–473 (1995).

175. Corry, J., Arora, N., Good, C. A., Sadovsky, Y. & Coyne, C. B. Organotypic models of type III interferon-mediated protection from Zika virus infections at the maternal-fetal interface. *Proc. Natl. Acad. Sci. USA* **114,** 9433–9438 (2017).
176. Bayer, A. *et al.* Type III Interferons Produced by Human Placental Trophoblasts Confer Protection against Zika Virus Infection. *Cell Host Microbe* **19,** 705–712 (2016).
177. Good, M. *et al.* Amniotic fluid inhibits Toll-like receptor 4 signaling in the fetal and neonatal intestinal epithelium. *Proc. Natl. Acad. Sci. USA* **109,** 11330–11335 (2012).
178. Rueda, C. M. *et al.* Lipopolysaccharide-Induced Chorioamnionitis Promotes IL-1-Dependent Inflammatory FOXP3+ CD4+ T Cells in the Fetal Rhesus Macaque. *J. Immunol.* **196,** 3706–3715 (2016).
179. Churlaud, G. *et al.* Human and Mouse CD8(+)CD25(+)FOXP3(+) Regulatory T Cells at Steady State and during Interleukin-2 Therapy. *Front. Immunol.* **6,** 171 (2015).
180. Wang, S. *et al.* The appropriate frequency and function of decidual Tim-3+CTLA-4+CD8+ T cells are important in maintaining normal pregnancy. *Cell Death Dis.* **10,** 407 (2019).